

**Mechanistic, Inhibitory, and Mutagenic Studies of Inositol
Dehydrogenase from *Bacillus subtilis***

A Thesis Submitted to
the College of Graduate Studies and Research
in Partial Fulfillment of the Requirements for
the Degree of Doctor of Philosophy
in the Department of Chemistry
University of Saskatchewan

by

Hongyan Zheng

PERMISSION TO USE

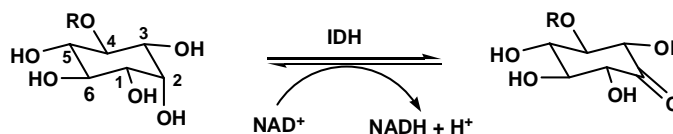
In presenting this dissertation in partial fulfillment of the requirements for a Postgraduate degree from the University of Saskatchewan, I agree that the libraries of this University may make it freely available for inspection. I further agree that permission for copying of this dissertation in any manner, in whole or in part, for scholarly purposes may be granted by the professor who supervised my dissertation work or, in his absence, by the Head of the Department or the Dean of the College in which my thesis work was done. It is understood that any copying or publication or use of this dissertation or parts thereof for financial gain shall not be allowed without my written permission. It is also understood that due recognition shall be given to me and to the University of Saskatchewan in any scholarly use which may be made of any material in my dissertation.

Requests for permission to copy or make other use of material in this dissertation in whole or in part should be addressed to:

The Head
Department of Chemistry
University of Saskatchewan
110 Science Place
Saskatoon, SK S7N 5C9
Canada

ABSTRACT

Inositol dehydrogenase (IDH, EC 1.1.1.18) from *Bacillus subtilis* catalyzes the reversible NAD^+ -dependent oxidation of the axial hydroxyl group of *myo*-inositol to form 2-keto-*myo*-inositol, NADH and H^+ . IDH is the first enzyme in catabolism of *myo*-inositol, and *Bacillus subtilis* is able to grow on *myo*-inositol as the sole carbon source. Our laboratory has previously shown that this enzyme has an unusual active site that can accommodate large hydrophobic substituents at 1L-4-position of *myo*-inositol.



In this dissertation, the further characterization of this IDH is described, with focus on the mechanism, inhibition, kinetics, substrate binding, and alteration of substrate specificity. A kinetic isotope effect study revealed that the chemical step of the reaction was not rate-limiting. In order to probe the inositol-binding site, five inositol analogues were synthesized and evaluated as competitive inhibitors. Recently the crystal structures of the *apo*-IDH, *holo*-IDH and ternary complex have been solved. Using structural information, as well as modeling and sequence alignment approaches, we predicted the active site structure of the enzyme. On the basis of these predictions, coenzyme specificity was converted from entirely NAD^+ -dependent to 6-fold preference for NADP^+ over NAD^+ by site-directed mutagenesis. The critical residues for coenzyme recognition were therefore identified. Besides coenzyme specificity alteration, eleven amino acid residues in and around the proposed *myo*-inositol active site were also modified to test their roles in order to improve our understanding of substrate binding and activation.

ACKNOWLEDGEMENTS

I want to express my sincerest thanks to my supervisor Dr. David R. J. Palmer for his brilliant research guidance, support, understanding, and encouragements throughout these years. He was a lighthouse during my struggles as a Ph.D. student. At times when success seemed far away, he was always there to help me with patience and smiles. Without his help, this dissertation could never be accomplished.

I benefited greatly from the members in Dr. Palmer's lab and Dr. Sanders' lab. Thanks to all the former members for initiating and progressing this IDH project. I want to say thank you to Richard Daniellou, David M. Langill, Christopher P. Phenix, Yunhua Jia, Maohai Fang, Josiah Obiero, Sarathy Karunan Partha, and Karen Ho for close collaboration, useful discussions, and their patient ears. I would especially like to thank Dr. Karin E. Van Straaten, who solved the structures of IDH and guided me in structure related work.

My thanks go to all my colleagues and friends from Department of Chemistry for their cooperation, research advice, and warm friendships.

Finally, I would like to extend my thanks to my parents and my brother for their complete support and understanding through these years.

TABLE OF CONTENTS

PERMISSION TO USE.....	i
ABSTRACT.....	ii
ACKNOWLEDGMENTS.....	iii
TABLE OF CONTENTS.....	iv
LIST OF TABLES.....	vii
LIST OF SCHEMES.....	ix
LIST OF FIGURES.....	x
LIST OF ABBREVIATIONS.....	xiii
1. INTRODUCTION	
1.1 Inositol.....	1
1.2 <i>myo</i> -Inositol catabolism.....	3
1.2.1 <i>myo</i> -Inositol catabolism in eukaryotes.....	4
1.2.2 <i>myo</i> -Inositol catabolism in bacteria.....	6
1.3 Dehydrogenases.....	9
1.3.1 NAD/NADP and the Rossmann fold.....	10
1.3.2 General mechanism of NAD/NADP-dependent dehydrogenases.....	12
1.3.3 Short-chain dehydrogenases/reductases.....	13
1.3.4 Medium-chain dehydrogenases/reductases.....	15
1.3.5 Long-chain dehydrogenases/reductases.....	15
1.4 <i>myo</i> -Inositol-2-dehydrogenase from <i>Bacillus subtilis</i>	16
1.4.1 Physical properties and catalytic properties of native <i>B. subtilis</i> IDH.....	17
1.4.2 Glucose-fructose oxidoreductase and IDH homology model.....	18
1.4.3 Substrate specificity.....	22
1.4.4 Inhibition.....	24
1.4.5 Bi Bi mechanism.....	27
1.4.6 Catalytic residues identification.....	30

1.5 Objectives of research.....	32
2. MATERIALS AND METHODS	
2.1 Reagents.....	33
2.2 Instrumentation.....	34
2.3 Media and plates.....	35
2.4 Plasmids, bacterial strains and growth conditions.....	36
2.5 Molecular biology techniques.....	36
2.5.1 DNA isolation and purification.....	36
2.5.2 Polymerase chain reaction (PCR).....	36
2.5.3 Site-directed mutagenesis.....	37
2.5.4 Restriction digestions.....	44
2.5.5 Transformation.....	44
2.6 Protein expression and purification.....	45
2.6.1 Overexpression of wild-type IDH and mutants.....	45
2.6.2 Purification of wild-type IDH and mutants.....	46
2.6.3 Protein concentration assay.....	47
2.7 Sequence analysis.....	47
2.8 Kinetic assays.....	48
2.8.1 Kinetic measuring system.....	48
2.8.2 Measurement of initial velocity.....	48
2.8.3 Apparent K_m (K_m^{app}) and k_{cat} determination.....	50
2.8.4 IC_{50} and K_i determination.....	52
2.8.5 K_m (<i>myo</i> -inositol) and K_m ($NAD^+/NADP^+$) determination.....	55
2.9 Chemical synthesis and compound characterization.....	57
3. RESULTS AND DISCUSSION	
3.1 Rate-limiting step.....	77
3.1.1 Kinetic isotope effect.....	77

3.1.2 Synthesis of 2- ² H- <i>myo</i> -inositol.....	79
3.1.3 Rate-limiting step determination.....	80
3.2 Exploring the substrate spectrum of IDH.....	81
3.2.1 Design of new potential substrates.....	81
3.2.2 Synthesis of new potential substrates.....	82
3.2.3 Apparent K_m (K_m^{app}) of new substrates.....	85
3.3 Inhibition studies.....	87
3.3.1 Design of potential competitive inhibitors.....	87
3.3.2 Synthesis of inhibitors.....	89
3.3.3 IC ₅₀ measurement and inhibitory properties.....	93
3.4 Mutagenic studies.....	95
3.4.1 Overview of IDH crystal structure.....	96
3.4.2 Structure alignment and implications.....	99
3.4.3 Alteration of coenzyme specificity.....	111
3.4.3.1 Overview of alteration of coenzyme specificity.....	111
3.4.3.2 Alteration of specificity on the basis of sequence alignment.....	112
3.4.3.3 Alteration of specificity on the basis of crystal structure.....	118
3.4.3.4 Summary.....	125
3.4.4 Alteration of substrate specificity from <i>myo</i> -inositol to <i>myo</i> -inositol 4- <i>O</i> -phosphate.....	127
3.4.5 Mutagenic study of the inositol-binding site.....	133
3.4.5.1 Overview of the inositol-binding pocket.....	133
3.4.5.2 Mutagenic studies of putative <i>myo</i> -inositol binding residues.....	134
3.4.5.3 Summary.....	147
4. SUMMARY AND FUTURE DIRECTIONS.....	149
REFERENCES.....	153
APPENDICES.....	168

LIST OF TABLES

Table 1.1	Coenzyme and active site conserved sequence motifs for five SDR families.....	13
Table 1.2	The characteristically graphic patterns of competitive, uncompetitive, and mixed inhibitor presented in double reciprocal plot, Dixon plot, and Cornish-Bowden plot, respectively.....	26
Table 1.3	Pattern of product inhibition observed for Equation 1.2 for differing kinetic mechanisms.....	29
Table 1.4	Pattern of dead-end inhibition observed for Equation 1.2 for differing kinetic mechanisms.....	30
Table 2.1	Primers used in site-directed mutagenesis.....	39
Table 3.1	Kinetic constants of the IDH catalyzed reactions using 2- ² H- <i>myo</i> -inositol and <i>myo</i> -inositol as substrates.....	81
Table 3.2	Kinetic constants of wild-type IDH with four synthesized substrates 1, 2, 3, 4 and D- <i>chiro</i> -inositol.....	85
Table 3.3	Kinetic constants of compounds 10-14 as potential competitive inhibitors of IDH.....	94
Table 3.4	Nine of IDH homologous enzymes.....	103
Table 3.5	Kinetic constants for the mutants D35S, G14A, and G14A/D35S.....	117
Table 3.6	Kinetic constants for the mutants G11K/D35S, G11K/D35S/V36R, D35S/V36R, A12K/D35S, and A12K/D35S/V36R.....	121
Table 3.7	Kinetic constants for the mutants D35S/A40K, D35S/V36R/A40R, and D35S/V36R/A40K.....	124
Table 3.8	Kinetic constants for the mutants at the sites of Asn157, Tyr233, Tyr235, Arg259, and Arg156.....	132

Table 3.9	Kinetic constants of mutants generated from the sites Lys97, Tyr280, Tyr235, and Trp272 in the proposed inositol-binding pocket.....	137
Table 3.10	Kinetic constants of mutants generated from the sites Asp179, Asn157, Met126, and His155 in the proposed inositol-binding pocket.....	142

LIST OF SCHEMES

Scheme 1.1	The diagrams of Bi Bi mechanisms.....	27
Scheme 2.1	A general scheme for one-substrate enzymatic reaction.....	50
Scheme 3.1	Synthesis of 2- ² H- <i>myo</i> -inositol.....	80
Scheme 3.2	Synthesis of inositol analogues.....	84
Scheme 3.3	Conversion of <i>myo</i> -inositol and D- <i>chiro</i> -inositol catalyzed by IoII and IDH(IoIG).....	86
Scheme 3.4	Chemical synthesis of intermediate 18	89
Scheme 3.5	Chemical syntheses of potential inhibitors 10, 11, 12 from intermediate 18	91
Scheme 3.6	Chemical syntheses of potential inhibitors 13, 14	93

LIST OF FIGURES

Figure 1.1	Structures and nomenclature of the inositols.....	2
Figure 1.2	Examples of the D/L naming system of <i>myo</i> -inositol and <i>myo</i> -inositol derivatives.....	3
Figure 1.3	The oxidation pathway of <i>myo</i> -inositol catabolism in eukaryotes.....	5
Figure 1.4	The proposed <i>myo</i> -inositol catabolic pathway in <i>B. subtilis</i>	8
Figure 1.5	Transformation between oxidized dinucleotide (NAD ⁺ /NADP ⁺) and reduced dinucleotide (NADH/NADPH).....	10
Figure 1.6	The model of Rossmann fold of dogfish M4 lactate dehydrogenase structure with NAD ⁺ binding inside.....	11
Figure 1.7	General chemical mechanism of an oxidation-reduction reaction catalyzed by an alcohol dehydrogenase.....	12
Figure 1.8	Examples of the SDR catalyzed reactions.....	14
Figure 1.9	Interconversion of <i>myo</i> -inositol and 2-keto- <i>myo</i> -inositol catalyzed by <i>myo</i> -inositol-2-dehydrogenase (IDH).....	17
Figure 1.10	The oxidation-reduction reaction GFOR catalyzed.....	19
Figure 1.11	Sequence alignment of IDH from <i>B. subtilis</i> and GFOR from <i>Z. mobilis</i>	20
Figure 1.12	Superpositioned models of the crystal structure of GFOR from <i>Zymomonas mobilis</i> and the homology model of IDH.....	21
Figure 1.13	The IDH hology model in which the proposed hydrophobic cavity formed by YGY.....	22
Figure 1.14	Compounds that can be oxidized by IDH.....	23
Figure 1.15	Three types of reversible inhibition.....	25
Figure 1.16	The proposed catalytic mechanism of IDH.....	31
Figure 2.1	A sample of A ₃₄₀ vs time graph.....	49

Figure 2.2	A saturation curve in which the velocity increases with the increase of substrate concentration until approaches a maximum velocity V_{\max}	51
Figure 2.3	Inhibitory property plots of 2-deoxy-2,2-difluoro- <i>myo</i> -inositol.....	53
Figure 2.4	Plot of the variation of velocity with varying <i>myo</i> -inositol concentrations at constant NAD^+ concentrations.....	56
Figure 2.5	Plot of the variation of velocity with varying NAD^+ concentrations at constant <i>myo</i> -inositol concentrations.....	56
Figure 3.1	Structures of potential substrates of IDH.....	82
Figure 3.2	Structures of potential competitive inhibitors of IDH.....	88
Figure 3.3	The model of a tetrameric IDH.....	97
Figure 3.4	The model of one IDH monomer.....	98
Figure 3.5	Structure alignment of IDH from <i>B. subtilis</i> and GPDH from <i>L. mesenteroides</i>	101
Figure 3.6	The structure alignment of the crystal structures of GPDH from <i>L. mesenteroides</i> (PDB code: 1DPG, blue) and IDH from <i>B. subtilis</i> (red).....	102
Figure 3.7	Comparison of coenzyme (NAD or NADP) binding mode in IDH (magenta carbon), GFOR from <i>Z. mobilis</i> (PDB code: 1OFG, yellow carbon), AFR from <i>S. morelense</i> (PDB code: 2GLX, green carbon), and a putative oxidoreductase from <i>T. maritima</i> (PDB code: 1ZH8, grey carbon), putative dehydrogenase from <i>S. typhimurium</i> (PDB code: 3EC7, cyans carbon), IolG1 from <i>L. plantarum</i> (PDB code: 3CEA, purple carbon) by superimposing the backbones of complexed structures.....	107
Figure 3.8	Multiple structure-based sequence alignment of IDH from <i>B. subtilis</i> and its homologs.....	110

Figure 3.9	The model of N-terminal of IDH homology model with Gly14 and Asp35.....	114
Figure 3.10	The model of N-terminal NADH-IDH complex structure with Gly14 and Asp35.....	116
Figure 3.11	Structure alignment of <i>apo</i> -IDH from <i>B. subtilis</i> and human 15-PGDH.....	118
Figure 3.12	The model of N-terminal domain of <i>holo</i> -IDH structure.....	123
Figure 3.13	The model of interface of IDH tetramer.....	128
Figure 3.14	Superpositioned models of the crystal structure of IDH (red) from <i>B. subtilis</i> and the homology model of IDH (blue).....	131
Figure 3.15	Proposed inositol-binding pocket.....	133
Figure 3.16	Superpositioned models of <i>apo</i> -IDH and <i>apo</i> -K97V.....	136
Figure 3.17	Superpositioned models of <i>apo</i> -IDH and <i>apo</i> -K97V.....	139
Figure 3.18	Proximity of bound <i>myo</i> -inositol and Trp272 in non-productive IDH ternary complex.....	141
Figure 3.19	Superpositioned models of <i>apo</i> -IDH and <i>apo</i> -N157S.....	144
Figure 3.20	Superpositioned backbones of <i>apo</i> -IDH and <i>apo</i> -126A.....	146

LIST OF ABBREVIATIONS

ADP	adenosine diphosphate
AIBN	2,2-azobis-(2-methylpropionitrile)
AMP	adenosine monophosphate
b. p.	boiling point
calc.	calculated
DAST	diethylaminosulfur trifluoride
ddH ₂ O	distilled, deionized water
DMAP	4-(dimethylamino)pyridine
DMF	<i>N,N</i> -dimethylformamide
DMSO	dimethyl sulfoxide
dNTP	deoxynucleoside triphosphate
FAD	flavin adenine dinucleotide
FCC	flash column chromatography
GFOR	glucose-fructose oxidoreductase
GPDH	glucose 6-phosphate dehydrogenase
HEPES	4-(2-hydroxyethyl)piperazine-1-ethanesulfonic acid
h	hour
IDH	<i>myo</i> -inositol-2-dehydrogenase
[I]	concentration of an inhibitor
k_{cat}	turnover number
$k_{\text{cat}}/K_{\text{m}}$	catalytic efficiency
K_{m}	Michaelis constant
$K_{\text{m}}^{\text{app}}$	apparent Michaelis constant
LDR	long-chain dehydrogenases/reductases
MW	molecular weight

MDR	medium-chain dehydrogenases/reductase
MIOX	<i>myo</i> -inositol oxygenase
m. p.	melting point
NAD	β -nicotinamide adenine dinucleotide
NADP	β -nicotinamide adenine dinucleotide phosphate
PCR	polymerase chain reactions
PDB	protein data bank
15-PGDH	15-hydroxyprostaglandin dehydrogenase
RMS	root mean square
r. t.	room temperature
[S]	concentration of a substrate
SDR	short-chain dehydrogenases/reductase
SDS-PAGE	sodium dodecyl sulphate-polyacrylamide gel electrophoresis
THF	tetrahydrofuran
TLC	thin layer chromatography
Tris	2-amino-2-(hydroxymethyl)-1,3-propanediol
v_0	initial velocity
v_i	initial velocity in the presence of an inhibitor
V_{\max}	maximum velocity
V_{\max}^{app}	apparent maximum velocity

1. INTRODUCTION

1.1 Inositol

A cyclohexanehexol was first isolated from muscle and named as “inosit” (from *inos*, the Greek root for muscle) by Scherer in 1850^{1,2}. Since then “inositol” became a term for 1,2,3,4,5,6-cyclohexanehexols in English, and it is also called “cyclitol” in some papers. There are nine possible stereoisomers of inositol: *allo*-inositol, *D-chiro*-inositol, *L-chiro*-inositol, *cis*-inositol, *epi*-inositol, *muco*-inositol, *myo*-inositol, *neo*-inositol, and *scyllo*-inositol (**Figure 1.1**). Of these nine stereoisomers, *myo*-, *scyllo*-, *D-chiro*-, *L-chiro*-, *muco*-, and *neo*-inositol are naturally occurring while *allo*-, *epi*-, and *cis*-inositol have not been found in nature, only known as chemically synthesized molecules³. *D-chiro*-inositol and *L-chiro*-inositol are an enantiomeric pair, and the remaining seven are optically inactive¹. *myo*-Inositol is the most prevalent inositol in nature so far, which is rich in soil and also common in plants and animals. Some microorganisms, including *Bacillus subtilis*⁴, *Cryptococcus melibiose*⁵, *Aerobacter aerogenes* (now reclassified as *Enterobacter aerogenes*)⁶, *Rhizobium leguminosarum* bv. *Viciae*⁷, *Sinorhizobium meliloti*⁸, *Sinorhizobium fredii*⁹, *Corynebacterium glutamicum*¹⁰, and *Lactobacillus casei*¹¹ are able to grow on *myo*-inositol by utilizing it as the sole carbon source.

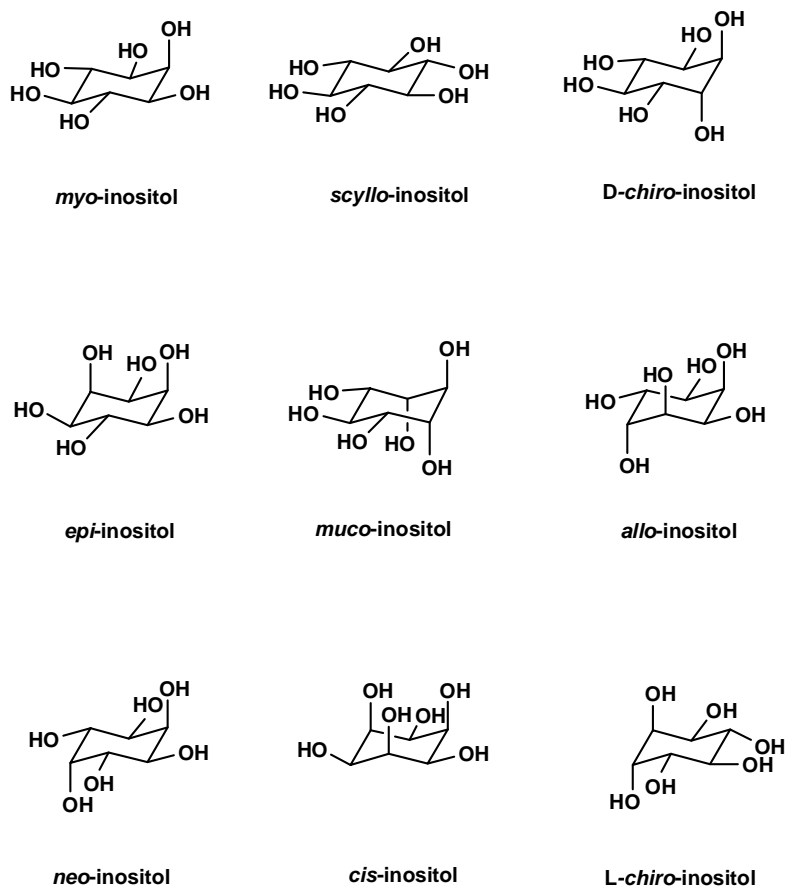


Figure 1.1 Structures and nomenclature of the inositols. When the term “inositol” is used without a prefix, it generally refers to be the *myo* isomer, whereas the term ‘inositols’ refers to all nine inositols. The term “cyclitol” can also be used to refer to the nine inositols collectively.

The numbering of the carbon chain of inositol is confusing since several different rules have been published. Of them, the D/L naming system according to the recommendations of the Nomenclature Committee of the International Union of Biochemistry (NC-IUB) is commonly used^{12,13}. *myo*-Inositol can be named as 1L-*myo*-inositol (clockwise) or 1D-*myo*-inositol (counterclockwise) depending on the substituent location as shown in **Figure 1.2**. To avoid confusion, the *myo*-inositol molecule can be visualized three dimensionally as a turtle, which is known as “Agranoff's turtle”^{1,12}. The head of this turtle always is positioned as number 2.

Looking down from above, the numbers are clockwise when the left front limb labels as number 1 (L system); the numbers are counterclockwise when the right front limb labels as number 1 (D system).

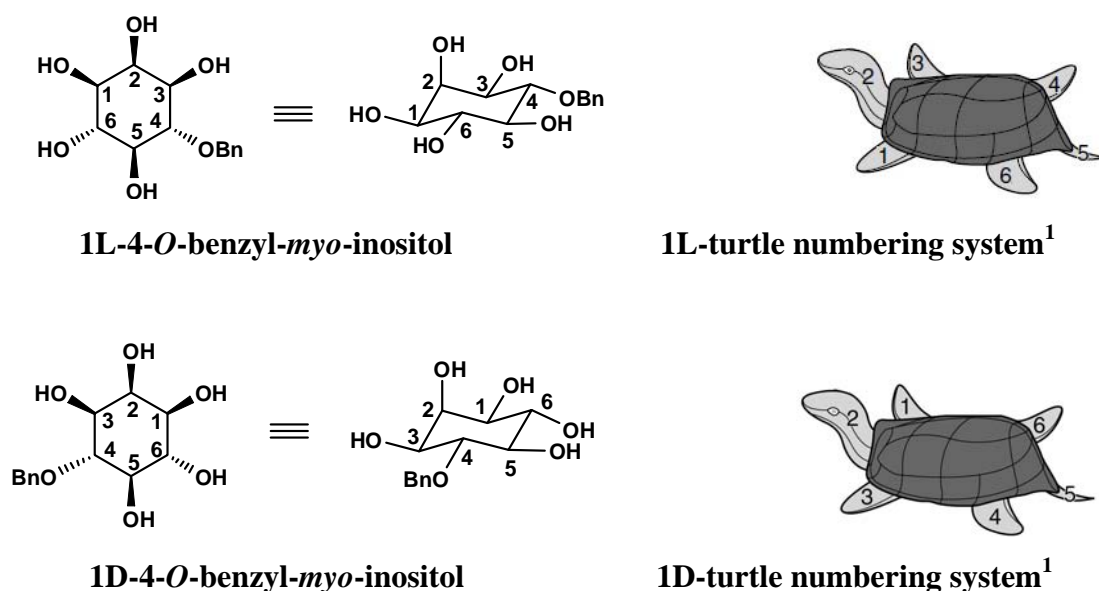


Figure 1.2 Examples of the D/L naming system of *myo*-inositol and *myo*-inositol derivatives.

For convenience, in the rest of this dissertation, when the word inositol is used without a prefix, it refers to *myo*-inositol and all the *myo*-inositol derivatives are named based on the 1L-*myo*-inositol system no matter the location of the substituent(s).

1.2 *myo*-Inositol catabolism

myo-Inositol and its derivatives are widely distributed in nature¹⁴. They play important roles in a myriad of cellular events such as membrane formation, signal transmission, growth regulation, stress response, seed germination, membrane trafficking, hormone

transport, protein anchoring, health maintenance, RNA export, and so on^{1, 15-25}. Two catabolic pathways have been discovered for the degradation of *myo*-inositol. It was found that the pathway in higher eukaryotes is completely different from the bacterial pathway²⁶.

1.2.1 *myo*-Inositol catabolism in eukaryotes

The catabolism pathway of *myo*-inositol in eukaryotes has been well studied, in which, *myo*-inositol is converted to D-glucuronate by the enzyme *myo*-inositol oxygenase (MIOX, EC 1.13.99.1). MIOX was first found in rat kidney in 1957²⁷, which catalyzes the cleavage of C1 and C6 of *myo*-inositol ring²⁸ (**Figure 1.3**). This oxidation reaction is the first step in the only known inositol catabolism pathway in mammals which is associated with diabetes. It has been suggested that inhibition of MIOX activity may be a future cure for diabetic complications²⁹.

In the following steps of *myo*-inositol catabolism pathway, two branches have been discovered. In animals and yeast, the subsequent steps of this inositol oxidation reaction are shown in **Figure 1.3**. The D-glucuronate is converted into L-gulonate, and then 3-keto-L-gulonate, L-xylulose, xylitol, D-xylulose, and D-xylulose 5-phosphate which enters the pentose phosphate cycle^{30,31}. In plants all oxygenase-generated glucuronate is transformed into D-glucuronate 1-phosphate and then into UDP-glucuronate which is a major precursor for nucleotide sugars such as UDP-galacturonate, UDP-D-apiose, UDP-xylose, UDP-L-arabinose^{15,32}.

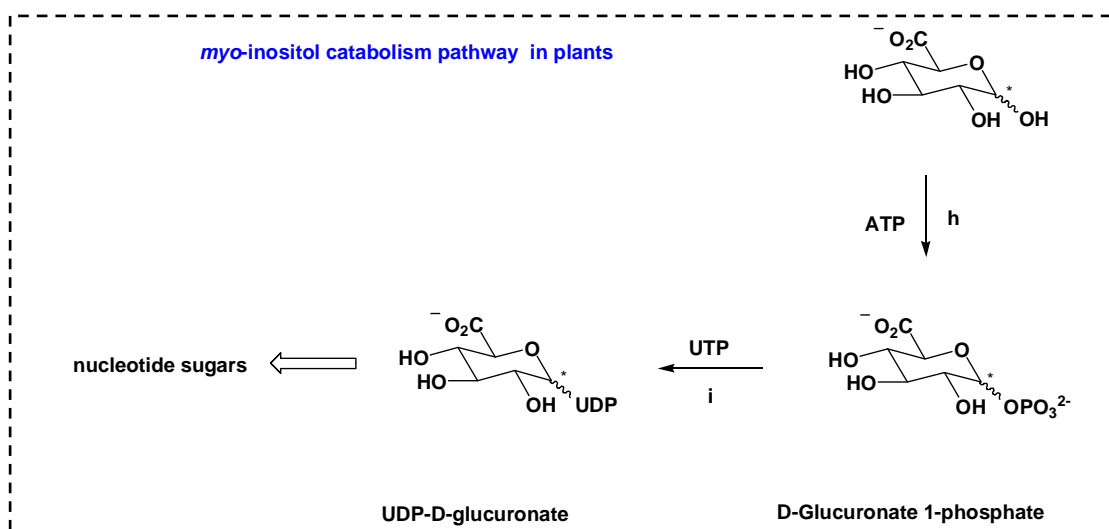
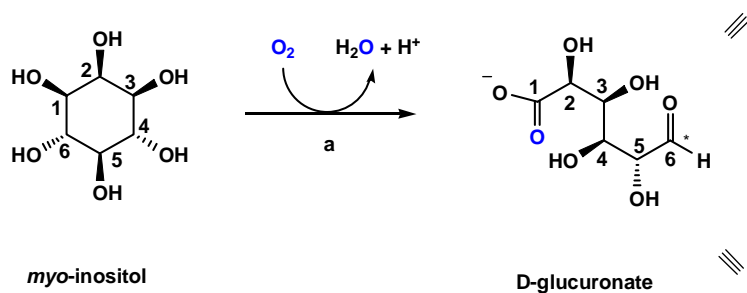
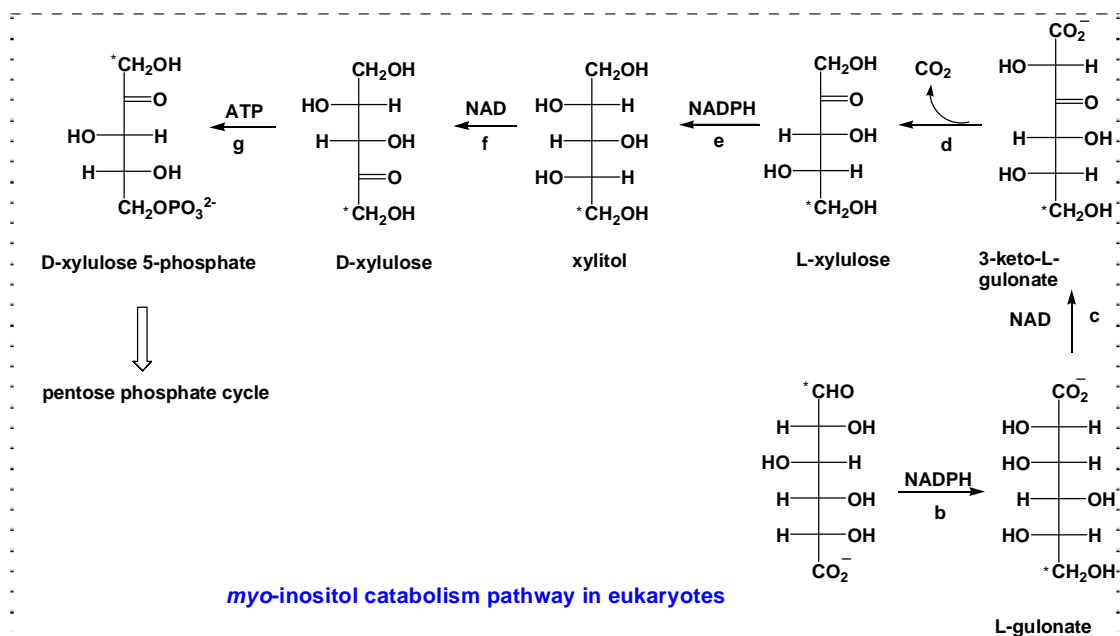


Figure 1.3 The oxidation pathway of *myo*-inositol catabolism in eukaryotes. a: *myo*-inositol oxygenase (MIOX); b: NADPH-dependent D-glucuronate reductase; c: L-gulonate-3-oxidoreductase; d: 3-keto-L-gulonate carboxylase; e: L-xylulose reductase; f: xylitol dehydrogenase; g: D-xylulokinase; h: glucuronokinase; i: glucuronate-1-phosphate uridylyltransferase.

1.2.2 *myo*-Inositol catabolism in bacteria

The breakdown of *myo*-inositol in bacteria follows a completely different pathway from eukaryotes. Relatively fewer studies have been done to demonstrate the *myo*-inositol catabolism pathway in bacteria. In 1971, Anderson *et al* reported the first proposed pathway in *Aerobacter aerogenes* (now reclassified as *Enterobacter aerogenes*) in which decomposition of *myo*-inositol yielded acetyl-CoA, dihydroxyacetone phosphate, and CO₂³³. Later, *myo*-inositol catabolism in *Bacillus subtilis* was explored, in which operon *iolABCDEFGHIIJ* was assigned for the function of inositol catabolism⁴. Experimental characterizations demonstrated *A. aerogenes* and *B. subtilis* shared a similar *myo*-inositol catabolism pathway which is shown in **Figure 1.4**³⁴. The only difference is the intermediate between D-2,3-diketo-4-deoxy-*epi*-inositol and 2-deoxy-5-keto-glucuronic acid. Anderson *et al* thought D-2,3-diketo-4-deoxy-*epi*-inositol was isomerized by keto-enol tautomerization and then the ring scission took place between C2 and C3 to form 2-deoxy-5-keto-glucuronic acid in *A. aerogenes*³³; whereas, 5-deoxy-glucuronic acid was reported as the intermediate in *B. subtilis*³⁴.

In *B. subtilis*, *myo*-inositol is first converted to 2-keto-*myo*-inositol by *myo*-inositol-2-dehydrogenase (IDH, encoded by gene *iolG*) instead of forming D-glucuronate³⁵ as mentioned in 1.2.1. The second step is a dehydration of previous product 2-keto-*myo*-inositol to D-2,3-diketo-4-deoxy-*epi*-inositol [also called 3D-(3,5/4)-trihydroxycyclohexane-1,2-dione], which is catalyzed by 2-keto-*myo*-inositol dehydratase (encoded by gene *iolE*)³⁶. Next, a hydrolase (encoded by gene *iolD*) cleaves the C2-C3 bond of the dehydration product to form 5-deoxy-D-glucuronic acid. The fourth step is catalyzed by an isomerase (encoded by gene *iolB*) to give 2-deoxy-5-keto-glucuronic acid which is phosphorylated in the fifth

step by a kinase (encoded by gene *iolC*)³⁴. The resulting 2-deoxy-5-keto-glucuronic acid 6-phosphate is cleaved into dihydroxyacetone phosphate and malonic semialdehyde by an aldolase (encoded by gene *iolJ*) in the sixth step. The last step is catalyzed by a malonic semialdehyde dehydrogenase (encoded by gene *iolA*), acting on malonic semialdehyde to produce acetyl-CoA and CO₂³⁷. Since the functions of enzymes involved inositol decomposition in *B. subtilis* have been identified, recently, many bacteria have been claimed to contain *myo*-inositol catabolism genes based on the sequence similarity to *B. subtilis iol* genes.

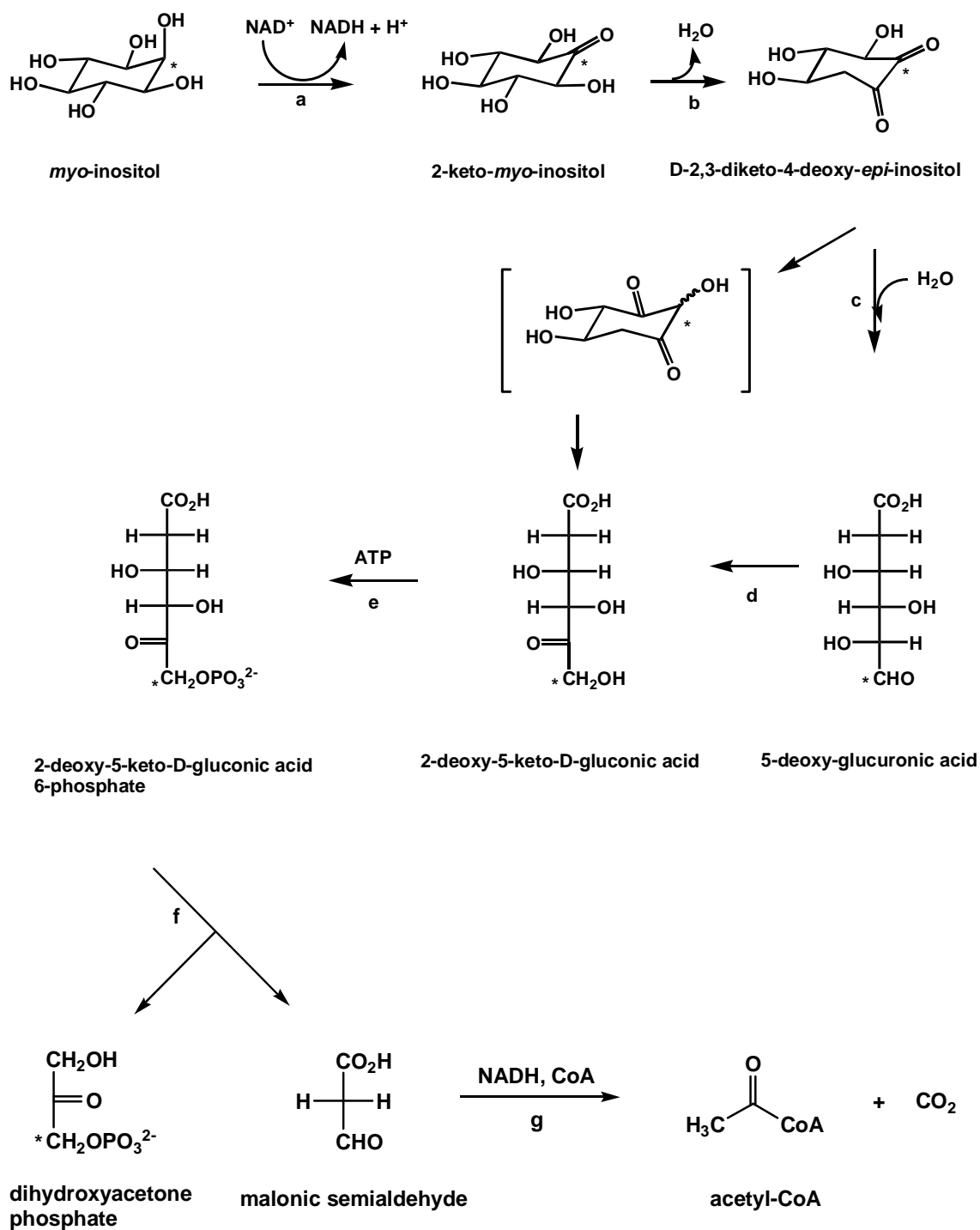


Figure 1.4 The proposed *myo*-inositol catabolic pathway in *B. subtilis*. a: *myo*-inositol-2-dehydrogenase (IDH, *IolG*); b: 2-keto-*myo*-inositol dehydratase (*IolE*); c: hydrolase (*IolD*); d: isomerase (*IolB*); e: kinase (*IolC*); f: aldolase (*IolJ*); g: malonic semialdehyde dehydrogenase (*IolA*). The molecule in blue is a proposed intermediate in *myo*-inositol catabolic pathway in *A. aerogenes*.

1.3 Dehydrogenases

Dehydrogenase, also called oxidoreductase, is an enzyme that catalyzes oxidation-reduction reaction by transferring a hydride between the substrate and coenzyme, and usually uses β -nicotinamide adenine dinucleotide (NAD), β -nicotinamide adenine dinucleotide phosphate (NADP), or flavin adenine dinucleotide (FAD) as a coenzyme. It is known that dehydrogenases comprise a large group of gene products within nearly every genome. It was reported that NAD is the most common coenzyme (41–49%), followed by NADP (30–38%), and FAD is the least common coenzyme (21%) in all organisms³⁸. Although NAD and NADP are structurally similar, their biochemistry is substantially different. NAD is used almost exclusively in the oxidative degradations and acts as an oxidant; however, NADP is, with a few exceptions, involved in the reactions of reductive biosynthesis and acts as a reductant³⁹. In this dissertation, NAD or NADP as a coenzyme will be discussed.

Based on distinct sequence motifs, protein chain length, mechanistic features and structural comparisons of dehydrogenases, superfamilies of short-, medium-, and long-chain dehydrogenases/reductases has been classified⁴⁰⁻⁴². This concept was first established in 1981⁴³. Of these three superfamilies, the long-chain dehydrogenases/reductases superfamily is the least defined one. In contrast, short-chain dehydrogenases/reductases superfamily and medium-chain dehydrogenases/reductases superfamily have been characterized in great detail including their structure-function relationships.

1.3.1 NAD/NADP and the Rossmann fold

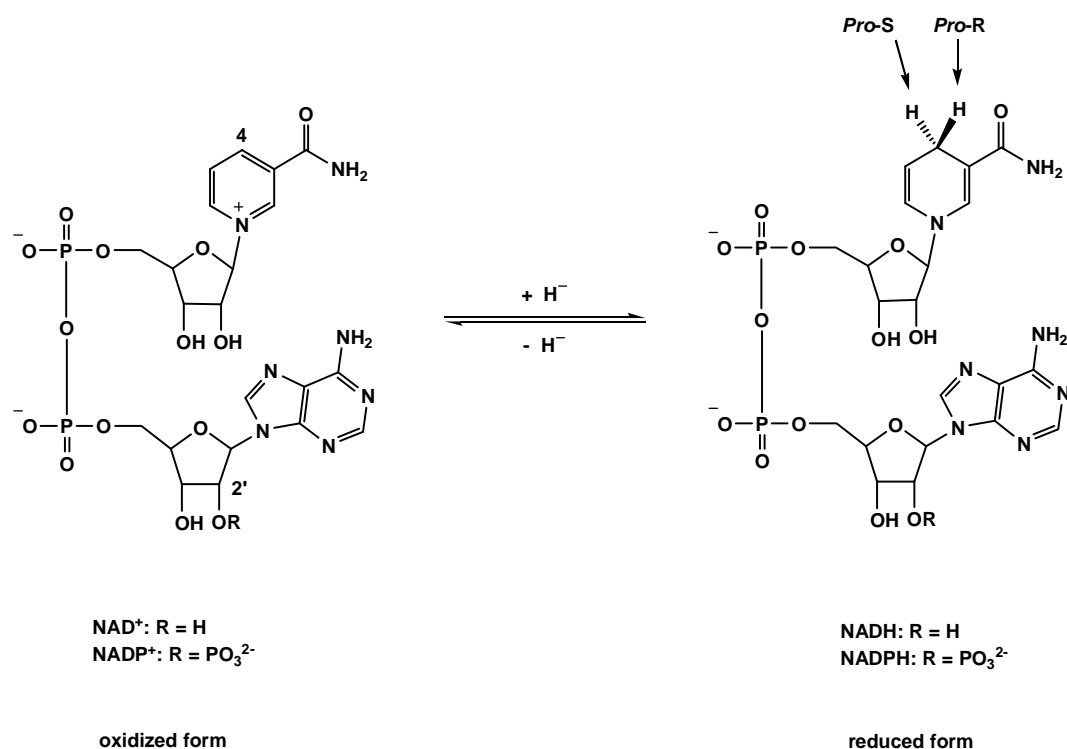


Figure 1.5 Transformation between oxidized dinucleotide ($\text{NAD}^+/\text{NADP}^+$) and reduced dinucleotide (NADH/NADPH).

β -Nicotinamide adenine dinucleotide (NAD) is a coenzyme that serves as a hydride carrier for the enzymatic oxidation-reduction reaction. There are two forms of NAD (**Figure 1.5**). NAD^+ is the oxidized form, and it accepts hydride from the substrate and becomes NADH which is the reduced form. Vice versa, NADH can donate a hydride to form NAD^+ . The reduced form NADH absorbs light at 340 nm, whereas the oxidized form NAD^+ does not. The nicotinamide ring of NAD^+ is the redox active moiety and the C4 position can reversibly accept hydrides, and thereby converts to the 1,4-dihydropyridine form of NADH. The C4 of nicotinamide ring is prochiral, and the enzymatic hydride transfer is stereospecific (attack from *re*-face or *si*-face of nicotinamide). Thus, the hydrogens on C4 of 1,4-dihydropyridine can be labelled as *pro-R* or *pro-S*. NADP is the phosphorylated NAD, as shown in **Figure 1.5**. NADP acts the same way as NAD chemically. Some enzymes are exclusive to NAD or

NADP, and a few enzymes can accommodate both NAD and NADP as coenzymes.

Most of the NAD/NADP-dependent dehydrogenases bind the coenzyme in a structurally conserved domain named the Rossman fold. This Rossman fold consists of a six-stranded parallel β -sheet and four associated α -helices with the topological order $\beta\alpha\beta\alpha\beta\alpha\beta$ in which α helix pairs are on both sides of the plane formed by β strands⁴⁴. A classical Rossmann fold is shown in **Figure 1.6** using dogfish M4 lactate dehydrogenase as an example. Almost all of the characterized Rossmann fold show glycine rich motif in a $GX_{1-2}GX_{1-2}G(A)$ pattern after $\beta 1$, where 'X' denotes any amino acid residue.

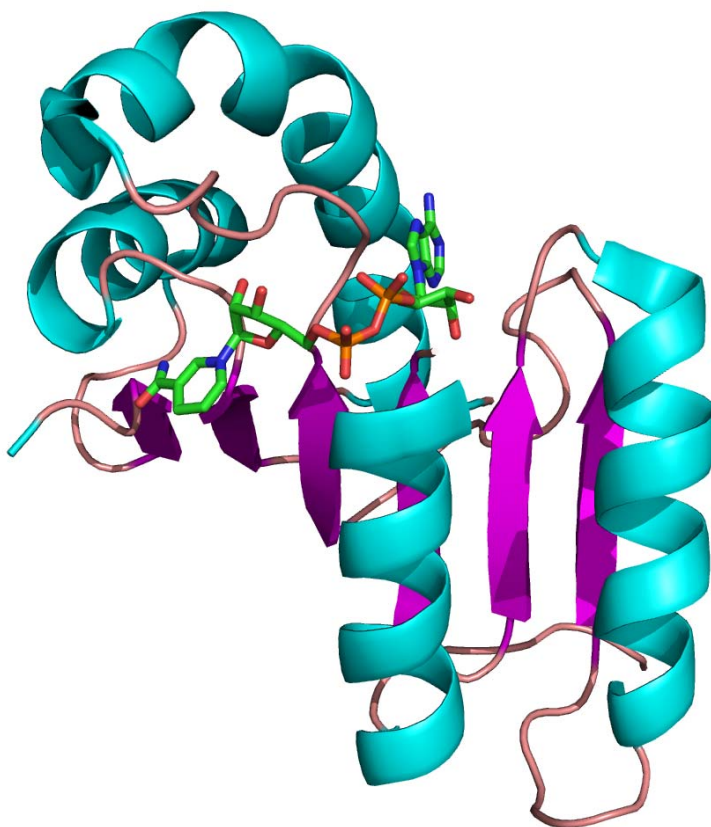
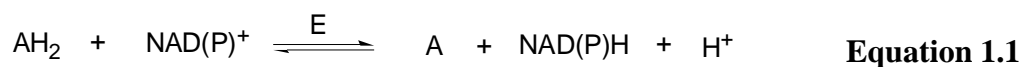


Figure 1.6 The model of Rossmann fold of dogfish M4 lactate dehydrogenase structure (PDB code: 3LDH) with NAD⁺ binding inside. NAD⁺ molecule is indicated in sticks (carbon in green, oxygen in red, phosphorus in orange, nitrogen in blue); α -helix is indicated in cyans; β -sheet is indicated in magenta; loop is indicated in salmon pink. Image was generated using PyMOL⁶⁸.

1.3.2 General mechanism of NAD/NADP-dependent dehydrogenases

The general reaction for NAD/NADP-dependent dehydrogenases can be represented by **Equation 1.1**, in which, AH_2 is a reduced form of substrate; A is an oxidized form; E is a dehydrogenase.



The general chemical mechanism of an alcohol dehydrogenase can be summarized as **Figure 1.7**. In the oxidation reaction, while a general base deprotonates a hydroxyl, the displaced hydride attacks C4 of the nicotinamide ring of NAD^+ to form the oxidized product and NADH. In the reverse direction, the hydride transfers from NADH to C of oxidized product and the carbonyl group is reprotonated, thus, alcohol and NAD^+ are produced.

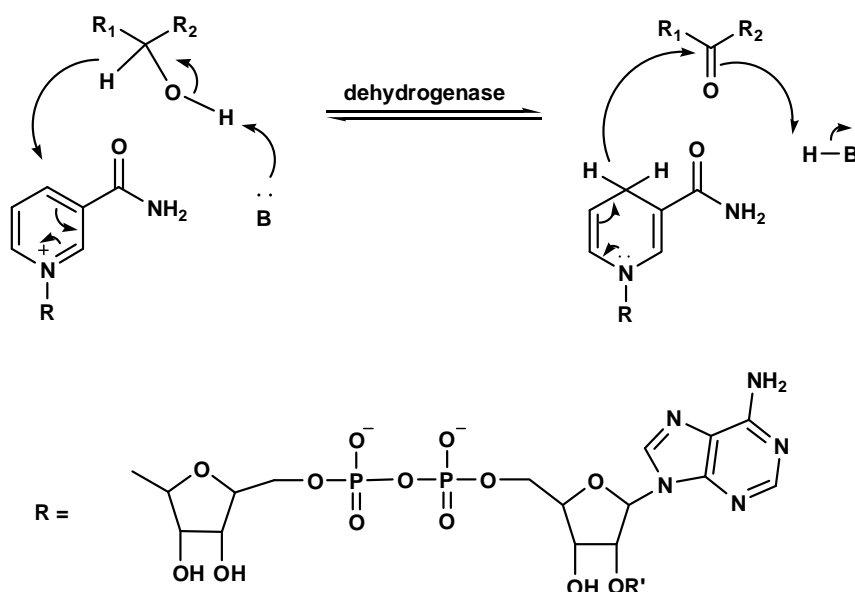


Figure 1.7 General chemical mechanism of an oxidation-reduction reaction catalyzed by an alcohol dehydrogenase. B is a general base, usually is Tyr, His, or Lys; R₁ and R₂ can be any substituent; R' = H, PO₃²⁻.

1.3.3 Short-chain dehydrogenases/reductases

Short-chain dehydrogenases/reductases (SDRs, with subunits typically of ~ 250 residues) is one of the largest enzyme superfamilies with 46,000 members and over 300 crystal structures deposited in protein data bank (PDB). About 25% of all dehydrogenases belong to the SDR superfamily and about 75% of all known SDR enzymes are from bacteria⁴⁵. SDR enzymes play critical roles in lipid, amino acid, carbohydrate, cofactor, hormone, retinoid, and xenobiotic metabolism as well as in redox sensor mechanisms. In humans over 70 SDR genes have been identified and a variety of inherited metabolic diseases have been identified as their underlying cause genetic defects in SDR genes^{46, 47}.

Table 1.1 Coenzyme and active site conserved sequence motifs for five SDR families.

Family	Coenzyme binding motif	Active site
Classical family	TGXXX[AG]XG	YXXXXK
Extended family	[ST]GXXGXXG	YXXXXK
Intermediate family	[GA]XXGXX[GA]	YXXXXK
Divergent family	GXXXXXSXA	YXXMXXXXK
Complex family	GGXGXXG	YXXN

According to the conserved sequence motifs and subunit size, the SDR superfamily is classified as classical family, extended family, divergent family, intermediate family, and complex family (**Table 1.1**)⁴⁸. Sequence identities of SDR enzymes are typically 15-30%, and the most conserved feature is the N-terminal Rossmann-fold where the coenzyme binds. Typically, the dinucleotide coenzyme binds in a conformation that allows transfer of the 4-*pro*-S hydride of nicotinamide to the substrate⁴⁵. Substrate specificity is determined by the variable C-terminal segment and the active site

contains a conserved Tyr as the general base/acid^{41,49}. SDR enzymes not only catalyze the interconversion of hydroxyl/carbonyl groups, but also catalyze reduction of C=C and C=N double bonds, dehydration, dehalogenation, isomerization, and decarboxylation reactions (**Figure 1.8**)⁵⁰. A database of SDR families is available on the website www.sdr-enzymes.org.

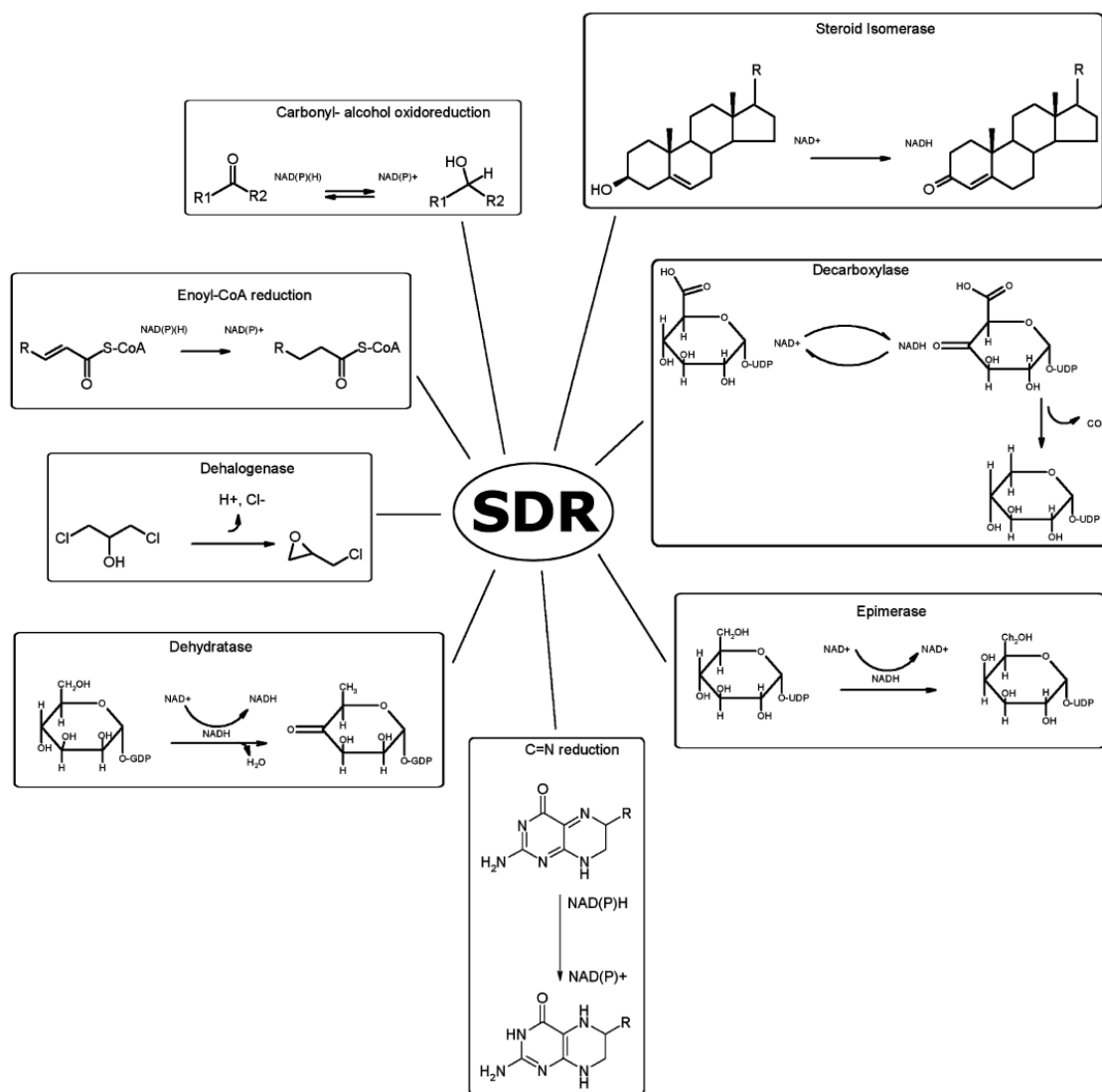


Figure 1.8 Examples of the SDR catalyzed reactions⁵⁰.

1.3.4 Medium-chain dehydrogenases/reductases

Medium-chain dehydrogenases/reductases (MDRs, with subunits typically of ~ 350 residues) comprise a superfamily that contains 2684 enzymes, and the structures of 43 enzymes have been solved as of 2009^{51,149}. MDRs are widely occurred and are involved in metabolism, regulatory processes, and protection against cell damage^{42,52}.

On the basis of sequence similarities analyzed, MDRs are classified into 29 families named from *mdr1* to *mdr29* and the sequence identity of each family varies from 30% to 70%. The Medium-Chain Dehydrogenase/Reductase Engineering Database (MDRED) has been created and is available on the website www.mdred.uni-stuttgart.de⁵¹. All identified MDRs use NAD or NADP as their coenzyme and the dinucleotide binds in a conformation that allows transfer of the 4-*pro*-R hydride of nicotinamide to the substrate⁵⁰. Some MDR members have one zinc ion with catalytic function binding at the active site. Therefore, MDRs are also divided into zinc-containing and non-zinc-containing MDRs^{42,53}.

1.3.5 Long-chain dehydrogenases/reductases

Long-chain dehydrogenases/reductases (LDRs, with subunits typically of ~ 360-550 residues) have not been well defined in terms of structural relationships among protein modules and functional properties. LDRs display similarities in some segments of the amino acid sequence but do not have entire chain homology. Unlike SDRs and MDRs, the number of strictly conserved residues in LDRs is extremely low⁴⁰. To my knowledge, only one family, polyol-specific long-chain dehydrogenases/reductases (PSLDRs), has been reported on the basis of sequence similarity, which consists of 66

NAD/NADP-dependent oxidoreductases^{54,55}. Besides PSLDRs, other NAD/NADP-dependent enzymes including D-glucose 6-phosphate dehydrogenases^{40,56}, isocitrate dehydrogenases⁵⁷, isopropylmalate dehydrogenases⁵⁸, tartrate dehydrogenases⁵⁹, malic enzyme⁶⁰, metalin dependent 6-phosphogluconate dehydrogenases⁶¹, UDP-glucose dehydrogenase⁶², and iron-activated long-chain dehydrogenases⁶³ also were reported as LDRs. In addition, some FAD-dependent enzymes such as fumarate reductase, succinate dehydrogenase, lipoamide dehydrogenase, methoxyneurosporene dehydrogenase, glycerol-3-phosphate dehydrogenase, glucose dehydrogenase, and flavine reductase⁴⁰ were also assigned to the LDR superfamily.

Although they have low amino acid sequence identity (for example, PSLDRs only have 3 residues strictly conserved), LDRs demonstrate similar domain architecture as MDRs and SDRs, which is constructed with the coenzyme-binding domain and the substrate-binding domain^{55,64}. A common feature to all three superfamilies of dehydrogenases/reductases (SDR, MDR, and LDR) is the occurrence of a Rossmann-fold dinucleotide-binding domain.

1.4 *myo*-Inositol-2-dehydrogenase from *Bacillus subtilis*

Bacillus subtilis is a spore-forming bacterium commonly found in soil, which is able to form a tough, protective endospore, allowing the organism to tolerate extreme environment conditions. Like other soil bacteria, *Bacillus subtilis* can grow on *myo*-inositol as the sole carbon source⁶⁵. After inositol is transported into the cell, *myo*-inositol is dehydrogenated to 2-keto-*myo*-inositol with the conversion of NAD⁺ to NADH by *myo*-inositol-2-dehydrogenase (IDH). This reaction is showed in **Figure 1.9**.

The whole inositol catabolism pathway in *Bacillus subtilis* has been described in 1.2.2.

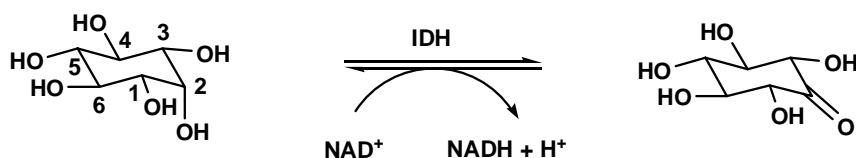


Figure 1.9 Interconversion of *myo*-inositol and 2-keto-*myo*-inositol catalyzed by *myo*-inositol-2-dehydrogenase (IDH).

1.4.1 Physical properties and catalytic properties of native *B. subtilis* IDH

A *myo*-inositol dehydrogenase (IDH, EC 1.1.1.18) was first discovered in vegetative cells of *B. subtilis* in 1976⁶⁶. Three years later, the native *B. subtilis* IDH was isolated and characterized. Ramaley *et al* reported that the active *B. subtilis* IDH is tetrameric, being composed of four identical subunits of 39,000 daltons, each with an independent active site⁶⁵. This enzyme reacts preferentially with *myo*-inositol, and also can recognize some other compounds such as D-glucose and D-xylose as its substrates. In addition, trace activity was observed with D-ribose and D-fructose, and no activity was observed with *scyllo*-inositol, D-mannose, D-sorbitol, D-mannitol, GDP-D-mannose, ADP-D-glucose, D-mannose-6-phosphate, CDP-D-glucose, D-glucose-6-phosphate, 2-deoxy-D-glucose-6-phosphate, D-erythrose, D-glucosamine, D-sorbitol, N-acetyl-D-glucosamine, and D-erythritol. It is apparent that IDH reacts with *myo*-inositol-like compounds, with only one axial hydroxyl group at position 2 (corresponding to position 1 of glucose). By measurement of transfer of tritium from 2-³H-*myo*-inositol, it was concluded that *myo*-inositol is oxidized by IDH at the 2-position to form 2-keto-*myo*-inositol (also called *scyllo*-inosose)⁶⁵. IDH is an exclusive NAD-dependent enzyme and can not recognize NADP as the coenzyme.

Optimum activity for the oxidation reaction presents at pH 9.5 and for reduction reaction presents at pH 7.0. Although IDH can react with D-glucose, it is distinct from glucose dehydrogenase (EC 1.1.1.47), which reacts with β -D-glucose or β -2-deoxy-D-glucose, but does not react with *myo*-inositol, and is able to use either NAD or NADP as a coenzyme^{65,67}.

B. subtilis IDH has not been assigned to any superfamily of SDR, MDR, or LDR, but its homolog D-glucose 6-phosphate dehydrogenase was reported as a member of LDR superfamily^{40,56}. The sequence of the gene *iolG* encoding the IDH enzyme and the regulation of this gene were reported in 1990s³⁵. And then the gene *iolG* was successfully cloned into pET-28b and overexpressed in *Escherichia coli* in this laboratory⁶⁹.

1.4.2 Glucose-fructose oxidoreductase and IDH homology model

B. subtilis IDH was assigned to the GFO/IDH/MOCA superfamily in Swiss-Prot. While some proteins identified by sequence alignment were named as inositol 2-dehydrogenase, there was no structural or functional information available until 2008, when the crystal structures of IolG1 (claimed as *myo*-inositol 2-dehydrogenase) from *Lactobacillus plantarum* WCFS1 (PDB code: 3CEA) and *myo*-inositol dehydrogenase from *Corynebacterium glutamicum* (PDB code: 3EUW) were deposited in RSCB protein data bank (www.rcsb.org/pdb) without reporting further functional characterization.

When we started the project, little was known about IDH and in particular no three-dimensional structure of IDH was solved. We knew, though, glucose-fructose oxidoreductase (GFOR, EC 1.1.99.28) from *Zymomonas mobilis*^{70,71}, a

NADP-dependent enzyme that catalyzes the coupled intermolecular oxidation-reduction of D-glucose and D-fructose in the sorbitol-gluconate pathway^{72,73} (**Figure 1.10**), was the best characterized member of the GFO/IDH/MOCA superfamily. In addition, the high-resolution crystal structures of the wild-type GFOR and several mutants have been determined by X-ray crystallography⁷⁴. *Z. mobilis* GFOR demonstrated 18% sequence identity with *B. subtilis* IDH. According to the sequence alignment in **Figure 1.11**, primary structures in N-terminal parts of IDH and GFOR show significant similarities. The fingerprint motif of the $\beta\alpha\beta$ dinucleotide binding fold, GXGXXG, is conserved in IDH, suggesting that the dinucleotide-binding domain contains the Rossmann fold. Another highly conserved motif in IDH is CEKP, which is proposed as the fingerprint of dehydrogenases whose substrates are structurally similar to glucose⁷⁵. In addition, the catalytic dyad in GFOR, Asp265 and Tyr269 (residue numbering taken from PDB file), aligns with Asp172 and His176 in IDH, which has a potential to act as a catalytic dyad. This sequence alignment allows us to predict the roles of corresponding residues in IDH.

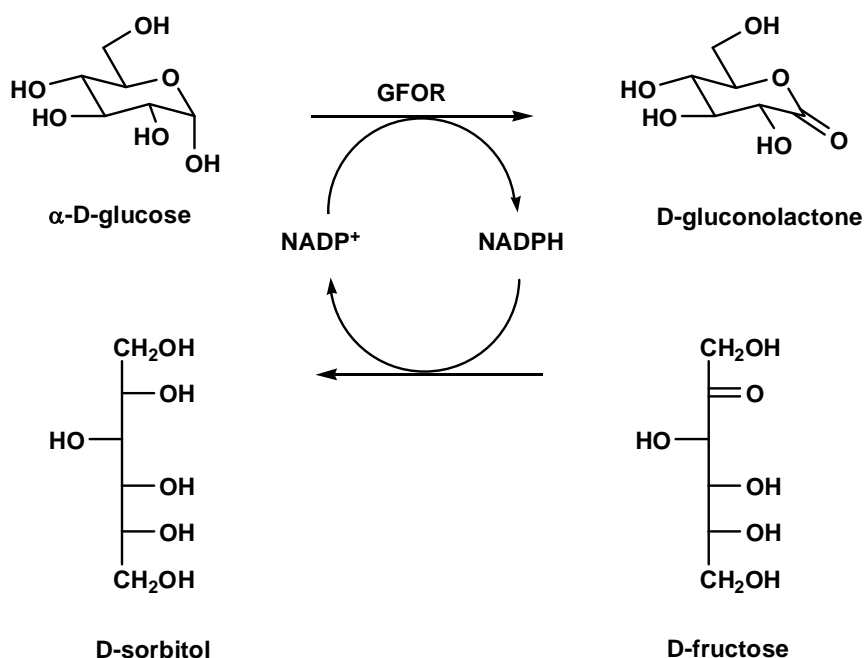




Figure 1.10 The oxidation-reduction reaction GFOR catalyzed.

	1	10	20	30	40
IDH	.MSLRIGVI	GTGAIGKEH	INRITNKL	SGAEIVAVTDVN	QEAQKVVEQYQ
GFOR	DRRFGYAIV	GLGKYALNQ	ILPGFAGCQHSR	IEALVSGNAEKAKIVAAEY	G

	50	60	70	80	90
IDH	LN...ATVYPND	DSLLADENV	DAVLVTSWGPA	HESVVKAIKAQKYVFCE	
GFOR	VDPRKIYDYSNFD	KIAKDPKIDAVYIILPNSL	HAEFAIRAFKAGKHVMCE		

	100	110	120	130	140
IDH	KPLATTAEGCMR	IVEEEIKVGKRLVQV	GFMRRYDSGYVQLKEALDNHVI	IG	
GFOR	KPMATSVADCQR	MIDAAKAANKKLM	IGYRCHYDPMNRAAVKLI	RENQLC	

	150	160	170	180
IDH	EPLMIHCAHRNPTVGDNYTTDMAVV	DTLVHEIDVLHWLVN	
GFOR	KLGMVTTDNSDVMDQNDPAQQWRLRREL	AGGSLMDIGIYGLNGTRY	ELG	





	190	200	210	220	230
IDH	DD.YESVQVIYP	PKKSKNALPHLKDPQ	IVVIETKGGIVINAEIYVNCKYGY		
GFOR	EEPIEVRAYTY	SDPNDERFVEVEDRI	IWQMRFRSGALSHGASSYSTTT..		

	240	250	260	270	280
IDH	DIQCEIVGEDGIIKLPEPSSISLRKEGRFSTDILMDWQRRFVAAY			
GFOR	TSRFSVQGDKAVLLMDPATGYQNL	ISVQTPGHANQSMMPQFIMPANNQF			

	290	300	310	320	330
IDH	DVEIQDFIDS IQKKGEV	SGPTAWDGYIAAVTTD	ACVKAQESGQKEKVELK		
GFOR	SAQLDHLAEAVINNKP	VRSP.GEEGMQDVRLIQ	AIYEAAARTGRPVNTDWG		

	340
IDH	EKPEFYQSFTTVQN
GFORYVRQGGY..

Figure 1.11 Sequence alignment of IDH from *B. subtilis* and GFOR from *Z. mobilis*. Amino acid sequences were aligned using CLUSTALW 1.83⁷⁶ and generated using ESPript⁷⁷, with the BLOSUM 62 scoring matrix (gap penalty = 10, gap extension penalty = 0.5). Red highlighted residues are identical residues. Asp265 and Tyr269 of GFOR are indicated by blue arrows .

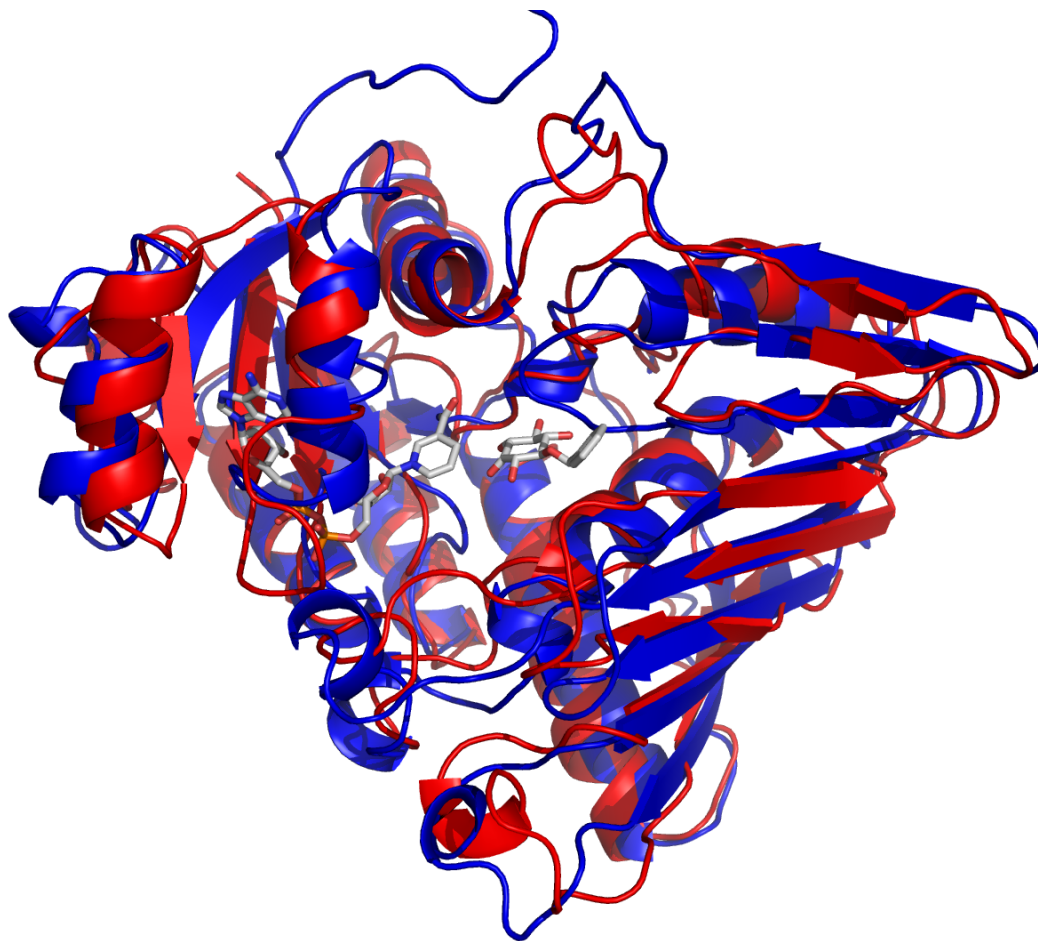


Figure 1.12 Superpositioned models of the crystal structure of GFOR from *Z. mobilis* (blue) and the homology model of IDH (red). NADH and 1L-4-*O*-benzyl-2-keto-*myo*-inositol docked in IDH are shown in sticks (oxygen in red, nitrogen in blue, phosphorus in orange, carbon in grey). Image was generated using PyMOL⁶⁸.

Since no three-dimensional structure of IDH was available at that time, a homology model was needed to make further predictions and activity interpretation. In 2007, the first IDH homology model was built using GFOR as the template and the coenzyme NADH and substrate 1L-4-*O*-benzyl-2-keto-*myo*-inositol were docked manually⁷⁸. The resulting model is shown in **Figure 1.12**. This homology model was used to predict active site residues and substrate/coenzyme binding properties before the IDH crystal structure was solved.

1.4.3 Substrate specificity

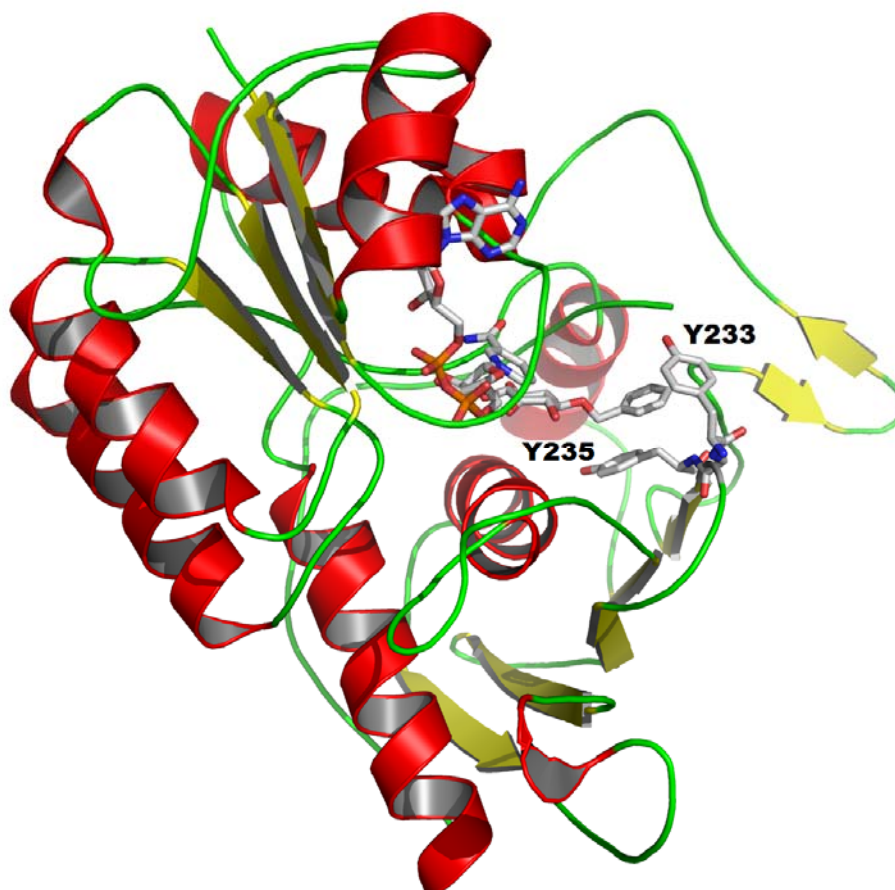


Figure 1.13 The IDH homology model in which the proposed hydrophobic cavity formed by the motif YGY. The coenzyme NAD^+ and substrate 1L-4-O-benzyl-*myo*-inositol are indicated in sticks (oxygen in red, nitrogen in blue, phosphorus in orange, carbon in grey). Image was generated using PyMOL⁶⁸.

As mentioned in **1.2.2**, IDH, a strictly NAD-dependent enzyme, catalyzes the first reaction in the inositol catabolism pathway. *myo*-Inositol is the natural substrate of IDH, and it is regioselectively oxidized at the 2-position, and D-glucose and D-xylose can be recognized as substrates⁶⁵. Previous results of this laboratory revealed that α -D-glucose, α -D-xylose, 1L-4-O-substituted *myo*-inositol, and 6-substituted α -D-glucose (**Figure 1.14**) were also substrates of IDH^{69,78}. Interestingly, derivatives

with charged substituents, *myo*-inositol-4-*O*-phosphate and glucose 6-phosphate, can not be oxidized as the substrates. It was thus proposed that there was a hydrophobic pocket formed by motif YGY near the inositol active site to accommodate those substituted groups⁶⁹ (**Figure 1.13**).

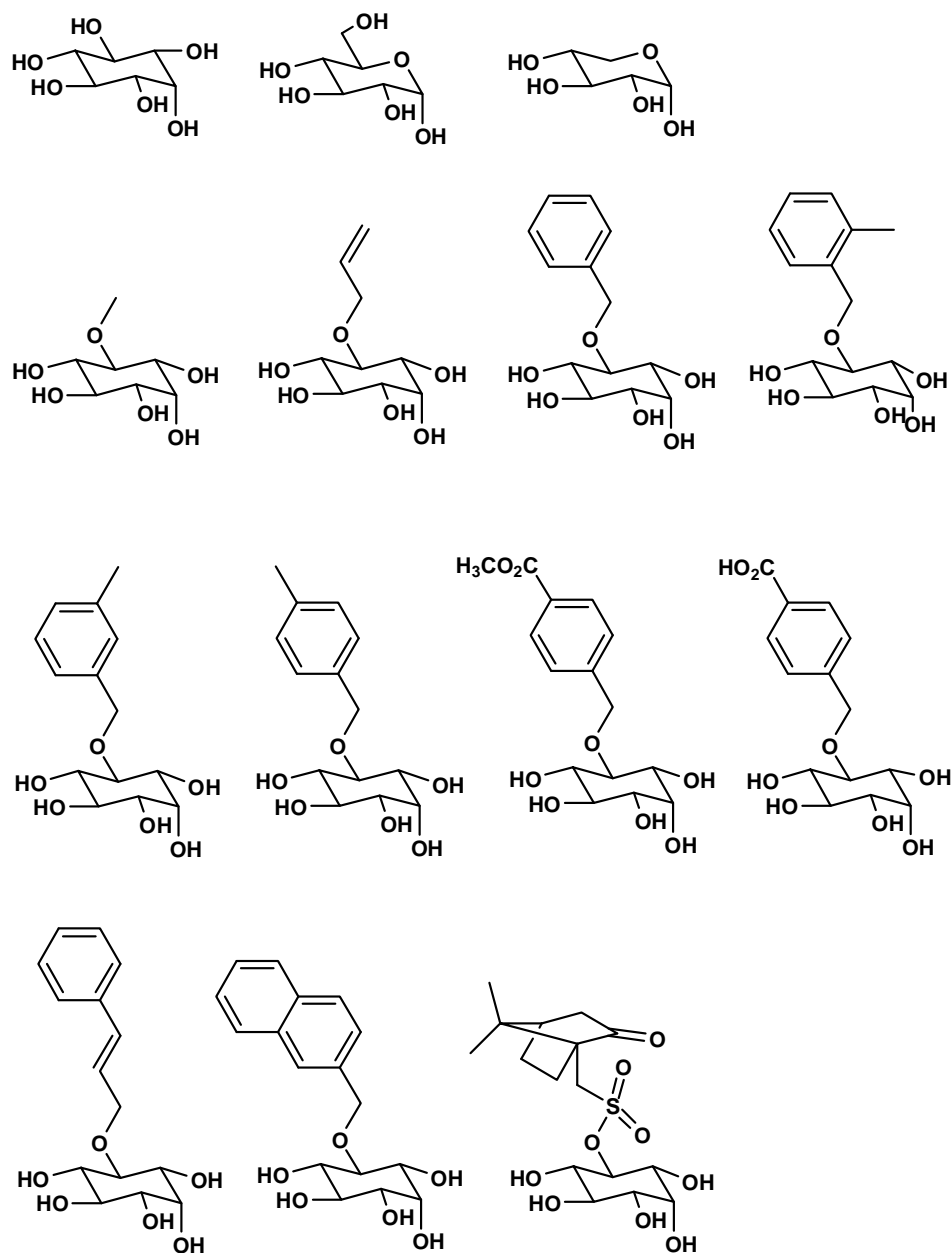


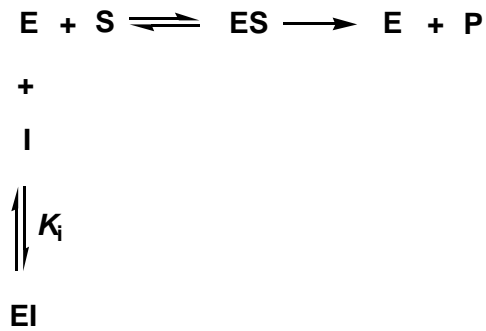
Figure 1.14 Compounds that can be oxidized by IDH.

1.4.4 Inhibition

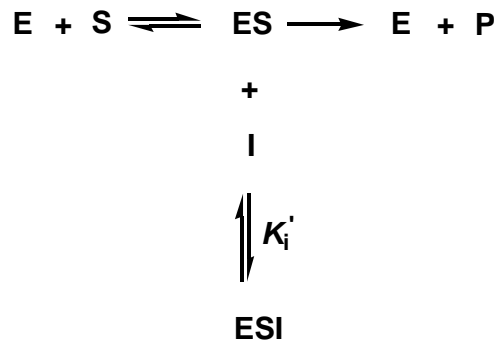
Inhibitors are compounds that interfere with catalysis, slowing or halting enzymatic reactions. As blocking an enzymatic activity can kill a pathogen or correct a metabolic imbalance, many drugs are enzyme inhibitors^{79,80}. The study of enzyme inhibitors also can provide valuable information about enzyme catalytic mechanisms and help define kinetic mechanisms in some cases (examples in **1.4.5**). The binding mode of an inhibitor to an enzyme is either reversible or irreversible. Irreversible inhibitors usually react with the enzyme and modify key amino acid residues needed for enzymatic activity. On the other hand, reversible inhibitors bind to enzymes non-covalently. On the basis of inhibitor binding sites and binding sequence, reversible inhibitors are further classified as competitive, uncompetitive, and mixed inhibitors (when the binding affinity of an inhibitor to free enzyme and to the ES complex is the same, the mixed inhibitor is called a noncompetitive inhibitor)⁸¹, and the corresponding binding modes are shown in **Figure 1.15**.

In order to diagnose the binding mode by which an inhibitor interacts with the enzyme, three sets of graphical methods could be utilized. They are the double reciprocal plot (or Lineweaver-Burk plot), Dixon plot, and Cornish-Bowden plot^{82,83}. These plots are generated by measuring the initial velocities of the enzymatic reaction as a function of several substrate concentrations at several fixed inhibitor concentrations. With the pattern of the straight lines exhibited in the corresponding plot, the inhibitor can be identified as a competitive, uncompetitive, or mixed inhibitor (**Table 1.2**).

a. Competitive inhibition



b. Uncompetitive inhibition



c. Mixed inhibition/noncompetitive inhibition

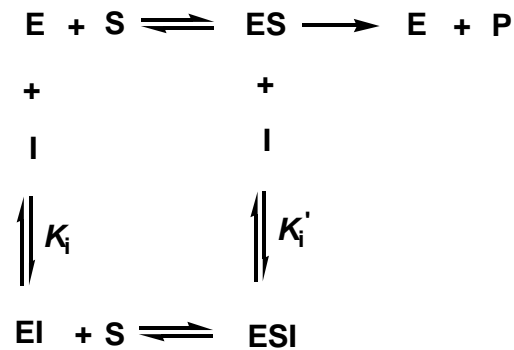


Figure 1.15 Three types of reversible inhibition. E represents an enzyme; S represents a substrate; I represents an inhibitor. K_i is the equilibrium constant for inhibitor binding to E; K_i' is the equilibrium constant for inhibitor binding to ES. (a) Competitive inhibitor binds to the active site. (b) Uncompetitive inhibitor binds at a separate site and binds only to the ES complex. (c) Mixed inhibitor binds at a separate site and can bind to either E or ES ($K_i = K_i'$, named as noncompetitive inhibitor).

Table 1.2 The characteristic patterns of competitive, uncompetitive, and mixed inhibitor presented in double reciprocal plot, Dixon plot, and Cornish-Bowden plot, respectively. a: competitive inhibitor; b: uncompetitive inhibitor; c: mixed inhibitor.

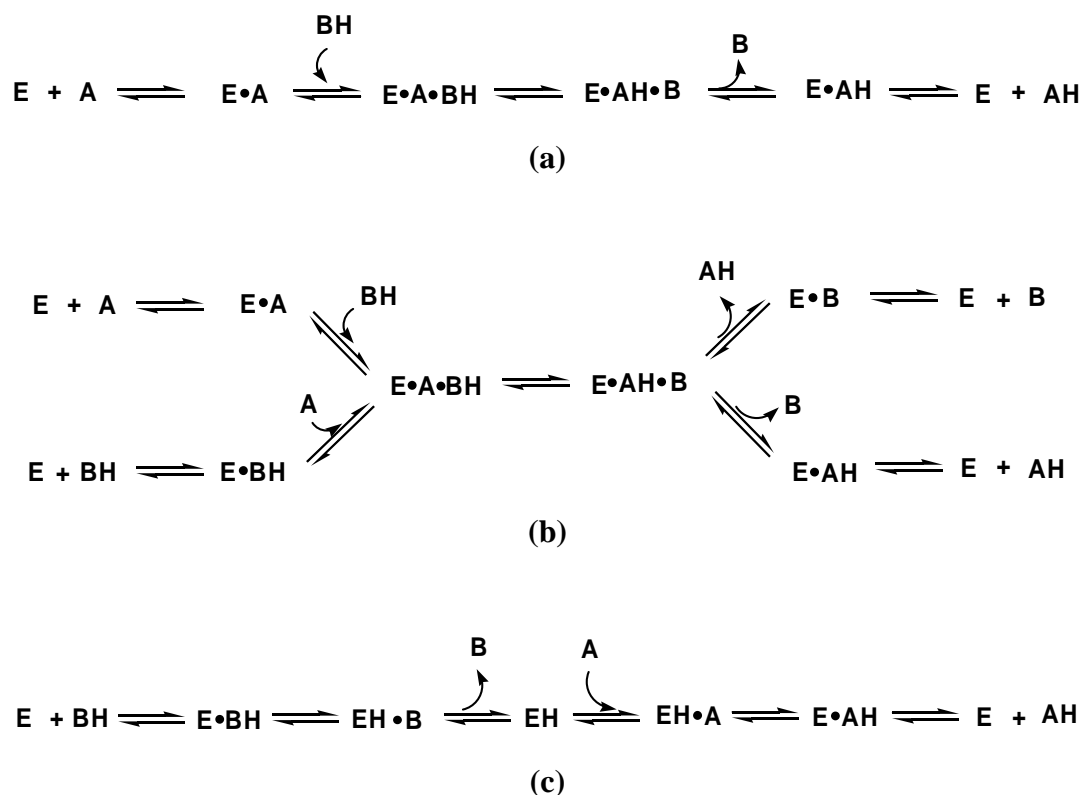
	Double reciprocal plot	Dixon plot	Cornish-Bowden plot
a			
b			
c			

1.4.5 Bi Bi mechanism

IDH requires NAD^+ and *myo*-inositol as its two substrates, and yields 2-keto-*myo*-inositol (also called as *scyllo*-inosose or inosose) and NADH as the two products. This enzymatic reaction is named as a Bi Bi reaction⁸², as shown in **Equation 1.2**,



in which A and BH represent substrates, AH and B represent products, and E represents an enzyme. This kind of reaction is classified into three mechanisms on the basis of the binding order of substrates and the release order of products, named as random ordered, compulsory ordered, and Ping-Pong Bi Bi mechanism (**Scheme 1.1**).



Scheme 1.1 The diagrams of Bi Bi mechanisms. a: compulsory ordered Bi Bi mechanism, b: random ordered Bi Bi mechanism, c: Ping-Pong Bi Bi mechanism.

Ordered and Ping-Pong Bi Bi mechanisms can be distinguished by double reciprocal plots. That is, the reaction velocity over a range of one substrate concentrations at several, fixed concentration of the other substrate and the resulting data is plotted as $1/v$ vs $1/[\text{substrate}]$. If the plots display a set of lines that converge to the left of the y axis, it means the reaction involves ternary complex formation, and follows an ordered Bi Bi mechanism. On the other hand, if the plots display a set of parallel lines, it means the reaction follows Ping-Pong Bi Bi mechanism. Unfortunately, it is not possible to further distinguish between compulsory and random ordered mechanism with the double reciprocal plot. Two methods, dead end inhibition and product inhibition, can be utilized to identify random ordered and compulsory ordered mechanism⁸². The patterns are summarized in **Table 1.3** and **Table 1.4**. By measuring the initial velocity of the reaction in the presence of several concentrations of competitive inhibitor or product, and varying the concentration of substrates A and BH, the reaction mechanism can be diagnosed by reference to the corresponding table.

The oxidation-reduction reaction catalyzed by *B. subtilis* IDH obeys a compulsory ordered Bi Bi mechanism, which was identified by product inhibition^{65,69}, in which NAD^+ binds first, and then inositol binds to form a ternary complex. After reaction, 2-keto-*myo*-inositol is released first, and NADH is the last one to be released (as shown in **Scheme 1.1a**, in which, E: IDH; A: NAD^+ ; BH: *myo*-inositol; B: 2-keto-*myo*-inositol; AH: NADH.).

Table 1.3 Pattern of product inhibition observed for Equation 1.2 for differing kinetic mechanisms.

Bi Bi mechanism	Product used as inhibitor	Varied [BH]		Varied [A]	
		Unsaturated [A]	Saturated [A]	Unsaturated [BH]	Saturated [BH]
Compulsory ordered with BH binding first	B	Mixed	Uncompetitive	Mixed	Mixed
Compulsory ordered with BH binding first	AH	Competitive	Competitive	Mixed	No inhibition
Compulsory ordered with A binding first	B	Mixed	No inhibition	Competitive	Competitive
Compulsory ordered with A binding first	AH	Mixed	Mixed	Mixed	Uncompetitive
Random ordered	B	Competitive	No inhibition	Competitive	No inhibition
Random ordered	AH	Competitive	No inhibition	Competitive	No inhibition
Ping-Pong	B	Mixed	No inhibition	Competitive	Competitive
Ping-Pong	AH	Competitive	Competitive	Mixed	No inhibition

Table 1.4 Pattern of dead-end inhibition observed for Equation 1.2 for differing kinetic mechanisms.

Bi Bi mechanism	Competitive inhibitor for substrate	Varied [BH]	Varied [A]
Compulsory ordered with BH binding first	BH	Competitive	Mixed
Compulsory ordered with BH binding first	A	Uncompetitive	Competitive
Compulsory ordered with A binding first	BH	Competitive	Uncompetitive
Compulsory ordered with A binding first	A	Mixed	Competitive
Random ordered	BH	Competitive	Mixed
Random ordered	A	Mixed	Competitive
Ping-Pong	BH	Competitive	Uncompetitive
Ping-Pong	A	Uncompetitive	Competitive

1.4.6 Catalytic residues identification

Daniellou⁷⁸ constructed a homology model of IDH which is mentioned in **1.4.2**. On the basis of the sequence alignment of IDH and GFOR (**Figure 1.11**), the residues His176 and Asp172 of IDH, corresponding to the catalytic residues Tyr269 and Asp265 of GFOR, were proposed as a catalytic dyad. His176 is the acid/base involved in proton transfer with the axial hydroxyl group of *myo*-inositol and Asp172 likely participates in this reaction in a secondary manner, as shown in **Figure 1.16**. The fact that mutant H176A leads to a 2000-fold decrease and mutant D172N leads to 5-fold decrease in activity strongly supports the catalytic dyad proposal⁷⁸. A similar catalytic mechanism has been proposed for other dehydrogenases, such as glucose 6-phosphate dehydrogenase⁸⁴ and 1,5-anhydro-D-fructose reductase⁸⁵.

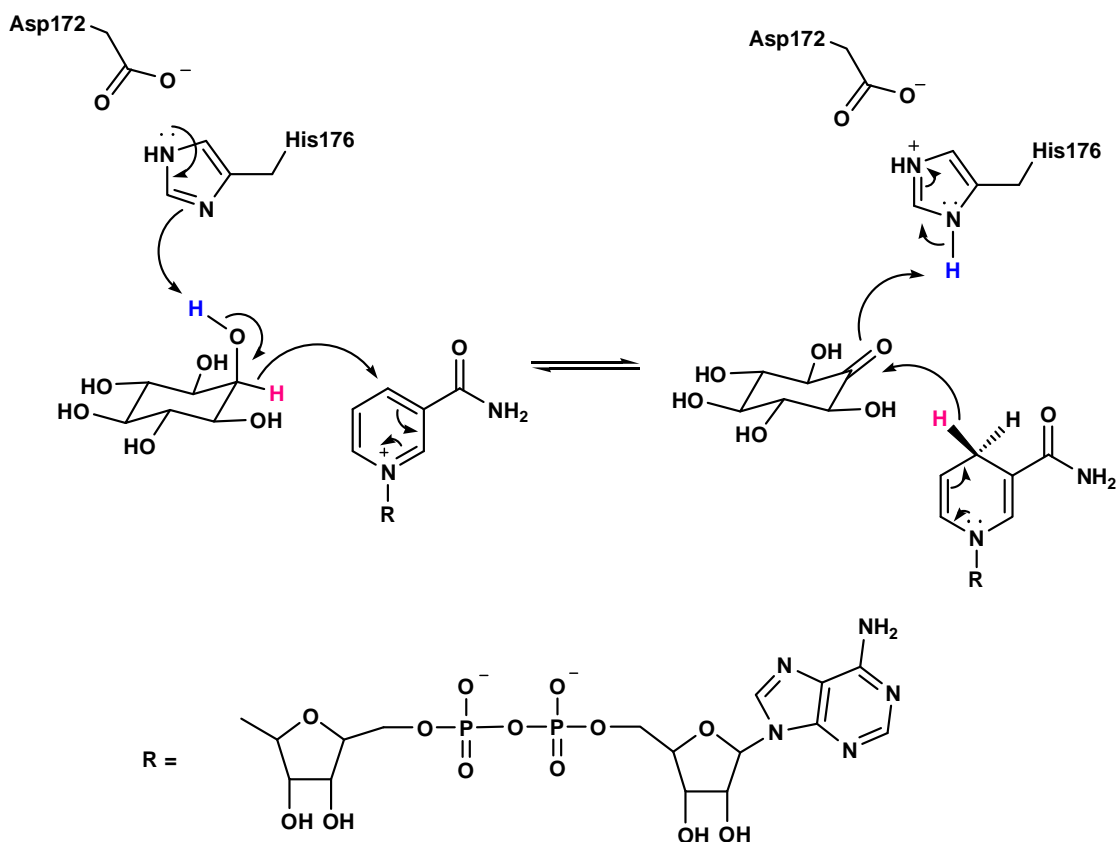


Figure 1.16 The proposed catalytic mechanism of IDH.

The chirality of hydride transferred was assigned based on the IDH homology model docked with NADH, in which the proposed inositol active site exits in the *re* face of NAD^+ . The hydride transferred from inositol was assumed to attack from the *re* face of the nicotinamide ring of NAD^+ , thus the hydride occupies the *pro-R* position of NADH. This hypothesis is consistent with the two facts: first, Alizade *et al* reported the same stereospecific transfer in *myo*-inositol dehydrogenase from *Klebsiella pneumoniae* which was measured by the assay using $[4\text{-}^3\text{H}]\text{-NAD}^+$ and *myo*-inositol dehydrogenase coupled with glutamate dehydrogenase⁸⁶; Second, *pro-R* hydride is transferred in GFOR and the motif EKP that orient nicotinamide ring of NADP^+ binding in GFOR is conserved in IDH.

1.5 Objectives of research

When I started the work in 2004, *B. subtilis* IDH gene *iolG* had been cloned into pET-28b (+) in this laboratory. The recombinant protein had been overexpressed⁶⁹. At that time, little was known on this enzyme other than substrate specificity and kinetic mechanism^{65,69}.

The aim of this research is to: (1) investigate the reaction mechanism, (2) broaden the substrate specificity, (3) study the inhibition property, (4) alter coenzyme/substrate specificity, and (5) probe the inositol-IDH interactions. Multiple approaches were undertaken by utilizing a combination of techniques in molecular biology, enzymology, and organic chemistry.

To begin with, the designed inositol analogues/derivatives were synthesized as proposed inhibitors/substrates of IDH since they were not commercially available. Once these compounds were obtained, research focused on characterizing inhibition property/dehydrogenase activity by steady-state kinetics.

In addition, mutagenesis experiments were carried out to attempt to alter the coenzyme specificity and probe inositol-binding site. Three methodologies were employed to predict the target amino acid residues including sequence alignment, structure alignment, structure-based engineering. Steady-state kinetics was employed to characterize the rationally designed mutants

2. MATERIALS AND METHODS

2.1 Reagents

QIAprep spin miniprep kit was purchased from Qiagen Inc. QuickChange site-directed mutagenesis kit and PfuUltra High-Fidelity DNA polymerase were purchased from Stratagene. Deoxynucleoside triphosphate (dNTP) mix (10 mM each) was purchased from Fermentas. DNA primers used for polymerase chain reactions (PCR) were synthesized by Integrated DNA Technologies (IDT). The restriction digestion enzymes used in mutagenesis and NDA analysis were purchased from New England Biolabs (NEB). Peptone, yeast extract, and agar were purchased from Becton, Dickinson and Company (BD). Prestained protein marker (7-175 kDa) and DNA ladder (1kb) were purchased from NEB. For kinetic studies, inositol analogues/derivatives were synthesized in this laboratory. All the other commercial available chemicals and solvents used in molecular biology, kinetic analysis, and chemical synthesis were purchased from Sigma-Aldrich Canada, VWR CanLab, or Tokyo Chemical Industry (TCI) and were used without further purification unless otherwise stated.

2.2 Instrumentation

Distilled, deionized water (ddH₂O) was purified by the nanopure diamond ultrapure water systems. All the sterile reagents were prepared using a VWR AccuSterilizer AS12. The Innova 4230 refrigerated incubator shaker and Innova 43 Large-Capacity Incubator Shaker were used to incubate bacterial cultures. The Beckman-Counter microfuge 18 and 22R centrifuges and the Beckman J2-HS centrifuge with JLA-10.500 and JA-25.50 rotors were used for DNA purification, cell harvesting, and protein preparation. Virsonic 600 ultrasonic cell disrupter was used for crude protein preparation. HiTrap Chelating HP columns purchased from GE Healthcare were used for protein purification. The BioCAD® Sprint Perfusion Chromatography system was used for large scale protein purifications. Spectra/Por 7 (MWCO: 25 kD) protein dialysis membrane was purchased from Spectrum Laboratories, Inc. BIO-RAD mini-protean 3 and sodium dodecyl sulphate-polyacrylamide gel electrophoresis (10% SDS-PAGE, stained with Coomassie blue) were used for protein analysis. BIO-RAD sub-cell GT agarose gel electrophoresis system and 1% agarose gel (visualized by ethidium bromide) were used for DNA electrophoresis. A Nanodrop ND-1000 spectrophotometer was used to measure DNA concentrations. Gene amplifications were performed using an Eppendorf gradient thermocycler Polymerase chain reaction machine. Water bath purchased from Sheldon manufacturing was used to maintain restriction digestion temperature. DNA sequencing reactions were performed at the DNA Technologies Unit, National Research Council (NRC), Plant Biotechnology Institute (PBI), Saskatoon. Spectrophotometric assays were performed with a Beckman DU 640 spectrophotometer with a circulating-bath-controlled temperature block.

Thin layer chromatography (TLC) was performed on Merck precoated Kieselgel 60F₂₅₄ silica gel plates (0.25 mm thickness) and visualized by ultraviolet light with radiation at 254 nm. If necessary, TLC plates were further developed with phosphomolybdic acid-ethanol reagent or 10% sulfuric acid in ethanol reagent followed by heating. Flash column chromatography was performed with Merck silica gel 60 (230-400 mesh). NMR spectra were collected with a Bruker 500 MHz spectrometer. Chemical shifts were reported on the δ scale in parts per million (ppm) and were referenced to the corresponding deuterated solvents. Melting points were measured on a Gallenkamp melting point apparatus and were uncorrected. Experiments that required anhydrous conditions were performed under an inert atmosphere of dry argon gas. Glassware was dried in the oven set at 120 °C and assembled under a stream of dry argon gas. The anhydrous solvents were dried by distillation under argon from an appropriate drying agent prior to use. For example, dry CH₂Cl₂, Et₂O were distilled over calcium hydride; dry toluene and THF were distilled over sodium and benzophenone; dry CCl₄ was dried over CaCl₂ and distilled.

2.3 Media and plates

Luria-Bertani (LB) medium was used to grow *E. coli* cells. One liter of LB medium contained 10 g of peptone, 5 g of yeast extract and 10 g of NaCl and the pH was adjusted to 7.5. After autoclaving, the media was stored at 4 °C.

LB plates were prepared with the same components as well as 15 g/L agar. When the autoclaved medium cooled down to about 60 °C, kanamycin was added as the antibiotic (final concentration was 50 µg/mL). The sufficiently mixed medium was poured into the sterile plates. These plates were stored at 4 °C after cooling down to room temperature.

2.4 Plasmids, bacterial strains and growth conditions

The gene *iolG* from operon *iolABCDEFGHIIJ* in *Bacillus subtilis* was cloned into pET-28b previously in this laboratory⁶⁹. All the *iolG* mutants were generated using wild-type recombinant plasmid as their template during polymerase chain reactions, in the other words, mutated *iolG* genes were also housed in pET-28b. *E. coli* XL1-Blue and BL21-Gold (DE3) were used as the host strain for the mutated plasmid construction and protein expression respectively. The *E. coli* strains harbouring the corresponding plasmids were routinely grown in LB medium with 50 µg/ml kanamycin at 37°C.

2.5 Molecular biology techniques

2.5.1 DNA isolation and purification

LB medium (5 mL) containing 50 µg/ml kanamycin was inoculated with a colony from XL1-Blue plate and grown overnight. The resulting pellets were harvested by centrifugation. The plasmid DNA was isolated by QIAprep miniprep kit following the manufacturer's protocol. The procedure is based on the alkaline lysis of bacterial cells followed by adsorption of DNA onto silica gel in the presence of high concentration of salt. The concentration of a DNA sample was measured using a nanodrop spectrophotometer based on the absorption at 260 nm.

2.5.2 Polymerase chain reaction (PCR)

Standard PCR methodology⁸⁷ was used in mutagenesis. The 50 μ L reactions were performed, which included: 40 μ L of sterile dd H₂O; 5 μ L of 10 \times PCR reaction buffer (200 mM Tris-HCl, pH 8.8; 100 mM KCl; 100 mM (NH₄)₂SO₄; 20 mM MgSO₄; 1% Triton X-100; 1 mg/mL BSA); 1 μ L of DNA template (30-50 ng/ μ L); 1.5 μ L of forward primer (100 ng/ μ L); 1.5 μ L of reversed primer (100 ng/ μ L); 1 μ L of dNTP (10 mM of dATP, dTTP, dCTP, dGTP); and 1 μ L of DNA polymerase. The thermocycler program was as follows: **1.** denaturation at 95°C for 30 seconds; **2.** annealing at 55°C or 53°C for 1 minute; **3.** extension at 72°C (PfuUltra High-Fidelity DNA polymerase) or 68°C (PfuTurbo DNA polymerase) for 13 minutes. **4.** repeating 17 cycles from **1** to **3**; **5.** final extension at 72°C or 68°C for 10 minutes. In the temperature program, double stranded DNA template was denatured to single stranded DNA. Short complementary piece of DNA (the primers) annealed to the complementary sequence of the single stranded fragments of DNA (template) upon coding. The 3'-end of the primers were used by DNA polymerase to synthesize a new DNA strand in the extension part.

2.5.3 Site-directed mutagenesis

The QuikChange Site-Directed Mutagenesis Kit was first used for introducing specific mutations. And then PfuUltra High-Fidelity DNA polymerase, dNTP mix, and Dpn1 restriction enzyme were bought separately. Complementary primers were designed with the mutated nucleotides in the middle region, and appropriate GC content (GC%) and melting temperature (T_m). All of the primers used are listed in **Table 2.1**. The oligonucleotide primers, each complementary to opposite strands of the template, were extended during thermocycler of PCR. The amplification product was then digested at

37°C with restriction enzyme Dpn1 which is specific for methylated and hemimethylated DNA and is used to digest the parental DNA template. This digestion did not affect the synthesized DNA containing the mutation. The more details about mechanism and procedure of this mutagenesis can be found in QuickChange Site-Directed Mutagenesis Kit instruction manual. After digestion, the nicked DNA containing the desired mutations was transformed into XL1-Blue competent cells for propagation. The QIAprep Miniprep kit was used for purification of the plasmid DNA. For the mutants with restriction sites designed in the primers, restriction analysis was performed on the plasmids with corresponding restriction enzymes.

Table 2.1 Primers used in site-directed mutagenesis. wt: wild-type; For each mutant, the first primer is forward, and the second primer is reverse. Red italic bases are mutated sites, bases underlined are restriction sites (some are created with silent mutations). Italic letters in red are mutated sites; Underlined letters are restriction sites.

Primers	Sequence (5' to 3')	Template	Substitution	Restriction enzyme
Y233F	GTCATCAATGCTGAAATCTATGT <u>TA</u> ACTGTAAATTCGGCTATGAC GTCATAGCCG <u>A</u> ATTACAGTT <u>A</u> ACATAGATTTCAGCATTGATGAC	wt IDH	G687T, A698T	HpaI
Y235F	GCTGAAATCTATGT <u>TA</u> ACTGTAAATACGGCTTTGACATTCAATGTG CACATTGAATGTCA <u>A</u> AGCCGTATTACAGTT <u>A</u> ACATAGATTTCAGC	wt IDH	G687T, A704T	HpaI
Y233R	CGTCATCAATGCTGAAATCTATGT <u>TA</u> ACTGTAAA <u>CG</u> CGGCTATGAC GTCATAGCCG <u>CG</u> TTTACAGTT <u>A</u> ACATAGATTTCAGCATTGATGACG	wt IDH	G687T, TA697CG	HpaI
Y235R	GTGAACTGTAAATACGGC <u>CG</u> TGACATTCAATGTGAAATC GATTCACATTGAATGTCA <u>CG</u> GCCGTATTACAGTTCAC	wt IDH	TA703CG	EaeI
M126A	<u>GCCTTGTTCA</u> <u>GG</u> TCGGCTTC <u>CG</u> CGCGCCGTTATGAC GTCATAACGGCGC <u>G</u> GAAGCCGAC <u>CTGAACAAGGC</u>	wt IDH	A366G AT376GC	ECoN1
M126S	<u>GCCTTGTTCA</u> <u>GG</u> TCGGCTTC <u>TC</u> CGCGCCGTTATGAC GTCATAACGGCGC <u>G</u> GAAGCCGAC <u>CTGAACAAGGC</u>	wt IDH	A366G, AT376TC	ECoN1
D35S	CGGAAATTGTAGCTGTAACGT <u>CTGT</u> TAA <u>C</u> CAAGAAGCTGC GCAGCTTCTTG <u>GTTAACA</u> <u>G</u> ACGTTACAGCTACAATTTCCG	wt IDH	GA103TC, T111C	HpaI

D179N	CGCTTGTTTCATGAAATT <u>AACGT</u> <u>T</u> CTCCACTGGC GCCAGTGGAG <u>AACGT</u> <u>T</u> AATTTTCATGAACAAGCG	wt IDH	G535A, G540T	Acl1
G14A	GGAAC TGGAG <u>C</u> GATCG <u>C</u> AAAAGAACATATTAACCG CGGTTAATATGTTCTTTT <u>G</u> CGAT <u>C</u> GCTCCAGTTCC	wt IDH	A36G, G41C	ASiS1
G14A/D35S	GGAAC TGGAG <u>C</u> GATCG <u>C</u> AAAAGAACATATTAACCG CGGTTAATATGTTCTTTT <u>G</u> CGAT <u>C</u> GCTCCAGTTCC	D35S	A36G, G41C	ASiS1
Y233F/Y235F	CTGTAAATTCGGCT <u>T</u> TGACATTCAATGTG CACATTGAATGTCA <u>A</u> AGCCGAATTTACAG	Y233F	A704T	
Y280F	GCTTTGTCGCTGCGT <u>T</u> TGATGTGGAAATCC GGATTTCCACATCA <u>A</u> ACGCAGCGACAAAGC	wt IDH	A839T	
W272A	GCACTGATATTTTGATGGAT <u>GC</u> GCAGAGACGCTTTGTCGC GCGACAAAGCGTCTCTGC <u>GC</u> ATCCATCAAAATATCAGTGC	wt IDH	TG814GC	
W272H	CACTGATATTTTGATGGAT <u>CAC</u> CAGAGACGCTTTGTCGCTGC GCAGCGACAAAGCGTCTCTG <u>GTG</u> ATCCATCAAAATATCAGTG	wt IDH	TGG814CAC	
K97V	CAGAAATATGTGTTCTGTGAA <u>GT</u> ACCGCTCGCGACAACGGC GCCGTTGTCGCGAGCGGT <u>ACT</u> TCACAGAACACATATTTCTG	wt IDH	AA289GT	

K97Q	GAAATATGTGTTCTGTGAA CA ACCGCTCGCGACAACGGC GCCGTTGTCGCGAGCGGTT GT TCACAGAACACATATTTC	wt IDH	A289C
K97R	GAAATATGTGTTCTGTGAAA G ACCGCTCGCGACAACGGC GCCGTTGTCGCGAGCGGT CT TCACAGAACACATATTTC	wt IDH	A290G
N157R	CACTGCGCGCACCGC CG CCCGACTGTAGGAG CTCCTACAGTCGGG CG GCGGTGCGCGCAGTG	wt IDH	AA469CG
N157S	CTGCGCGCACCGCA G CCCGACTGTAGGAG CTCCTACAGTCGGG CT GCGGTGCGCGCAG	wt IDH	A470G
H155K	CTCTTATGATTCACTGCGCG AAG CGCAACCCGACTGTAGGAG CTCCTACAGTCGGGTTGCG CTT CGCGCAGTGAATCATAAGAG	wt IDH	CAC463AAG
H155F	CTCTTATGATTCACTGCGCG TT CCGCAACCCGACTGTAGG CCTACAGTCGGGTTGCGG AA CGCGCAGTGAATCATAAGAG	wt IDH	CA 463TT
G11K/D35S	GGCGTAATTGGA AA AGCAATCGGAAAAGAAC GTTCTTTTCCGATTGC TT AGTTCCAATTACGCC	D35S	GG31AA
D35S/V36R	GTAGCTGTAACGTCT CG TAATCAAGAAGCTGCAC GTGCAGCTTCTTGATT AG AGACGTTACAGCTAC	D35S	GT106CG

G11K/D35S/V	GGCGTAATTGGAAC TA AGCAATCGGAAAAGAAC	D35S/V36R	GG31AA
36R	GTTCTTTTCCGATTGC TT AGTTCCAATTACGCC		
A12K/D35S	GGCGTAATTGGAAC TGA AAATCGGAAAAGAAC	D35S	GC34AA
	GTTCTTTTCCGATT TT TCCAGTTCCAATTACGCC		
A12K/D35S/V	GGCGTAATTGGAAC TGA AAATCGGAAAAGAAC	D35S/V36R	GC34AA
36R	GTTCTTTTCCGATT TT TCCAGTTCCAATTACGCC		
D35S/A40K	CGTCTGTAAACCAAGAA AG GCACAAAAGGTCGTTGAGC	D35S	GCT118AAG
	GCTCAACGACCTTTTGTGC CT TTCTTGTTAACAGACG		
R259Q	GCCATCAAGCATCAGCTTG CA AAAAGAAGGCAGATTCAGC	wt IDH	AG775CA
	GCTGAATCTGCCTTCTTT TG CAAGCTGATGCTTGATGGC		
R156Q	GATTCAGTGC GCGCACC AG AACCCGACTGTAGGAG	wt IDH	GC467AG
	CTCCTACAGTCGGGTT CT GGTGCGCGCAGTGAATC		
R259A	GCCATCAAGCATCAGCTTG GC AAAAGAAGGCAGATTCAGC	wt IDH	AG775GC
	GCTGAATCTGCCTTCTTT GC CAAGCTGATGCTTGATGGC		
R259E	GCCATCAAGCATCAGCTTG GA AAAAGAAGGCAGATTCAGC	wt IDH	AG775GA
	GCTGAATCTGCCTTCTTT TC CAAGCTGATGCTTGATGGC		

R259Y	GCCATCAAGCATCAGCTTG TAC AAAGAAGGCAGATTCAGC GCTGAATCTGCCTTCTTT GT ACAAGCTGATGCTTGATGGC	wt IDH	AGA775TAC
Y233R/R259A	GCCATCAAGCATCAGCTTG GC AAAAGAAGGCAGATTCAGC GCTGAATCTGCCTTCTTT GC CAAGCTGATGCTTGATGGC	Y233R	AG775GC
Y233R/R259E	GCCATCAAGCATCAGCTTG GA AAAAGAAGGCAGATTCAGC GCTGAATCTGCCTTCTTT TC CAAGCTGATGCTTGATGGC	Y233R	AG775GA
Y233R/R259Q	GCCATCAAGCATCAGCTTG CA AAAAGAAGGCAGATTCAGC GCTGAATCTGCCTTCTTT TG CAAGCTGATGCTTGATGGC	Y233R	AG775CA
Y233R/R259Y	GCCATCAAGCATCAGCTTG TAC AAAGAAGGCAGATTCAGC GCTGAATCTGCCTTCTTT GT ACAAGCTGATGCTTGATGGC	Y233R	AGA775TAC
D35S/V36R/A 40K	CGTCTCGTAATCAAGAA AAG GCACAAAAGGTCGTTGAG CTCAACGACCTTTTGTGC CTT TTCTTGATTACGAGACG	D35S/V36R	GCT118AAG
D35S/V36R/A 40R	CGTCTCGTAATCAAGAA CGT GCACAAAAGGTCGTTG CAACGACCTTTTGTGC ACG TTCTTGATTACGAGACG	D35S/V36R	GC118CG

2.5.4 Restriction digestions

Colonies visible on the plates were used to inoculate separate test tubes containing 5 mL of LB with kanamycin. These cultures were allowed to incubate overnight. Plasmids were extracted in the same manner as **2.5.1** and subjected to a corresponding digest [typically 8 μ L plasmid (about 400 ng), 1 μ L digest enzyme (500 units), 1 μ L digest buffer, 37°C, 1 h, or follow corresponding instruction]. The conditions were performed according to the instruction with the enzymes. The resulting mutant digests were loaded onto a 1% agarose gel along with digested wild-type IDH plasmid. The digests were electrophoresed at 110V and visualized with ethidium bromide under UV light. The expected results (shown in Appendix 1) were calculated on the basis of the restriction map generated with online program NEB cutter (<http://tools.neb.com/NEBcutter2/index.php>).

2.5.5 Transformation

The competent cells XL1-Blue or BL21-Gold were prepared using the CaCl_2 method¹⁵⁰. Competent cells were inoculated in 5 mL of LB medium containing 50 $\mu\text{g/mL}$ of tetracycline at 37°C overnight. Overnight culture (5 μL) was transferred to 50 mL of LB medium with 50 $\mu\text{g/mL}$ tetracycline. The culture was incubated at 37°C until the optical density (O.D.) at 595 nm reached 0.4, and then the cells were harvested by centrifugation. The pellet was resuspended in 20 mL of transformation buffer (25 mM Tris, 50 mM CaCl_2 , pH 7.5) and incubated on ice for 30 min. The resuspended cells were centrifuged again and the pellet was resuspended in 1 mL of transformation buffer. The resulting cells were aliquoted into 100 μL and were ready

to perform transformation. The unused competent cell aliquots were supplemented with glycerol (final concentration: 15%) and were stored at -80°C.

Competent cells (100 µL) were transferred into a pre-chilled 14 mL Falcon polypropylene round bottom tube. Plasmid (1 µL) from Miniprep (2.5.1) or PCR (2.5.3) mixture was added and the solution was incubated on ice for 30 minutes. The tube was heat-shocked in a 42°C water bath for 45-60 seconds. After heat shock, the solution was incubated on ice for 2 minutes and 1 mL of preheated LB medium without any antibiotics was added. The medium was incubated at 37°C with shaking at 250 rpm for 1 h. After incubation, 50-500 µL of the transformation mixture was spread on a LB agar plate with kanamycin. The plates were incubated at 37°C overnight to allow colonies grow.

2.6 Protein expression and purification

2.6.1 Overexpression of wild-type IDH and mutants

The *iolG* or mutated *iolG* pET-28b recombinant plasmids were isolated from XL1-Blue cells and transformed into BL21-Gold (DE3) cells which were used as the host for protein expression. The transformed cells were streaked on an agar plate with 50 µg/mL of kanamycin and incubated at 37°C overnight. A single colony picked from the plate was incubated in 5 mL of LB medium containing 50 µg/mL of kanamycin at 37°C overnight. 50 µL of the overnight culture was transferred into 50 mL of LB medium containing 50 µg/mL of kanamycin and kept shaking at 37°C at 250 rpm until OD₅₉₅ was about 0.5. The protein overexpression was induced by addition of isopropyl

β -D-thiogalactoside (IPTG, final concentration is 1 mM). After induction, the culture was incubated for three more hours. Cells were harvested by centrifugation and stored at -20°C for purification.

2.6.2 Purification of wild-type IDH and mutants

Proteins (wild-type IDH or mutants) were purified from the bacterial extracts by using a HiTrap chelating HP column. Frozen cell pellets (**2.6.1**) from 50 mL of LB medium were thawed on ice and resuspended in 2.5 mL of binding buffer (20 mM Tris, 500 mM NaCl, 5 mM imidazole, 10% glycerol, pH 7.9), then lysed by sonication for 4 × 20 s (2 s on and 3 s off) on ice with the sonicator setting at level 3. The supernatant was separated from cell debris by centrifugation for 10 minutes at 4°C and filtered through 0.45 μ m membrane. The supernatant was loaded onto the 1 mL HiTrap chelating HP column, which had been rinsed with 5 mL of charging buffer (50 mM NiSO₄, pH 4.0) and 3 mL of binding buffer. After the protein was loaded, the column was washed with 4 mL of binding buffer followed with 4 mL of washing buffer (20 mM Tris, 500 mM NaCl, 60 mM imidazole, 10% glycerol, pH 7.9). The protein was then eluted with 9 mL of eluting buffer (1:1 v/v of binding buffer and strip buffer). The column was stripped with 6 mL of strip buffer (100 mM EDTA, 500 mM NaCl, 20 mM Tris, 10% glycerol, pH 7.9). The purity of the resultant fraction of protein was verified by 10% SDS-PAGE⁸⁸ in which target protein exhibited a molecular weight of approximately 40 kDa. The pure protein was combined and dialyzed against 50 mM phosphate buffer (1 L), pH 6.5, containing 50% (v/v) glycerol and 0.1 mM DL-dithiothreitol (DTT), and stored at -20°C.

2.6.3 Protein concentration assay

The purified protein concentration was determined by absorbance assay at 280 nm. Due to the presence of aromatic amino acids, mainly tyrosine and tryptophan, protein in solution absorbs UV light at the wavelength of 280 nm. The extinction coefficient (ϵ) of a protein at 280 nm can be predicted based on its amino acid composition (<http://ca.expasy.org/tools/protparam.html>) although an extinction coefficient can be affected by other factors, like pH, temperature, and ionic strengths. According to the Beer-Lambert law, protein concentration could be calculated as $C = A_{280}/(\epsilon_{280} \text{ L})$. The protein solution was diluted two times to perform the same measurement, and the average concentration value is the final concentration used in kinetic studies.

2.7 Sequence analysis

Multiple sequence alignment was generated using ClustalW 2 multiple sequence alignment at EBI (<http://www.ebi.ac.uk/Tools/clustalw2/index.html>) utilizing default parameters (Gonnet scoring matrix, gap open penalty = 10, gap extension penalty = 0.2). When generating structural based sequence alignment, DaliLite Pairwise comparison of protein structures online programme (<http://www.ebi.ac.uk/Tools/dalilite/index.html>) was used to superimpose the structures of homologous enzymes, and then structural based sequence alignment was performed utilizing software SEQUOIA (<http://rotatingpenguin.com/sequoia/index.html>), which is used for the superposition of homologous protein atomic coordinates. The aligned sequences of both sequence alignment and structure based sequence alignment were visualized by using ESPript 2.2 (<http://esprict.ibcp.fr/ESPript/cgi-bin/ESPript.cgi>).

2.8 Kinetic assays

2.8.1 Kinetic measuring system

As mentioned in 1.4.1, the pH dependence of the reactions catalyzed by IDH was characterized in 1979 by Ramaley *et al*⁶⁵. Optimum activity for the oxidation reaction from *myo*-inositol to 2-keto-*myo*-inositol was observed at pH 9.5 in a 100 mM Tris-HCl buffer, and for the reverse reaction, the optimum activity was observed at pH 7.0 in HEPES buffer. All the kinetic assays in this dissertation were measured in the oxidation reaction, and 100 mM Tris-HCl at pH 9.0 was used as a reaction buffer.

Kinetic assays were performed in cuvettes with total reaction volume of 1 mL. Reaction progress was monitored spectrophotometrically at 340 nm by detecting the formation of NADH or NADPH ($\epsilon_{340} = 6220 \text{ M}^{-1} \text{ cm}^{-1}$) with measurements taken at 10/15-second intervals. The spectrophotometer was blanked using corresponding assay solution and then the reaction was initiated by adding either IDH or *myo*-inositol. The measured data from spectrophotometer was converted into a Microsoft Excel file using DU600/700 file utility software (version 1.0), and then generated absorbance *versus* time plots to calculate initial velocity.

2.8.2 Measurement of initial velocity

During the steady-state period the product concentration increases linearly with time. The rate of the appearance of product is called the initial velocity (v_0) of the reaction. The initial velocity phase typically persists for several seconds to several hundred seconds. This duration depends upon many factors, such as the equilibrium constant,

the fractional saturation of the enzyme with substrates and products, the buffering capacity of medium, and the concentration ratio of the least abundant substrate relative to the enzyme. A reliable initial velocity measurement is important for achieving a faithful analysis of an enzymatic reaction.

One set of kinetic experiments was used to explain the measurement of initial velocity. For example, when IDH, 0.5 mM of NAD^+ , and 80 mM of *myo*-inositol were mixed together in Tris-HCl buffer at pH 9.0, the accumulation of product (NADH) was measured at 340 nm over time. A graph of A_{340} versus time was obtained (**Figure 2.1**) and was used to calculate initial velocity. In this kind of graph, at very early time points, the product concentration increases linearly with time. At later time, the curve starts to level off. Eventually the concentration of product reaches a plateau and does not change with time. In **Figure 2.1**, first 90 seconds was almost linear and used to calculate the initial velocity using equation $v_0 = \text{slope}/(\epsilon \times l) = \Delta A_{340} \div (\Delta t \times \epsilon_{340} \times l)$, in which $\epsilon_{340} = 6220 \text{ M}^{-1}\text{cm}^{-1}$, $l = 1 \text{ cm}$, ΔA_{340} and Δt were measured, so $v_0 = 0.1654 \div (90 \text{ s} \times 6220 \text{ M}^{-1}\text{cm}^{-1} \times 1 \text{ cm}) = 2.955 \times 10^{-7} \text{ M}\cdot\text{s}^{-1} = 1.773 \times 10^{-5} \text{ M}\cdot\text{min}^{-1}$. Velocity was expressed in terms of molarity changes per unit time.

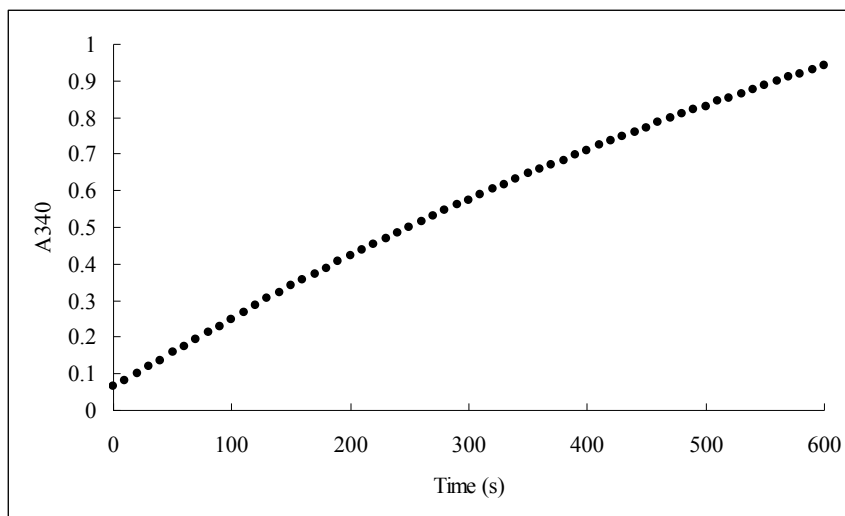
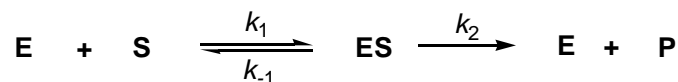


Figure 2.1 A sample of A_{340} vs time graph.

2.8.3 Apparent K_m (K_m^{app}) and k_{cat} determination



Scheme 2.1 A general scheme for one-substrate enzymatic reaction. E: enzyme; S: substrate; ES: the complex of enzyme and substrate; P: product; k_1 : association constants of ES; k_{-1} , k_2 : dissociation constants of ES.

In general, the single substrate enzyme catalyzed reaction or the reaction can be simplified as **Scheme 2.1**, the relationship between substrate concentration and reaction rate can be expressed by Michaelis-Menten equation:

$$v_0 = \frac{V_{max}[S]}{K_m + [S]}$$

in which, maximum velocity $V_{max} = k_2[E]$; Michaelis constant $K_m = (k_2 + k_{-1})/k_1$ and is equivalent to the substrate concentration at which V_0 is one-half of V_{max} . When k_2 is rate-limiting, $k_2 \ll k_{-1}$ and K_m reduces to k_{-1}/k_1 , which is defined as the dissociation constant. Therefore, K_m is an indication of the affinity of the enzyme with the substrate. The lower the K_m , the higher is the affinity.

IDH is a two-substrate enzyme, and K_m was measured when NAD^+ was saturated (50 mM, $K_m = 80 \mu\text{M}$), consequently, the resulting Michaelis constant was an apparent K_m (K_m^{app}). To measure K_m^{app} , initial velocities were calculated at varied concentrations (5, 10, 20, 40, 80, 160, 320 mM) of inositol and the data points ($[S]$ and v_0) were fitted to the Michaelis-Menten equation using Leonara software⁸³. A saturation curve was generated as shown in **Figure 2.2**, and K_m^{app} and V_{max} values were obtained.

The turnover number, k_{cat} , which defines how fast the enzymatic reaction takes place, represents the number of substrate molecules converted to product in a given unit of

time on a single enzyme molecule when the enzyme is saturated with substrate, is calculated by equation $k_{\text{cat}} = \frac{V_{\text{max}}}{[E]_0}$ (k_{cat} is equal to k_2 in Michaelis-Menten equation).

The ratio k_{cat}/K_m , the specificity constant, a second order rate constant, is a measure of how good the enzyme is at its catalysis. A high specificity constant means a reaction goes fast (k_{cat} is high) and the enzyme does not need a high concentration of the substrate (K_m is small). From the free energy point of view, the specificity constant relates to the activation energy ($\Delta G_{\text{ES}}^\ddagger$). When the enzyme can catalyze different substrates, the substrate demonstrates highest specificity constant is the preferred substrate for the enzyme. The top value range for this value is 10^8 - $10^9 \text{ M}^{-1}\text{s}^{-1}$ due to the diffusion limit.

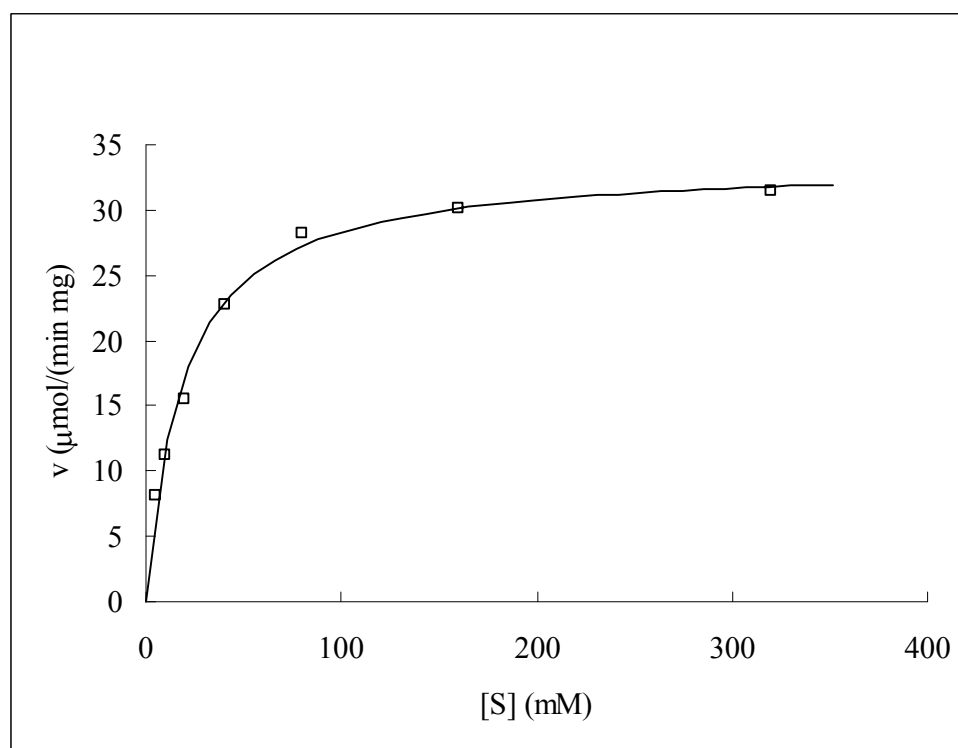


Figure 2.2 A saturation curve in which the velocity increases with the increase of substrate concentration until approaches a maximum velocity V_{max} . Empty square (\square) represents measured data points. $K_m^{\text{app}} = 19 \text{ mM}$; $V_{\text{max}} = 34 \text{ } \mu\text{mol} \cdot \text{min}^{-1} \cdot \text{mg}^{-1}$.

2.8.4 IC₅₀ and K_i determination

Inositol analogues were designed as the potential competitive inhibitors, which competed with inositol for active site to form an EI complex but without leading to products. In the presence of a competitive inhibitor, V_{\max} can still be reached if sufficient substrate is available; one-half V_{\max} requires a higher [S] than in the absence of inhibitor and thus V_{\max} is same as before and K_m^{app} is larger.

When a competitive inhibitor is present in the enzymatic reaction, the Michaelis-Menten equation becomes,

$$v_i = \frac{V_{\max}[S]}{K_m \left(1 + \frac{[I]}{K_i} \right) + [S]}$$

In which, v_i is initial velocity in the presence of an inhibitor; [I] is the concentration of inhibitor; K_i is dissociation constant of complex EI.

IC₅₀ represents the inhibitor concentration at which 50% enzyme activity is inhibited, so when [I] = IC₅₀, $v_i = \frac{1}{2} v_0$, after rearrangement,

$$K_i = \frac{IC_{50}}{1 + \frac{[S]}{K_m}} \quad \text{Equation 2.1}$$

since [S] is fixed during the kinetic assay and K_m can be measured as mentioned in

2.7.3. If IC₅₀ is known, K_i can be calculated using **Equation 2.1**⁸⁹.

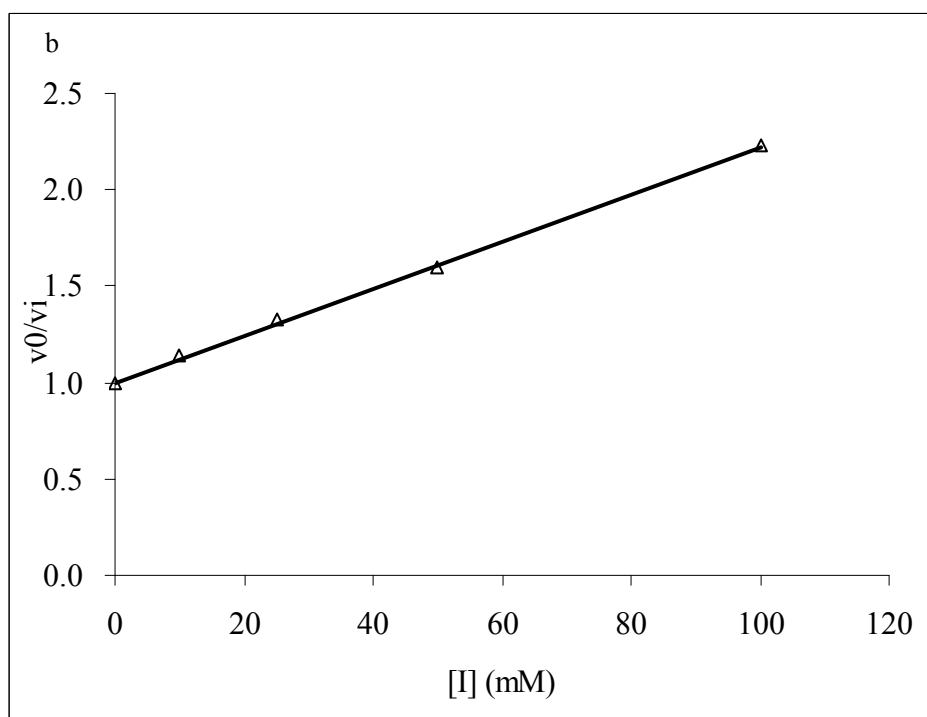
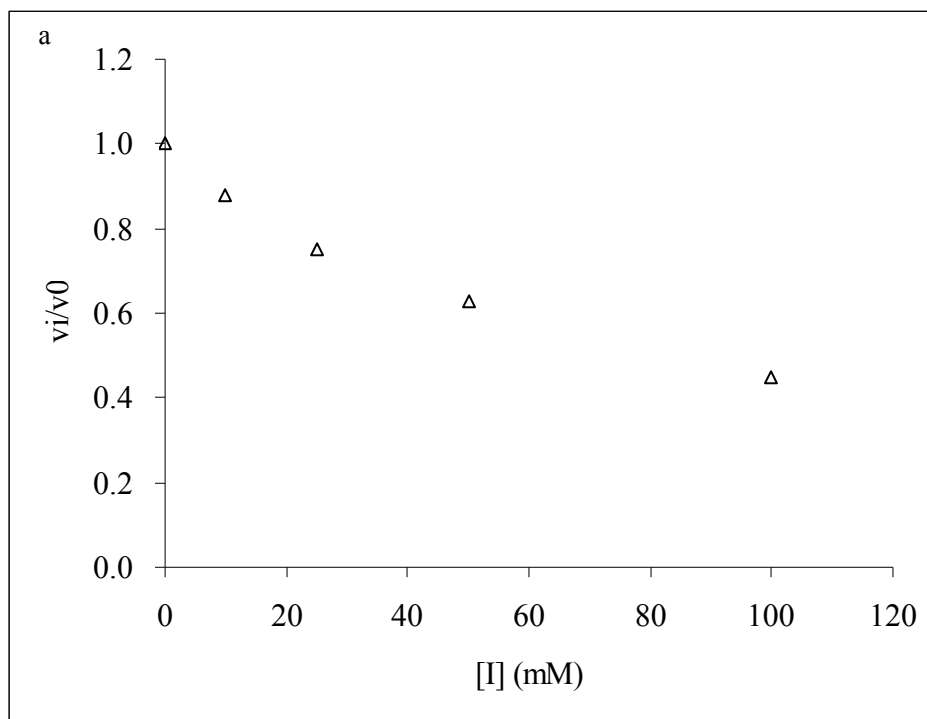


Figure 2.3 Inhibitory property plots of 2-deoxy-2,2-difluoro-*myo*-inositol. a) v_i/v_0 vs $[I]$ plot. b) v_0/v_i vs $[I]$ plot. Empty triangle (Δ) represents the measured data points; $[I]$ represents the concentration of compound 2-deoxy-2,2-difluoro-*myo*-inositol.

In this dissertation, all the inhibition experiments were performed under the same conditions. The assay mixture contained about 2 $\mu\text{g/mL}$ of IDH, 0.5 mM of NAD^+ , 20 mM of *myo*-inositol and four to six varied concentrations of inhibitors in 100 mM Tris-HCl buffer at pH 9.0, and a total volume of 1 mL. The kinetic assays were performed at 25°C for 10 min. Before the oxidation reactions were initiated, inhibitors were incubated with IDH for 5 min at room temperature. The inhibitory properties were determined by measuring the initial velocities in the absence and in the presence of various concentrations of inhibitors with the fixed 20 mM inositol. An inhibitor 2-deoxy-2,2-difluoro-*myo*-inositol is used as an example here, 0, 10, 25, 50, 100 mM of 2-deoxy-2,2-difluoro-*myo*-inositol were incubated with IDH in the presence of 0.5 mM NAD^+ in Tris-HCl buffer for 5 min at room temperature, and then *myo*-inositol was added to initiate the reaction (final concentration was 20 mM) and the formation of NADH was monitored at 340 nm. After the calculation of initial velocities, inhibitory activity (v_i/v_0) was plotted against concentrations of inhibitor (**Figure 2.3 a**). IC_{50} was calculated by plotting reciprocal of inhibitory activity (v_0/v_i) against concentrations of the inhibitor (**Figure 2.3 b**). When $y = v_0/v_i = 2$, $x = [\text{I}] = \text{IC}_{50} = 82$ mM. According to **Equation 2.1**, $K_i = 82/(1 + 20/18) = 39$ mM.

2.8.5 K_m (*myo*-inositol) and K_m ($\text{NAD}^+/\text{NADP}^+$) determination

As mentioned in 1.4.5, the IDH catalyzed reaction follows a compulsory ordered Bi Bi mechanism, which is shown in **Scheme 1.1a**. The initial velocity equation of steady state for such kind of reaction is given in **Equation 2.2**⁸²

$$v = \frac{V_{\max}[A][BH]}{K_{iA}K_{mBH} + K_{mBH}[A] + K_{mA}[BH] + [A][BH]} \quad \text{Equation 2.2}$$

where $[A]$ is the concentration of the substrate that first binds (NAD^+), $[BH]$ is the concentration of the second substrate (*myo*-inositol), K_{iA} is the dissociation constant for $E \cdot A$ complex, K_{mA} and K_{mBH} are the respective Michaelis constants for the substrates A and BH, and V_{\max} is the maximum velocity when both substrates are in saturating condition.

In this dissertation, **Equation 2.2** was used to measure K_{mA} and K_{mBH} . For example, in the reaction catalyzed by IDH, Michaelis constants of two substrates NAD^+ and *myo*-inositol could be determined by a series of kinetic experiments. Initial velocities were measured over a range of concentrations of *myo*-inositol (10, 20, 40, 80, 120, 200 mM) at several fixed concentrations of NAD^+ (0.1, 0.3, 0.6, 1.0, 2.0 mM) in 100 mM Tris-HCl pH 9.0 at 25°C. These data points ($[\text{inositol}]$, $[\text{NAD}^+]$, v_0) were fitted to **Equation 2.2** using Leonora software⁸³ and the kinetic constants were determined ($K_{mA} = 0.075 \pm 0.007$ mM, $K_{mBH} = 4.36 \pm 0.48$ mM, and $V_{\max} = 86 \pm 1$ $\mu\text{mol} \cdot \text{min}^{-1} \cdot \text{mg}^{-1}$). The fitted graphs are shown in **Figure 2.4** and **Figure 2.5**. The catalytic constant k_{cat} and the specificity constant k_{cat}/K_m were calculated in the same way as mentioned in 2.8.3.

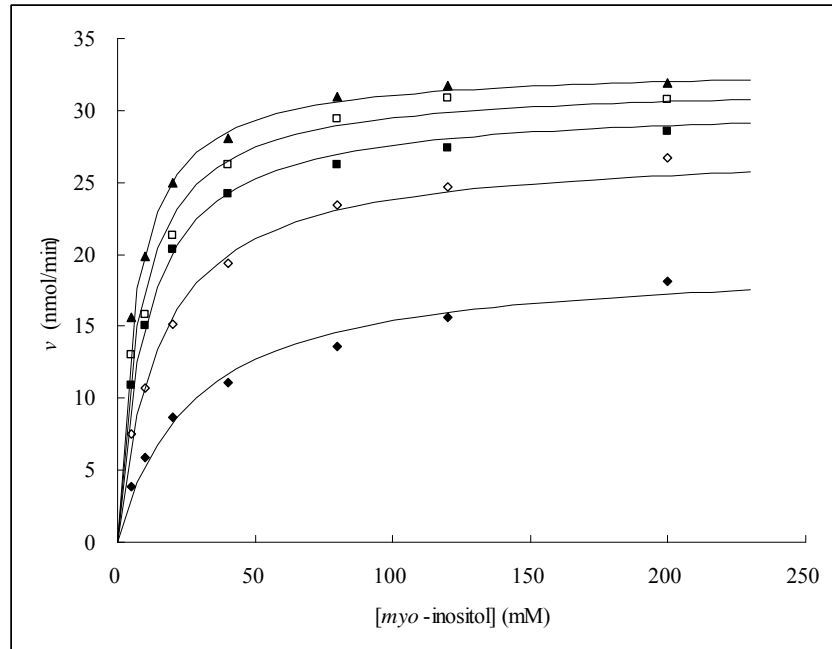


Figure 2.4 Plot of the variation of velocity with varying *myo*-inositol concentrations at constant NAD^+ concentrations: 0.1 mM (\blacklozenge), 0.3 mM (\diamond), 0.6 mM (\blacksquare), 1.0 mM (\square), 2.0 mM (\blacktriangle).

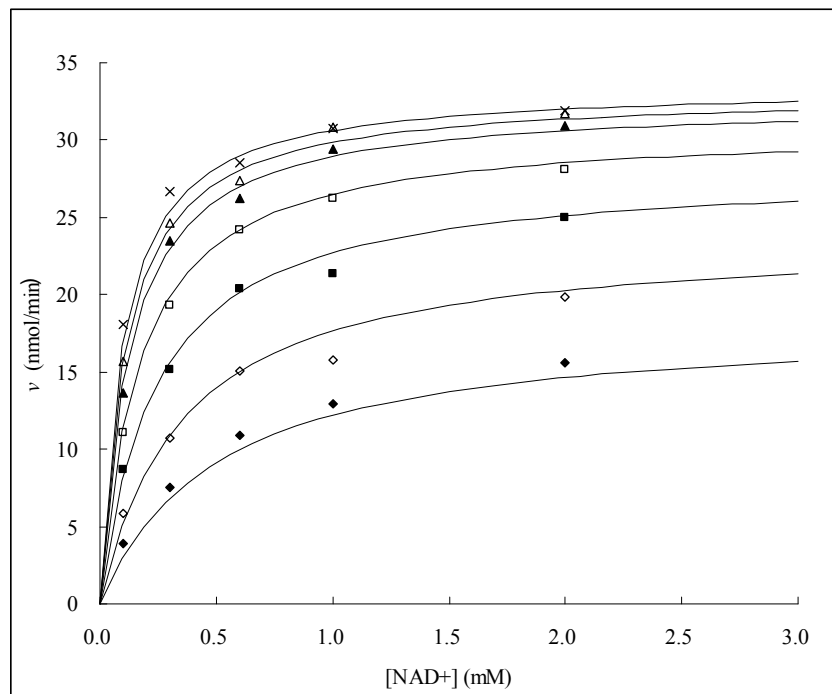
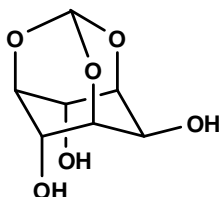


Figure 2.5 Plot of the variation of velocity with varying NAD^+ concentrations at constant *myo*-inositol concentrations: 5 mM (\blacklozenge), 10 mM (\diamond), 20 mM (\blacksquare), 40 mM (\square), 80 mM (\blacktriangle), 120 mM (\triangle), 200 mM (\times).

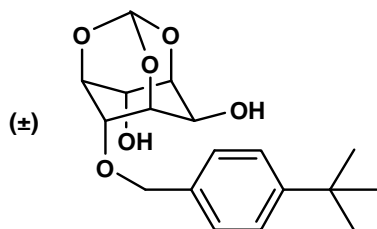
2.9 Chemical synthesis and compound characterization



***myo*-Inositol 1,3,5-monoorthoformate 5**

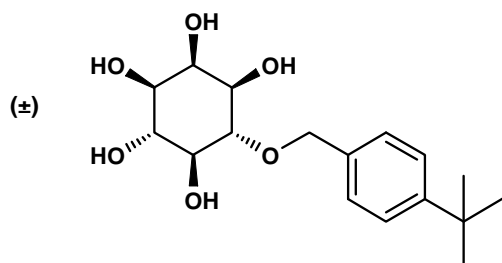
This compound was made as described in the literature⁹⁰.

¹H NMR (D₂O) δ 5.47(1H, s), 4.45 (2H, dd, J = 3.5 Hz), 4.20 (1H, m), 4.13 (1H, m), 4.10 (2H, m).

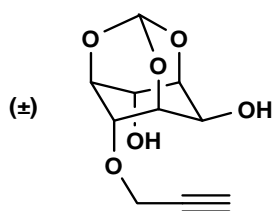


(±)-4-*O*-(4-*tert*-Butyl)benzyl-*myo*-inositol 1,3,5-monoorthoformate 7 To a solution of *myo*-inositol 1,3,5-monoorthoformate (2.0 g, 10.5 mmol) in 40 mL of DMF was added 0.42 g of NaH (60%). The suspension was stirred in ice-water bath for 15 min, and then 4-*tert*-butylbenzyl bromide (1.93 mL, 10.5 mmol) was added with syringe. The mixture was warmed to room temperature slowly and stirred overnight. After quenching and removing the solvent, the remaining syrup was partitioned between water and ethyl acetate. The organic layer was dried over MgSO₄ and the solvent was removed. The remaining was purified by FCC [ethyl acetate-toluene (2:3)], and the product (±)-4-*O*-(4-*tert*-butyl)benzyl-*myo*-inositol 1,3,5-monoorthoformate (2.74 g, 77%) was obtained as a white solid. ¹H NMR (CDCl₃) δ 7.40 (2H, d, J = 8.5 Hz), 7.24 (2H, d, J = 8.5 Hz), 5.45 (1H, s), 4.64 (2H, dd, J = 11.5 Hz), 4.48-4.42 (2H, m), 4.30-4.26 (2H, m), 4.22 (1H, m), 4.10 (1H, m), 1.33 (9H, s); ¹³C NMR (CDCl₃) δ

152.03, 132.75, 128.01, 125.85, 102.75, 74.77, 73.97, 72.85, 72.22, 67.89, 67.25, 60.74, 34.69, 31.03; Mass: 336.1567 (EI, MW, calc. 336.1573); m.p. 113-114°C.

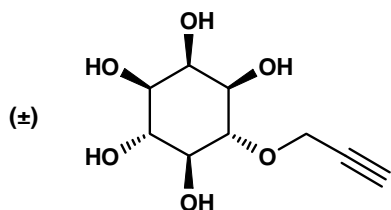


(±)-4-O-(4-*tert*-Butylbenzyl)-*myo*-inositol 2 To a solution of (±)-4-*O-tert*-butylbenzyl-*myo*-inositol 1,3,5-monoorthoformate (2.67 g, 7.95 mmol) in methanol (50 mL) was added Dowex 50X8 (H⁺, 200-400 mesh). The suspension was stirred overnight, and then filtered and washed by water. Methanol in the filtrate was removed by vacuum evaporation and then dried by freeze dryer. White solid (2.50 g, 97%) was obtained. ¹H NMR (CD₃OD) δ 7.39-7.35 (4H, m), 4.85-4.80 (2H, m), 3.94 (1H, dd, J = 2.5 Hz), 3.66-3.60 (2H, m), 3.48 (1H, dd, J = 10 Hz, 2.5 Hz), 3.34-3.27 (2H, m), 1.30 (9H, s); ¹³C NMR (D₂O) δ 150.15, 136.14, 127.76, 124.63, 81.75, 75.07, 74.50, 73.08, 73.05, 71.98, 71.89, 33.94, 30.42; Mass: 326.1727 (TOF, MW + HCO₂⁻, calc. 371.1706); m.p. 200-201°C.

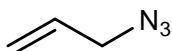


(±)-4-O-Propargyl-*myo*-inositol 1,3,5-monoorthoformate 8 To the solution of *myo*-inositol 1,3,5-monoorthoformate (2.0 g, 10.5 mmol) in 40 mL of DMF was

added NaH (0.42 g, 60%). The suspension was stirred in an ice-water bath for 15 min. Propargyl bromide in toluene solution (1.13 mL, ~ 10.5 mmol) was then added dropwise. The mixture was warmed to r.t. slowly and stirred overnight. After removing the solvent, the remaining syrup was partitioned between water and ethyl acetate. The organic layer was dried over MgSO₄ and the solvent was removed. The residue was purified by FCC [ethyl acetate-toluene (1:1)] to give a yellow oil (1.45 g, 60%). ¹H NMR (CDCl₃) δ 5.47 (1H, s), 4.56 (1H, m), 4.47 (1H, s), 4.36 (2H, m), 4.31 (2H, d, J = 2.5 Hz), 4.21 (1H, m), 4.06 (1H, s), 2.59 (1H, t, J = 2.5 Hz); ¹³C NMR (CDCl₃) δ 102.73, 77.91, 76.75, 74.75, 74.64, 72.10, 67.81, 67.39, 60.54, 58.51; Mass: 229.0715 (TOF, MW + H⁺, calc. 228.0634).



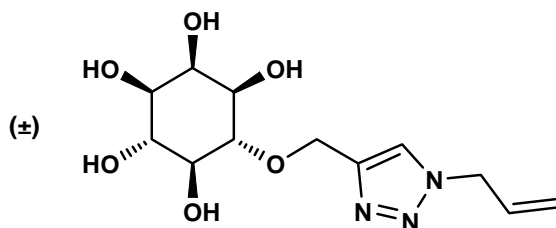
(±)-4-*O*-Propargyl-*myo*-inositol 3 To a solution of (±)-4-*O*-propargyl-*myo*-inositol 1,3,5-monoorthoformate (1.3 g, 5.7 mmol) in methanol (30 mL) was added Dowex 50X8 (H⁺, 200-400 mesh). The suspension was stirred overnight, and then filtered. Dowex was washed with water. The filtrate was concentrated and then dried by freeze drier. A white solid (1.0 g, 99%) was obtained. ¹H NMR (D₂O) δ 4.46 (2H, d, J = 2.5 Hz), 4.01 (1H, m), 3.63-3.56 (3H, m), 3.47 (1H, dd, J = 10 Hz, 2.5 Hz), 3.34-3.30 (1H, m), 2.85 (1H, t, J = 2.5 Hz); ¹³C NMR (D₂O) δ 83.21, 82.32, 78.31, 76.37, 74.84, 74.75, 73.49, 73.30, 62.34; Mass: 236.1130 (TOF, MW + NH₄⁺, calc. 236.1134); m.p. 156-157°C.



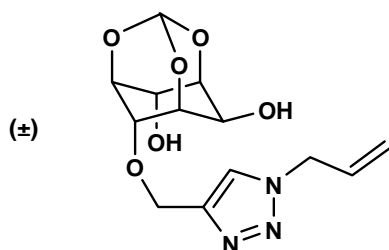
Allyl azide⁹¹

This compound was made as described in the literature.

¹H NMR (CDCl₃) δ 5.88 (1H, m), 5.31 (2H, m), 3.77 (2H, s).

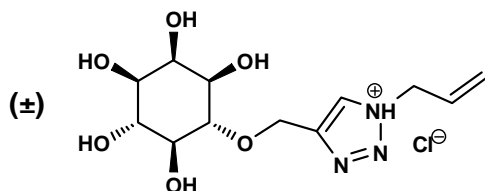


(±)-4-*O*-(1-Allyl-4-methylene-1,2,3-triazole)-*myo*-inositol 4 (±)-4-*O*-propargyl-*myo*-inositol (0.5 g, 2.3 mmol) and allyl azide (0.29 g, 3.5 mmol) were dissolved in THF (10 mL). While stirring, CuSO₄·5H₂O aqueous solution (5 mL, 5% mol) and sodium L-ascorbate aqueous solution (5 mL, 10% mol) were added. The reaction mixture was stirred at r. t. for 24 h, and then the solvent was evaporated. The yellow residue was purified by FCC [chloroform-methanol (3:1, v/v) with 5% triethylamine], (±)-4-*O*-(1-allyl-4-methylene-1,2,3-triazole)-*myo*-inositol (0.49 g, 71%) was obtained as a yellow solid. ¹H NMR (D₂O) δ 7.98 (1H, s), 6.01 (1H, ddt, *J* = 16.9 Hz, 10.5 Hz, 5.7 Hz), 5.28 (1H, d, *J* = 10.3 Hz), 5.15 (1H, d, *J* = 16.6 Hz), 4.98 (2H, d, *J* = 5.7 Hz), 4.87 (2H, dd, *J* = 14.5 Hz), 3.98 (1H, m), 3.58 (3H, m), 3.43 (1H, dd, *J* = 10 Hz, 2.8 Hz), 3.30 (1H, dd, *J* = 8.9 Hz); ¹³C NMR (D₂O) δ 131.7, 125.6, 119.8, 118.33, 81.7, 74.32, 72.79, 72.68, 71.38, 71.21, 65.35, 52.89; NOE difference spectrometry confirmed the 1,4-disubstituted triazole structure (*anti*). Irradiation of H₁ resulted in enhancement of H₂, H₃, H₄, H₅, H₆, and H₇. (Spectrum shown in Appendix 2); Mass: 300.1193 (TOF, MW-H, calc. 300.1196).



(±)-4-*O*-(1-Allyl-4-methylene-1,2,3-triazole)-*myo*-inositol 1,3,5-mono-orthoformate

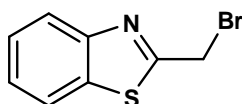
9 (±)-4-*O*-Propargyl-*myo*-inositol 1,3,5-monoorthoformate (2.16 g, 9.47 mmol) and allyl azide (1.18 g, 14.21 mmol) were dissolved in THF (30 mL). While stirring, CuSO₄·5H₂O aqueous solution (15 mL, 5% mol) and sodium L-ascorbate aqueous solution (15 mL, 10% mol) were added. The reaction mixture was stirred at r. t. for 24 h. The solvent was evaporated and the yellow residue was purified by FCC [chloroform-toluene (1:1) with 5% triethylamine], (±)-4-*O*-(1-allyl-4-methylene-1,2,3-triazole)-*myo*-inositol 1,3,5-monoorthoformate was obtained as light yellow oil (1.33 g, 45%). ¹H NMR (CDCl₃) δ 7.58 (1H, s), 6.01 (1H, ddt, J = 17 Hz, 10 Hz, 6 Hz), 5.44 (1H, s), 5.38 (1H, d, J = 10 Hz), 5.33 (1H, d, J = 17 Hz), 4.99 (2H, d, J = 5.7 Hz), 4.80 (2H, dd, J = 12 Hz), 4.51 (1H, m), 4.46 (1H, m), 4.29 (2H, m), 4.19 (1H, m), 4.05 (1H, d, J = 10.5 Hz); ¹³C NMR (CDCl₃) δ 143.41, 130.84, 122.64, 120.81, 102.74, 74.65, 74.61, 72.12, 67.84, 67.31, 63.85, 60.55, 52.93; Mass: 312.1205 (TOF, MW + H, calc. 312.1196).



(±)-4-*O*-(1-Allyl-4-methylene-1,2,3-triazole)-*myo*-inositol hydrochloride

4 To a solution of (±)-4-*O*-(1-allyl-4-methylene-1,2,3-triazole)-*myo*-inositol 1,3,5-monoorthoformate (1.30 g, 4.18 mmol) in methanol (30 mL) was added Dowex 50X8 (H⁺, 200-400 mesh). The suspension was stirred overnight, and then filtered. Dowex

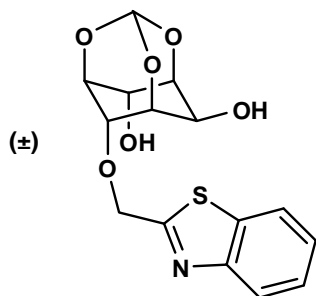
was washed with water. After evaporation, 90 mg (7%) of white solid was obtained. The resin was then washed with 1M HCl. The aqueous solution was evaporated to dryness. 0.99 g (76%) of (\pm)-4-*O*-(1-allyl-4-methylene-1,2,3-triazole)-*myo*-inositol hydrochloride was obtained as a white solid. ^1H NMR (D_2O) δ 7.97 (1H, s), 5.93 (1H, ddt, J = 17 Hz, 10 Hz, 6 Hz), 5.22 (1H, d, J = 10 Hz), 5.11 (1H, d, J = 17 Hz), 4.93 (2H, d, J = 6 Hz), 4.82 (2H, dd, J = 14.5 Hz), 3.90 (1H, dd, J = 2.3 Hz), 3.48 (3H, m), 3.35 (1H, dd, J = 10 Hz, 3 Hz), 3.24 (1H, m).



2-(Bromomethyl)benzothiazole

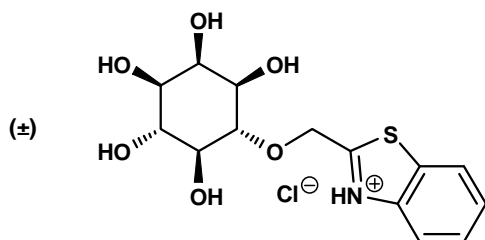
This compound was made as described in the literature⁹².

^1H NMR (CDCl_3) δ 8.02 (1H, d, J = 8.0 Hz), 7.87 (1H, d, J = 8.0 Hz), 7.50 (1H, dd, J = 8.0 Hz, 7.0 Hz), 7.42 (1H, dd, J = 8.0 Hz, 7.0 Hz), 4.81 (2H, s).

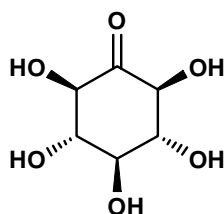


(\pm)-4-*O*-(2-Benzothiazolylmethoxy)-*myo*-inositol 1,3,5-monoorthoformate 6 To the solution of *myo*-inositol 1, 3, 5-monoorthoformate (1.10 g, 5.79 mmol) in 40 mL of DMF was added NaH (0.23 g, 60%). The suspension was stirred in an ice-water bath for 15 min, then 2-(bromomethyl)benzothiazole (1.32 g, 5.79 mmol) was added. The mixture was warmed to r. t. slowly and stirred overnight. After removing the

solvent, the remaining syrup was partitioned between water and ethyl acetate. The organic layer was dried over MgSO_4 , filtered, and concentrated to a residue that was purified by FCC [ethyl acetate-toluene (1:1, v/v)]. (\pm)-4-*O*-(2-benzothiazolylmethoxy)-*myo*-inositol 1,3,5-monoorthoformate (1.39 g, 71%) was obtained as a yellow solid. ^1H NMR (CDCl_3) δ 8.04 (1H, d, J = 8.5 Hz), 7.91 (1H, d, J = 8.0 Hz), 7.53 (1H, dd, J = 7.5 Hz, 7.0 Hz), 7.46 (1H, dd, J = 7.5 Hz, 7.0 Hz), 5.47 (1H, s), 5.13 (1H, d, J = 13.5 Hz), 5.06 (1H, d, J = 14.0 Hz), 4.58 (1H, m), 4.55 (1H, m), 4.42 (1H, m), 4.37 (1H, m), 4.25 (1H, m), 4.18 (1H, m); ^{13}C NMR (CDCl_3) δ 166.61, 152.74, 134.86, 126.67, 125.93, 123.44, 121.96, 102.78, 75.86, 74.60, 72.08, 70.06, 67.79, 67.50, 60.65; Mass: 338.0684 (TOF, MW + H, calc. 338.0698); m. p. 139-140°C.



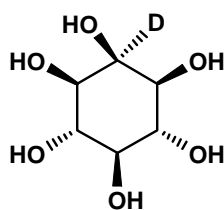
(\pm)-4-*O*-(2-Benzothiazolylmethoxy)-*myo*-inositol 1 To a solution of (\pm)-4-*O*-(2-benzothiazolylmethoxy)-*myo*-inositol 1,3,5-monoorthoformate (1.0 g, 2.97 mmol) in methanol (30 mL) was added Dowex 50X8 (H^+ , 200-400 mesh). The suspension was stirred overnight, and then filtered. The resin was then washed with 1M HCl. Methanol was evaporated and the aqueous solution was dried by freeze dryer. (\pm)-4-*O*-(2-Benzothiazolylmethoxy)-*myo*-inositol (0.50 g, 59%) was obtained as a white solid. ^1H NMR (D_2O) δ 7.89 (1H, d, J = 8.0 Hz), 7.78 (1H, d, J = 8.5 Hz), 7.47 (1H, dd, J = 7.5 Hz, 8.0 Hz), 7.39 (1H, dd, J = 7.5 Hz, 7.5 Hz), 5.17 (2H, s), 3.91 (1H, m), 3.59-3.58 (2H, m), 3.51 (1H, dd, J = 9.5 Hz, 9.5 Hz), 3.39-3.33 (2H, m); ^{13}C NMR (D_2O) δ 173.50, 147.60, 133.00, 127.50, 126.41, 122.65, 120.41, 83.11, 73.83, 72.38, 72.89, 70.87, 70.76, 70.32; Mass: 328.0847 (TOF, MW, calc. 328.0849); m. p. 113-115°C.



2-Keto-*myo*-inositol (*scyllo*-Inosose or Inosose)

This compound was made as described in the literature⁹³.

¹H NMR (D₂O) δ 4.3 (2H, d, J = 10.3 Hz), 3.7 (1H, dd, J = 9.4 Hz), 3.4-3.2 (2H, m).

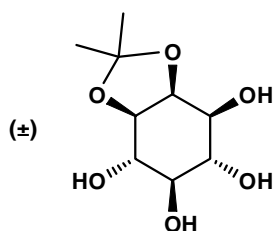


2-²H-*myo*-Inositol

This compound was made as described in the literature¹¹⁹ with modification. In a 100-mL round bottom flask containing 27 mL of ddH₂O, 2-keto-*myo*-inositol (0.53 g, 3.00 mmol) and NaBD₄ (0.30 g, 7.14 mmol) was added, and the reaction was allowed to stir at r. t. overnight. The reaction was quenched with 5 mL of acetone and stirred with Dowex 50X8 (H⁺, 200-400 mesh) for about 30 min to neutralize. After filtration and evaporation, 0.93 g of crude product was obtained as a solid.

Purification of 2-²H-*myo*-inositol 1) **acetylation of 2-²H-*myo*-inositol** Crude 2-²H-*myo*-inositol (1.7 g) was added into a mixture of 60 mL of Ac₂O and 25 mL of pyridine. The solution was heated at 100°C for 24 h, and then poured into ice and left overnight. The suspension was filtered, washed with water (15 mL), and then dried. The resulting filtrate was concentrated and the residue was purified by FCC [ethyl acetate-hexanes (1:1, v/v)]. The product (1.06 g total) as a white solid was obtained. ¹H NMR (CDCl₃) 5.51 (2H, dd, J = 10.3 Hz), 5.19 (1H, dd, J = 9.8 Hz), 5.10 (2H, d, J = 10.5 Hz), 2.22 (3H, s), 2.02 (15H, m).

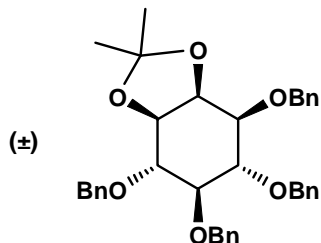
2) Deacetylation A mixture of inositol acetate (1.58 g, 3.65 mmol) in 40 mL of methanol was heated to boiling. NaOCH₃ (5 mL, 2 M solution) was added and heated to reflux for an additional 10 min, and then the solution was cooled to room temperature. A white solid was obtained by filtration. Since there was NaOCH₃ in the solid, it was redissolved in water and stirred with Dowex 50X8 (H⁺, 200-400 mesh) to neutralize. After filtration and evaporation, 2-²H-*myo*-inositol (0.65 g, 98%) was obtained as a white solid. ¹H NMR (D₂O) δ 3.51 (2H, dd, J = 9.8 Hz, 9.5 Hz), 3.41 (2H, d, J = 10.0 Hz), 3.16 (1H, dd, J = 9.3 Hz, 9.4 Hz); ²H NMR (H₂O) δ 4.3 (s); ¹³C NMR (D₂O) δ 74.73, 72.78, 72.13 (t, J = 22.4 Hz), 71.44; Mass: 204.0600 (TOF, MW + Na, calc. 204.0593).



(±)-1,2-*O*-Isopropylidene-*myo*-inositol 15

This compound was made as described in the literature⁹⁴.

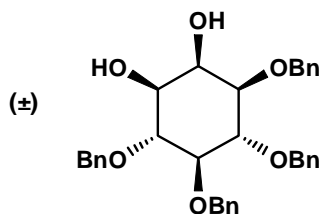
¹H NMR (D₂O) δ 1.31 (3H, s), 1.45 (3H, s), 3.18 (1H, ddd, J = 9.6 Hz, 9.6 Hz, 1.6 Hz), 3.48-3.58 (2H, m), 3.77 (1H, dd, J = 9.9 Hz, 4.2 Hz), 3.96-3.99 (1H, m), 4.40 (1H, dd, J = 4.6 Hz).



(±)-3,4,5,6-*O*-Tetrabenzyl-1,2-*O*-isopropylidene-*myo*-inositol 16

This compound was made as described in the literature⁹⁵.

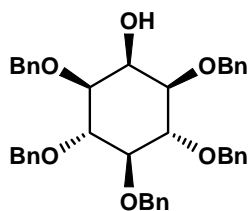
¹H NMR (CDCl₃), 1.39 (3H, s), 1.54 (3H, s), 3.45 (1H, dd, J = 9.0 Hz), 3.72 (1H, dd, J = 8.8 Hz, 3.8 Hz), 3.82 (1H, dd, J = 9.4 Hz, 6.9 Hz), 3.97 (1H, dd, J = 8.6 Hz), 4.13 (1H, dd, J = 6.2 Hz), 4.30 (1H, dd, J = 5.5 Hz, 4.0 Hz), 4.75-4.90 (8H, m), 7.28-7.40 (20H, m).



(±)-3,4,5,6-O-Tetrabenzyl-*myo*-inositol 17

This compound was made as described in the literature⁹⁵.

¹H NMR (CDCl₃), δ 3.48-3.52 (3H, m), 3.86 (1H, dd, J = 9.5 Hz), 3.99 (1H, dd, J = 9.5 Hz), 4.23 (1H, dd, J = 2.5 Hz), 4.71-4.98 (8H, m), 7.28-7.37 (20H, m).

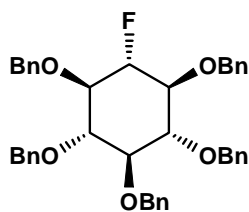


1,3,4,5,6-O-Pentabenzyl-*myo*-inositol 18

1) Preparation from (±)-3,4,5,6-O-tetrabenzyl-*myo*-inositol⁹⁶ A mixture of 3,4,5,6-O-tetrabenzyl-*myo*-inositol (5.4 g, 10 mmol), tetrabutylammonium bromide (3.54 g, 11 mmol), dibutyltin oxide (2.74 g, 11 mmol) and benzyl bromide (1.88 g, 15.8 mmol) was heated to reflux in 150 mL of acetonitrile for 24 h. The reaction mixture was cooled to room temperature. After removing the solvent, the remaining syrup was partitioned between water and ethyl acetate. The organic layer was separated and stirred with an aqueous solution of NaHCO₃ for 1 h, and then filtered

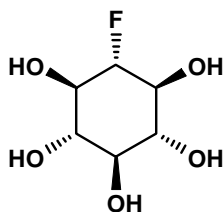
through celite and washed with ethyl acetate. The organic layer was dried over MgSO_4 , and then the solvent was removed. The solid was recrystallized from methanol to give white crystals (4.4 g). The remaining filtrate was purified by FCC [ethyl acetate-hexanes (1:5 to 1:3, v/v)]. Yellow solid (0.78 g) was afforded with total yield 82%.

2) Preparation from 1,2,3,4,5,6-*O*-hexabenzyl-*myo*-inositol⁹⁷ To a solution of 1,2,3,4,5,6-*O*-hexabenzyl-*myo*-inositol (6.0 g, 8.3 mmol) in dry dichloromethane (50 mL) was added tin chloride (8.3 mL, 8.3 mmol) dropwise at r. t. under argon. After the solution was stirred for 1 h, the reaction was quenched with water. The mixture was extracted with dichloromethane. FCC [ethyl acetate-hexanes (1:4 to 1:3, v/v)] gave 1,3,4,5,6-*O*-pentabenzyl-*myo*-inositol (2.1 g, 41%) as a light yellow solid. Starting material 1,2,3,4,5,6-*O*-hexabenzyl-*myo*-inositol (3.1 g 51%) was recovered. ^1H NMR (CDCl_3) δ 3.42 (2H, dd, $J = 9.7$ Hz, 2.6 Hz), 3.49 (1H, dd, $J = 9.4$ Hz), 4.04 (2H, dd, $J = 9.5$ Hz), 4.26 (1H, dd, $J = 2.6$ Hz), 4.71-4.77 (4H, m), 4.87-4.95 (6H, m), 7.28-7.37 (25H, m).



1,3,4,5,6-*O*-Pentabenzyl-2-deoxy-2-fluoro-*scyllo*-inositol 19

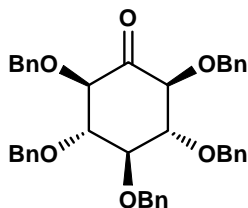
This compound was made as described in the literature^{98,99}. ^1H NMR (CDCl_3) δ 3.56-3.64 (3H, m), 3.69-3.75 (2H, m), 4.64 (1H, ddd, $J = 51$ Hz, 9 Hz, 9 Hz), 4.78-4.95 (10H, m), 7.33-7.43 (25H, m).



2-Deoxy-2-fluoro-*scyllo*-inositol 11

This compound was made as described in the literature¹⁰⁰.

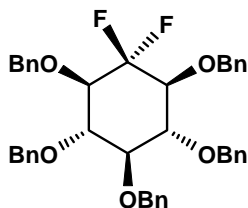
¹H NMR (D₂O) δ 3.25-3.34 (3H, m), 3.53-3.61 (2H, m), 4.18 (1H, ddd, J = 52.0 Hz, 9.2 Hz, 9.2 Hz); ¹³C NMR (D₂O) δ 72.18 (d, J = 17.6 Hz), 72.88 (d, J = 11.8 Hz), 73.75, 94.92 (d, J = 177.9 Hz).



1,3,4,5,6-*O*-Pentabenzyl-2-keto-*myo*-inositol 21

This compound was made as described in the literature¹⁰⁰.

¹H NMR (CDCl₃), δ 3.65 (2H, dd, J = 9.5 Hz), 3.90 (1H, dd, J = 9.2 Hz), 4.21 (2H, d, J = 9.3 Hz), 4.57 (2H, d, J = 11.5 Hz), 4.80 (2H, d, J = 10.7 Hz), 4.91-5.00 (6H, m), 7.21-7.41 (25H, m).

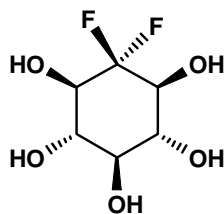


1,3,4,5,6-*O*-Pentabenzyl-2-deoxy-2,2-difluoro-*myo*-inositol

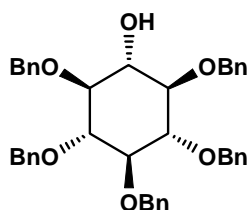
22^{98,101}

Diethyl-

aminosulfur trifluoride (DAST, 0.23 ml, 1.76 mmol) was added to a stirred solution of 1,3,4,5,6-*O*-pentabenzyl-2-keto-*myo*-inositol (0.50 g, 0.80 mmol) dissolved in dichloromethane (10 ml). The stirring was continued at r. t. for 20 h before addition of water. The mixture was separated and the organic layer was concentrated. FCC [toluene, 100%] afforded product (0.41 g, 79%) as a white solid. ^1H NMR (CDCl_3), δ 3.59 (1H, dd, $J = 9.1$ Hz, 9.0 Hz), 3.65-3.75 (4H, m), 4.80-4.98 (10H, m), 7.28-7.36 (25H, m); ^{13}C NMR (CDCl_3) δ 76.34, 76.36, 76.54, 76.68, 80.10 (t, $J = 18.6$ Hz), 81.25 (d, $J = 9.4$ Hz), 82.57, 120.82 (t, $J = 250.0$ Hz), 128.19, 128.20, 128.39, 128.45, 128.65, 128.85, 128.88, 137.94, 138.63, 138.67; ^{19}F NMR (CDCl_3), δ -129.46 (1F, ddd, $J = 252$ Hz, 20 Hz, 20 Hz), -115.65 (1F, d, $J = 252$ Hz); Mass: 673.2748 (TOF, MW + Na, calc. 673.2741).



2-Deoxy-2,2-difluoro-*myo*-inositol 12¹⁰⁰ A solution of 1,3,4,5,6-*O*-pentabenzyl-2-deoxy-2,2-difluoro-*myo*-inositol (1.23 g, 1.89 mmol) in THF- H_2O (50 mL, 4:1, v/v) was stirred in the presence of 10% Pd-C (0.3 g). The suspension was hydrogenated at r. t. under H_2 atmosphere using a balloon for 3 days. The mixture was filtered through celite and the filtrate was concentrated to dryness. Product was obtained as a light yellow solid (0.35 g, 97%). ^1H NMR (D_2O) δ 3.30-3.39 (3H, m), 3.66-3.72 (2H, m); ^{13}C NMR (D_2O) δ 71.31 (t, $J = 19.49$ Hz), 72.43 (d, $J = 8.9$ Hz), 73.45, 119.63 (t, $J = 244.8$ Hz).



1,2,3,4,5-*O*-Pentabenzyl-scyлло-inositol 24 was synthesized in 3 steps:

1)Triflate derivative 20

This compound was made as described in the literature⁹⁹.

¹H NMR (CDCl₃) δ 3.47-3.51 (3H, m), 3.89 (2H, dd, J = 9.6 Hz), 4.60-5.00 (10H, m), 5.29 (1H, dd, J = 2.1 Hz), 7.26-7.36 (25H, m).

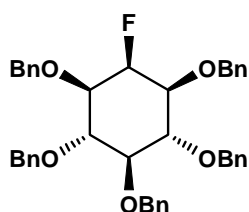
2)Trifluoroacetate derivative 23

This compound was made as described in the literature⁹⁹.

3) 1,2,3,4,5-*O*-Pentabenzyl-scyлло-inositol 24

This compound was made as described in the literature⁹⁹.

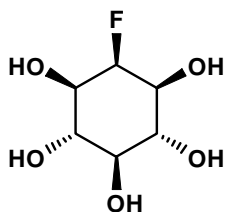
¹H NMR (CDCl₃) δ 3.45 (2H, dd, J = 8.7 Hz), 3.57-3.66 (4H, m), 4.82-4.93 (10H, m), 7.28-7.35 (25H, m).



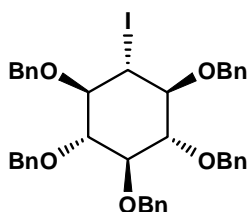
1,3,4,5,6-*O*-Pentabenzyl-2-deoxy-2-fluoro-myо-inositol 25

This compound was made as described in the literature^{102,103}.

¹H NMR (CDCl₃) δ 3.39 (2H, ddd, J = 28.8 Hz, 9.8 Hz, 1.7 Hz), 3.51 (1H, dd, J = 9.4 Hz), 3.98 (2H, dd, J = 9.4 Hz), 4.72 (4H, s), 4.84-4.95 (7H, m), 7.28-7.36 (25H, m).

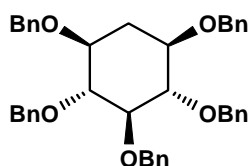


2-Deoxy-2-fluoro-*myo*-inositol **10**¹⁰⁰ 1,3,4,5,6-*O*-Pentabenzyl-2-deoxy-2-fluoro-*myo*-inositol (1.11 g, 1.76 mmol) was dissolved in THF-H₂O (60 mL, 4:1, v/v) containing 10% Pd-C (0.20 g) as a catalyst. The suspension was hydrogenated at r. t. using a balloon for 2 days. The mixture was filtered through a bed of celite, which was washed with water. The solvent was removed by rotary evaporation, resulting in 2-deoxy-2-fluoro-*myo*-inositol (0.32 g, 99%) as a grey solid. ¹H NMR (D₂O) δ 3.23 (1H, dd, J = 9.0 Hz), 3.51-3.60 (4H, m), 4.69 (1H, m); ¹³C NMR (D₂O) δ 70.46 (d, J = 17.2 Hz), 72.65 (d, J = 3.8 Hz), 73.23, 94.47 (d, J = 175.2 Hz).

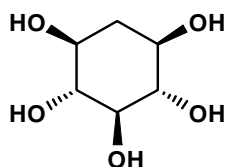


1,3,4,5,6-*O*-Pentabenzyl-2-deoxy-2-iodo-*scyllo*-inositol **26**^{104,105} To a solution of 1,3,4,5,6-*O*-pentabenzyl-*myo*-inositol (4.4 g, 7.0 mmol), triphenylphosphine (3.7 g, 14.0 mmol), and imidazole (1.2 g, 17.5 mmol) in dry toluene (100 mL) was added iodine (3.5 g, 14.0 mmol). The mixture was stirred at reflux for 24 h under argon, and then cooled to room temperature. Saturated NaHCO₃ aqueous solution (50 mL) was added, and the stirring was continued for 5 min. After the mixture was transferred to a separatory funnel, the organic layer was diluted with toluene and washed with aqueous sodium thiosulphate to remove excess iodine. The yellow solid was obtained after the organic layer was dried and concentrated. Triphenylphosphine oxide was separated by redissolving the solid in diethyl ether, followed by filtration. The filtrate was concentrated and then subjected to FCC [petroleum ether-ethyl acetate (12:1, v/v)]

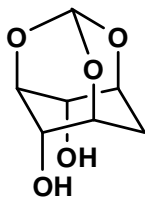
to afford the desired product as a white solid (4.28 g, 82%). ^1H NMR (CDCl_3) δ 3.61 (2H, dd, $J = 9.3$ Hz, 9.5 Hz), 3.71 (1H, dd, $J = 9.6$ Hz, 9.5 Hz), 3.78 (2H, dd, $J = 9.2$ Hz, 10.9 Hz), 4.18 (1H, dd, $J = 11.0$ Hz), 4.95-5.08 (10H, m), 7.36-7.53 (25H, m); ^{13}C NMR (CDCl_3) δ 34.44, 76.18, 76.32, 76.48, 82.95, 83.31, 84.65, 128.21, 128.23, 128.32, 128.42, 128.53, 128.70, 128.89, 128.91, 128.95, 138.22, 138.68, 138.71. Mass: 763.1878 (TOF, MW + Na, calc. 763.1896).



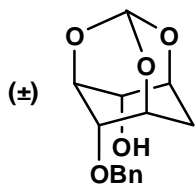
1,3,4,5,6-*O*-Pentabenzyl-2-deoxy-*myo*-inositol **27**^{104,106} A solution of 1,3,4,5,6-*O*-pentabenzyl-2-deoxy-2-iodo-*scyllo*-inositol (4.79 g, 6.47 mmol), tri-*n*-butyltin hydride (3.43 mL, 12.94 mmol) and 2,2-azobis-(2-methylpropionitrile) (AIBN, 0.10 g, 11.00 mmol) in dry toluene (150 mL) was degassed by bubbling argon through for 15 min. The stirring mixture was heated to reflux under argon for 30 min. After evaporation, the residue was purified by FCC [petroleum ether-ethyl acetate (8:1, v/v)] to afford the desired product as a white solid (3.97 g, 100%). ^1H NMR (CDCl_3) δ 1.50 (1H, dd, $J = 12.0$ Hz), 2.43 (1H, ddd, $J = 12.6$ Hz, 4.3 Hz, 4.2 Hz), 3.44-3.50 (3H, m), 3.58 (2H, dd, $J = 9.3$ Hz, 9.2 Hz), 4.69-5.02 (10H, m), 7.28-7.48 (25H, m); ^{13}C NMR (CDCl_3) δ 33.31, 72.98, 76.17, 76.47, 83.64, 85.93, 127.96, 128.07, 128.12, 128.31, 128.38, 128.75, 128.82, 138.82, 139.08, 139.17; Mass: 615.3128 (MW + H, calc. 615.3110); 637.3000 (TOF, MW + Na, calc. 637.2924); m. p. 107-108°C.



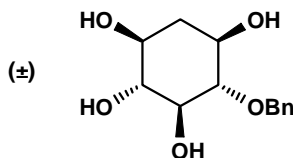
2-Deoxy-*myo*-inositol 13 To a solution of 1,3,4,5,6-*O*-pentabenzyl-2-deoxy-*myo*-inositol (1.74 g, 2.83 mmol) in THF-H₂O (60 mL, 4:1, v/v) was added 10% Pd-C (0.20 g). The black suspension was hydrogenated at r. t. using balloon for 2 days. The mixture was filtered through a bed of celite, which was washed with water. The filtrate was evaporated to yield 2-deoxy-*myo*-inositol (0.45 g, 98%) as a white solid. ¹H NMR (D₂O) δ 1.36 (1H, dd, J = 12.0 Hz), 2.10 (1H, ddd, J = 12.3 Hz, 4.6 Hz, 4.6 Hz), 3.13-3.22 (3H, m), 3.43-3.48 (2H, m).



2-Deoxy-*myo*-inositol 1,3,5-monoorthoformate 28 A mixture of 2-deoxy-*myo*-inositol (0.72 g, 4.39 mmol), *p*-toluenesulfonic acid monohydrate (0.20 g, 1.05 mmol), and triethylorthoformate (2.2 mL, 13.17 mmol) in dry DMF (15 mL) was stirred in an oil bath at 120-130°C for 2 h. The solvent was removed by evaporation. FCC [ethyl acetate-petroleum ether (3:1, v/v)] produced 2-deoxy-*myo*-inositol 1,3,5-monoorthoformate (0.57 g, 75%) as a white solid. ¹H NMR (D₂O) δ 2.22 (1H, d, J = 14.6 Hz), 2.34 (1H, dd, J = 14.6 Hz, J = 4.1 Hz), 4.18 (2H, m), 4.25 (1H, m), 4.31 (2H, m), 5.58 (1H, s)

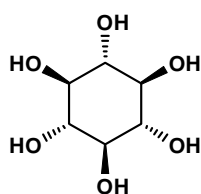


(±)-4-*O*-Benzyl-2-deoxy-*myo*-inositol 1,3,5-monoorthoformate 29 2-Deoxy-*myo*-inositol 1,3,5-monoorthoformate (0.52 g, 3.0 mmol) was treated with sodium hydride (0.12 g, 60%, 3.0 mmol) in DMF (10 mL) in ice bath. After 30 min, benzyl bromide (0.35 mL, 3.0 mmol) was added dropwise at 0°C, and then warmed to r. t. gradually and stirred overnight. The reaction mixture was quenched with water and the solvent was evaporated. The yellow residue was extracted with ethyl acetate and water. The organic layer was dried over MgSO₄. After removing the solvent, the yellow residue was purified by FCC [ethyl acetate-toluene (1:12, v/v)]. The product (±)-4-*O*-benzyl-2-deoxy-*myo*-inositol 1,3,5-monoorthoformate (0.44 g, 56%) were yielded as a white solid, and byproduct 4,6-*O*-dibenzyl-2-deoxy-*myo*-inositol 1,3,5-monoorthoformate (0.04 g, 4%) was also obtained. ¹H NMR (CDCl₃) δ 2.23 (1H, dd, J = 14.1 Hz, 1.4 Hz), 2.44 (1H, d, J = 14.0 Hz), 4.20-4.34 (5H, m), 4.68 (2H, s), 5.52 (1H, s), 7.33-7.40 (5H, m); ¹³C NMR (CDCl₃) δ 22.86, 66.84, 68.04, 68.54, 70.52, 73.15, 73.46, 103.56, 128.44, 129.07, 129.24, 136.65; Mass: 265.1078 (TOF, MW + H, calc. 265.1076). Byproduct 4,6-*O*-dibenzyl-2-deoxy-*myo*-inositol 1,3,5-monoorthoformate ¹H NMR (CDCl₃) δ 2.40 (2H, m), 4.25 (4H, m), 4.54 (1H, s), 4.61 (2H, d, J = 11.5 Hz), 4.72 (2H, d, J = 11.5 Hz), 5.57 (1H, s), 7.27-7.32 (10H, m).

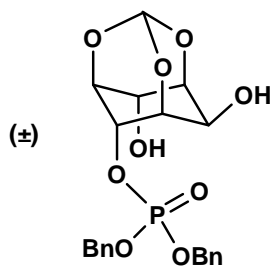


(±)-4-*O*-Benzyl-2-deoxy-*myo*-inositol 14 A solution of (±)-4-*O*-benzyl-2-deoxy-*myo*-inositol 1,3,5-monoorthoformate (0.42 g, 1.6 mmol) in methanol (30 mL) was

stirred with Dowex 50X8 (H^+ , 200-400 mesh) at r. t. overnight. The mixture was filtered and washed with methanol. The solvent was evaporated, and (\pm)-4-*O*-benzyl-2-deoxy-*myo*-inositol (0.38 g, 95%) was yielded as a white solid. ^1H NMR (D_2O) δ 1.39 (1H, dd, $J = 12.0$ Hz), 2.09 (1H, ddd, $J = 12.3$ Hz, 4.6 Hz, 4.6 Hz), 3.20-3.26 (3H, m), 3.41-3.44 (1H, m), 3.54-3.57 (1H, m), 4.73 (2H, s), 7.29-7.39 (5H, m); ^{13}C NMR (D_2O) δ 37.23, 68.66, 68.73, 74.23, 75.32, 77.26, 85.59, 128.74, 129.05, 129.24, 138.01; Mass: 277.1036 (TOF, $\text{M} + \text{Na}$, calc. 277.1052).



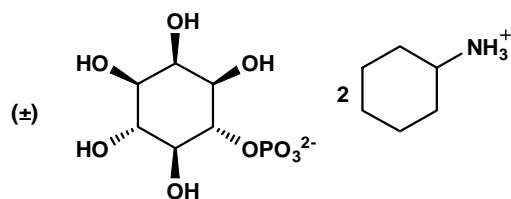
***scyllo*-Inositol** To a solution of 1,2,3,4,5-*O*-pentabenzyl-*scyllo*-inositol (1 g, 1.6 mmol) in 40 mL of THF- H_2O (3:1, v/v) was added 0.5 g of 10% Pd-C. The suspension was hydrogenated at r. t. for a day. The mixture was filtered and washed with water. The filtrate was dried by freeze drier, and *scyllo*-inositol (0.2 g, 70%) was obtained as a light yellow solid. ^1H NMR (D_2O) δ 3.22 (s); ^{13}C NMR (D_2O) δ 74.5.



(\pm)-4-(Dibenzyloxyposphoryloxy)-*myo*-inositol 1,3,5-monoorthoformate

This compound was made as described in the literature¹⁰⁷.

^1H NMR (CDCl_3) δ 7.35 (10H, m), 5.40 (1H, s), 5.16-5.02 (4H, m), 4.94 (1H, br s), 4.50 (1H, br s), 4.30 (1H, br s), 4.14 (1H, br s), 4.04 (1H, br s), 3.94 (1H, br s).



(±)-*myo*-Inositol-4-phosphate

This compound was made as described in the literature¹⁰⁷.

¹H NMR (D₂O) δ 3.95 (1H, m), 3.91 (1H, br s), 3.56 (1H, dd, J = 9.5 Hz), 3.48 (1H, d, J = 9.5 Hz), 3.42 (1H, d, J = 10 Hz), 3.27 (1H, dd, J = 9.5 Hz), 3.01 (2H, br s), 1.84 (4H, br s), 1.67 (4H, br s), 1.51 (2H, d, J = 12.5 Hz), 1.20 (8H, br s), 1.04 (2H, br s).

3. RESULTS AND DISCUSSION

3.1 Rate-limiting step

The kinetic mechanism for IDH was established as a compulsory ordered Bi Bi mechanism, as mentioned in **1.4.5**. The complete steady-state rate constants were determined by Daniellou in 2006¹⁰⁸. On the basis of these values, it seems that the breakdown of the ternary complex and the liberation of NADH constitute the rate limiting step. The rate-limiting step of reactions catalyzed by dehydrogenases typically is not the chemical reaction step. To determine whether the chemical step is the rate-limiting step for IDH catalyzed reaction, a kinetic isotope effect experiment was carried out.

3.1.1 Kinetic isotope effect

Kinetic isotope effect (KIE), a useful method to elucidate the rate-limiting step in a reaction mechanism, has been used to study chemical reactions for almost half a century. A kinetic isotope effect is a change in the rate when an atom is replaced by its

isotopic atom in the same reaction¹⁰⁹. This isotopic substitution can influence equilibrium and also affect reaction rates based on the differences in the mass of different isotopes. The calculated or observed isotope effect is normally presented by the ratio between the rate with an unlabeled molecule and the rate with the molecule containing a heavy isotope (for example, k_H/k_D)¹¹⁰.

The magnitude of the isotope effect depends on the location of the isotope. KIE commonly is classified into primary KIE and secondary KIE. A primary KIE is observed when the rate change is due to isotopic substitution at a site of bond breaking or bond making in the rate determining step of a mechanism. On the other hand, if rate changes due to isotopic substitution at a site not undergoing bond breaking or bond making in the rate determining step of a mechanism, this is a secondary KIE¹¹¹. A secondary KIE is weaker than a primary KIE.

The magnitude of isotope effect also depends on the relative mass difference between the atom and its isotope. Hydrogen is a common atom used in KIE as the effect is significant since deuterium is twice as massive as hydrogen and tritium is three times as massive as hydrogen. Theoretically, the maximum value of primary deuterium KIE (k_H/k_D) is 6.9 and the maximum value of primary tritium KIE (k_H/k_T) is 18 at room temperature, whereas, the maximum value of secondary deuterium KIE (k_H/k_D) is only 1.2¹¹⁰.

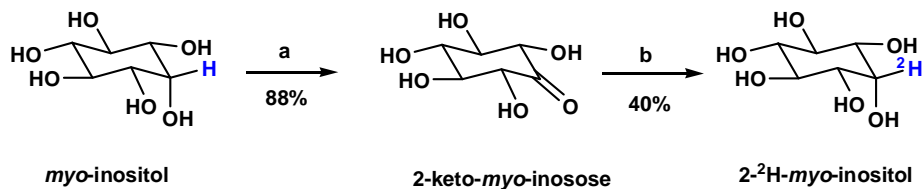
The theory of kinetic isotope effects is applicable to enzymatic reactions, however, the chemical step(s) of an enzymatic reaction is often not totally rate limiting because of the strong binding affinity between the enzyme and its substrates/products¹¹¹. A kinetic isotope effect on a rate constant of enzymatic reaction is normally presented by $^xV_{\max}$,

$^x(\frac{V_{\max}}{K_m})$, or $^x(\frac{k_{cat}}{K_m})$. The superscript x is D, T, ^{13}C , ^{14}C , ^{15}N , ^{17}O , or ^{18}O isotope effects. The magnitude of KIE observed for enzymatic reactions varies widely and the interpretation can be complex^{112,113}.

In many cases of dehydrogenases, the observed primary KIE on deuterium substituted substrate is in the range of 1-2, indicating that interconversion of substrates and products is not rate limiting or only partly rate limiting, and release of product(s) is primarily rate limiting¹¹⁴⁻¹¹⁸. In this research, deuterium labeling was employed to determine the rate limiting step of IDH catalyzed reaction. The deuterium-substituted compound 2- ^2H -*myo*-inositol, in which deuterium was incorporated into the reaction center C2, was designed as the substrate. A significant primary KIE should be detected if the hydride transfer is the rate-limiting step or part of the rate-limiting step.

3.1.2 Synthesis of 2- ^2H -*myo*-inositol

The compound 2- ^2H -*myo*-inositol was synthesized by using *myo*-inositol as starting material, and the synthetic route is shown in **Scheme 3.1**. Oxidation of *myo*-inositol to 2-keto-*myo*-inositol was completed by *Gluconobacter oxidans* ATCC621 as described in the literature in 88% isolated yield⁹³. The stereoselective reduction of 2-keto-*myo*-inositol with NaBD₄ in H₂O at r. t. produced 2- ^2H -*myo*-inositol^{119,120}. The deuterium is added to carbonyl from the face which is *anti* to the substituents at the two contiguous carbons, resulting in product 2- ^2H -*myo*-inositol. Acetylation and deacetylation were used for purification. Neutralization with Dowex 50X8 (H⁺ form, 200-300 mesh) gave 2- ^2H -*myo*-inositol as a white solid in 35% overall yield.



Scheme 3.1 Synthesis of 2-²H-*myo*-inositol. Reagents and conditions: a) *Gluconobacter oxidans*, 88%. b) (1) NaBD₄, H₂O, r. t., overnight; (2) Ac₂O, pyridine, 100°C, 24 h (overall yield of (1) and (2): 41 %); (3) NaOCH₃, CH₃OH, reflux 10 min, Dowex 50X8 (H⁺ form), 98 %.

3.1.3 Rate-limiting step determination

During the kinetic analysis, the cofactor NAD⁺ was kept constant and saturating, thus the two-substrate enzymatic reaction was simplified to a one-substrate reaction and the rate of the reaction depended on the amount of the IDH-NAD⁺ complex. Initial velocities, K_m^{app} , and V_{max}^{app} were determined as described in 2.8.2 and 2.8.3. The kinetic isotope effect upon $V_{max}^{app} / K_m^{app}$ was measured via generating saturation curves with commercial *myo*-inositol and synthesized 2-²H-*myo*-inositol. In order to get consistent data to make the results more convincing, this assay was also carried out using synthesized *myo*-inositol made by sodium borohydride reacting with 2-keto-*myo*-inositol. It turned out that the kinetic result using synthesized *myo*-inositol showed no difference from that using the commercial *myo*-inositol. The kinetic constants were shown in **Table 3.1**.

No kinetic isotope effect was observed on $^D V_{max}^{app}$ ($^D V = 1.0$) and the isotope effect on

$^D \left(\frac{V_{max}^{app}}{K_m^{app}} \right)$ was 1.1 ± 0.1 , suggesting no KIE was observed. Therefore, the chemical

reaction is not the rate-limiting step of the oxidation-reduction reaction that IDH

catalyzed. This result combined with those of rate constants determination¹⁰⁸, reveals that the breakdown of ternary complex and liberation of NADH constitute the rate-limiting step.

Table 3.1 Kinetic constants of the IDH catalyzed reactions using 2-²H-*myo*-inositol and *myo*-inositol as substrates.

Substrate	K_m^{app} (mM)	V_{max}^{app} [$\mu\text{mol} \cdot \text{min}^{-1} (\text{mg protein})^{-1}$]
2- ² H- <i>myo</i> -inositol	20 ± 1	9.0 ± 0.1
Commercial <i>myo</i> -inositol	18 ± 1	9.0 ± 0.1
Synthesized <i>myo</i> -inositol	18 ± 1	9.0 ± 0.1

Conditions: 100 mM Tris-HCl, pH 9.0, 25°C.

3.2 Exploring the substrate spectrum of IDH

3.2.1 Design of new potential substrates

As mentioned in **1.4.3**, IDH demonstrates broad substrate specificity. The 1L-4-*O*-substituted *myo*-inositol derivatives listed in **Figure 1.14** had been synthesized and proved to be substrates in this laboratory. In order to probe the pocket that accommodates 4-substituted groups, four new shapes of inositol derivatives were designed as potential substrates. These four compounds were 1L-4-*O*-(2-benzothiazolylmethyl)-*myo*-inositol **1**, 1L-4-*O*-(4-*tert*-butylbenzyl)-*myo*-inositol **2**, 1L-4-*O*-propargyl-*myo*-inositol **3**, and 1L-4-*O*-(1-allyl-4-methylene-1,2,3-triazol)-*myo*-inositol **4** as shown in **Figure 3.1**. Besides the shape differences, compounds **1** and **4** also introduce heterocycles that possess the potential to interact with amino acid residue(s) of the binding pocket.

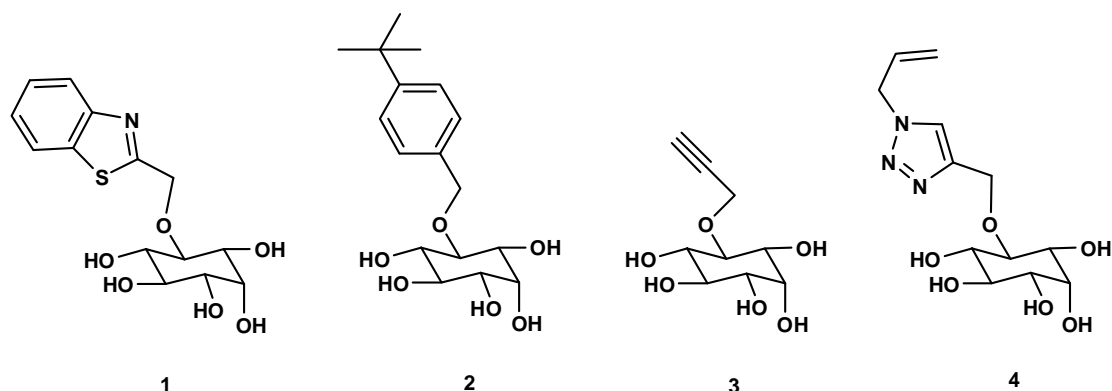


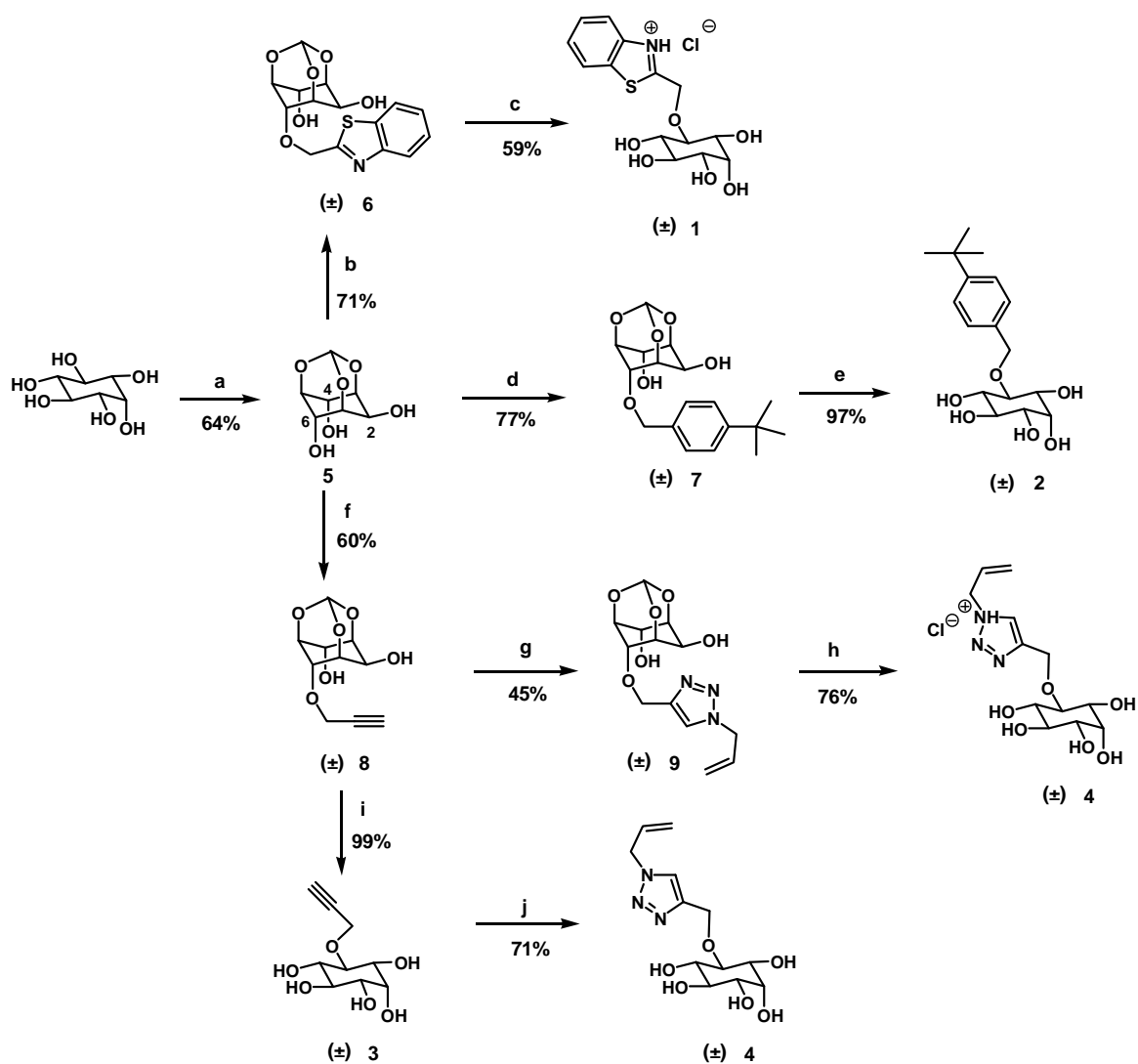
Figure 3.1 Structures of potential substrates of IDH.

3.2.2 Synthesis of new potential substrates

Three proposed IDH substrates **1**, **2**, and **3** were synthesized employing a similar synthetic route as published previously⁶⁹. The method began with the commercially available *myo*-inositol as shown in **Scheme 3.2**. Selective protection with triethylorthoformate formed *myo*-inositol 1,3,5-monoorthoformate **5**, in which all of the hydroxyl groups are in the axial orientation relative to the inositol ring except the hydroxyl at the C2. Compound **5** was an attractive structure because of the regioselectivity displayed by three free hydroxyl groups¹²¹. The axial hydroxyl groups of C4 and C6 are chemically equivalent and more acidic than C2 hydroxyl group. In the presence of 1.1 mole equivalent of NaH, a C4/6 hydroxyl group is deprotonated to the corresponding anion available for subsequent addition of an electrophile. Therefore, these anions allowed formation of racemic products **6**, **7**, and **8** after addition with 2-(bromomethyl)benzothiazole, *tert*-butylbenzyl bromide, or propargyl bromide respectively. After removal of orthoformate by treatment with Dowex 50X8 (H⁺ form) in methanol, the racemic compounds **1**, **2**, and **3** were obtained. (±)-**4** was

successfully synthesized from racemic compound **8** by two routes in which allyl azide was “clicked” on to compound **8** or **3** to form a triazole ring. The 1,4-disubstituted (*anti*) triazole structure of **4** was determined by NOE difference. The analogue of compound **4** that would be formed when “clicked” with methyl azide may show a lower value of Michaelis constant. Unfortunately, this analogue has not been tried since methyl azide exists as a gas at room temperature (b. p. 18°C)⁹¹.

Although only one enantiomer of *myo*-inositol derivatives (1L-4-*O*- attached) is the potential substrate, the other enantiomer will not affect the enzymatic reaction according to our previous measurements⁶⁹. Therefore, the racemic compounds **1**, **2**, **3**, and **4** were tested as potential substrates of IDH.



Scheme 3.2 Synthesis of inositol analogues. Reagents and conditions: a) (1) Triethylorthoformate, *p*-toluenesulfonic acid monohydrate, DMF, 120-130°C; (2) Pyridine and Ac₂O; (3) NaOCH₃. b) 2-(bromomethyl)benzothiazole, NaH, DMF. c) Dowex 50X8 (H⁺), methanol. d) *tert*-butylbenzyl bromide, NaH, DMF. e) Dowex 50X8 (H⁺), methanol. f) propargyl bromide, NaH, DMF. g) allyl azide, CuSO₄·5H₂O, sodium L-ascorbate, THF/H₂O. h) Dowex 50X8 (H⁺), methanol. i) Dowex 50X8 (H⁺), methanol. j) allyl azide, CuSO₄·5H₂O, sodium L-ascorbate, THF/H₂O.

3.2.3 Apparent K_m (K_m^{app}) of new substrates

Table 3.2 Kinetic constants of wild-type IDH with four synthesized substrates 1, 2, 3, 4 and D-chiro-inositol.

Compounds	K_m^{app} (mM)	V_{max}^{app} [$\mu\text{mol} \cdot \text{min}^{-1} (\text{mg protein})^{-1}$]	$V_{max}^{app} / K_m^{app}$
<i>myo</i> -inositol	18 ± 1	35 ± 4	1.9
D- <i>chiro</i> -inositol	37 ± 3	22 ± 2	0.6
(\pm) 1	16 ± 2	12 ± 1	0.8
(\pm) 2	42 ± 16	$7 \pm 2^*$	0.2
(\pm) 3	83 ± 7	15 ± 1	0.2
(\pm) 4	45 ± 4	15 ± 1	0.3

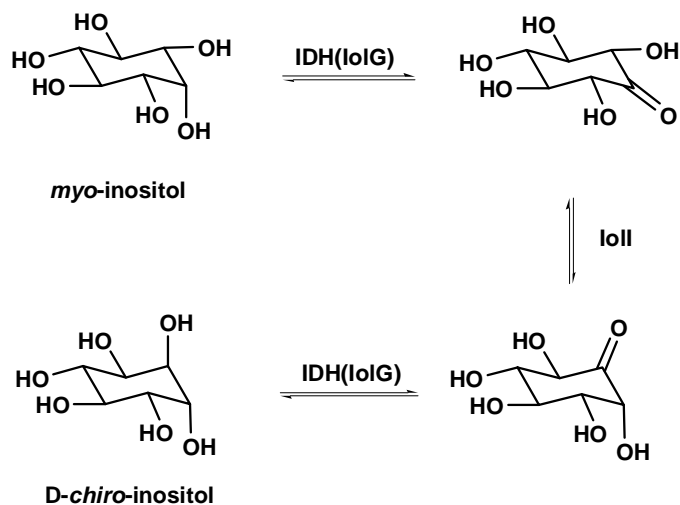
Conditions: 100 mM Tris-HCl pH 9.0, 25°C, $[\text{NAD}^+] = 0.5 \text{ mM}$;

*20% DMSO in 100 mM Tris-HCl at pH 9.0.

The kinetic method described in **2.8.3** was used to evaluate the proposed substrates. The results revealed that all four synthesized compounds, **1**, **2**, **3**, and **4**, were substrates of IDH. Since the solubility of compound **2** in aqueous buffers is very poor, the corresponding kinetics experiments were carried out in Tris-HCl buffer in the presence of 20% DMSO (IDH is fully active in 20% DMSO⁷⁸). As all four compounds are racemic compounds, the K_m^{app} values of the reactive enantiomers are equal to half of the values listed in **Table 3.2**. Therefore, the values of K_m^{app} of compounds **2** and **4** were comparable to the value of *myo*-inositol, whereas the value of K_m^{app} of 1L-**1** was half and 1L-**3** was twice that of *myo*-inositol. Hydrogen bonding interaction may be introduced by the nitrogen atom in the heterocycle of compound **1**, which can act as hydrogen bond acceptor and enhance the binding affinity. In contrast, compound **4** also incorporates a nitrogen atom, but the K_m^{app} value is almost three times of the value of

compound **1**. It seems that the triazole ring armed with a long allyl side chain is not accommodated well by IDH compared to benzothiazole ring.

In 2006, the *in vitro* interconversion of *myo*-inositol and *D-chiro*-inositol catalyzed by the enzymes IDH and IolI (encoded by genes *iolG* and *iolI* in *Bacillus subtilis*) was reported¹²², the details are shown in **Scheme 3.3**. Therefore, *D-chiro*-inositol was tried as a substrate for IDH in this laboratory. As expected, *D-chiro*-inositol is a substrate of IDH, but demonstrates higher value of K_m^{app} and lower value of V_{max}^{app} than those of *myo*-inositol.



Scheme 3.3 Conversion of *myo*-inositol and *D-chiro*-inositol catalyzed by **IolI** and **IDH(IolG)**. IolI is an inosose isomerase.

3.3 Inhibition studies

3.3.1 Design of potential competitive inhibitors

A competitive inhibitor typically competes with the substrate for binding in the same active site to form an enzyme-inhibitor complex which is not able to undergo a reaction. In most cases, a competitive inhibitor resembles the corresponding substrate. This character makes it possible to rationally design potential competitive inhibitors for IDH.

The C2 alcohol of *myo*-inositol is oxidized during the IDH catalyzed reaction. Based on the proposed mechanism of dehydrogenases (**Figure 1.16**), removal of the axial hydroxyl group at the 2-position will produce inactive substrate. In order to probe the active site, a series of analogues of *myo*-inositol modified at the 2-position were synthesized and tested as inhibitors of IDH. These analogues are 2-deoxy-2-fluoro-*myo*-inositol **10**, 2-deoxy-2-fluoro-*scyllo*-inositol **11**, 2-deoxy-2,2-difluoro-*myo*-inositol **12**, 2-deoxy-*myo*-inositol **13**, and 1L-4-*O*-benzyl-2-deoxy-*myo*-inositol **14**. For clarity, the compounds are named using the 1L-*myo*-inositol numbering system, and the structures are shown in **Figure 3.2**.

Fluorine, the most electronegative element, is a good hydroxyl surrogate since it is close in size (C-F bond length is 1.39 Å and C-O bond length is 1.43 Å). In addition, fluorine is able to act as a hydrogen bond acceptor, participating in interactions with -OH and -NH- donors, and also can form hydrogen-bonding interactions with H-C¹²³. Thus fluorinated compounds **10** and **11** should provide good *myo*- and *scyllo*-inositol mimics respectively. Although fluorine and hydrogen demonstrate different van der Waals radii (r_w : 1.47 Å vs 1.20 Å), fluorine is often regarded as an isostere of

hydrogen¹²⁴. The replacement of hydrogen by fluorine in compound **12** alters electronically the properties of the molecule and affects the dipole moment. Deoxy compounds **13** and **14** were also expected to be inhibitors of IDH. Since the hydrogen atom is unable to act as hydrogen bond donor or acceptor, these inhibitors can probe the importance of having hydrogen bond accepting/donating functionality at the 2-position of *myo*-inositol. The ability of fluorinated and deoxy analogues to inhibit IDH will indicate the role of hydroxyl group in binding to the active site.

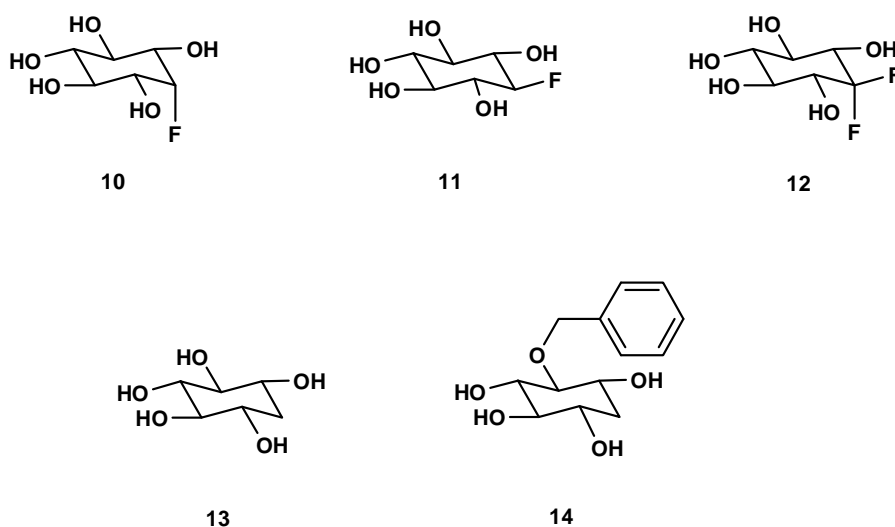
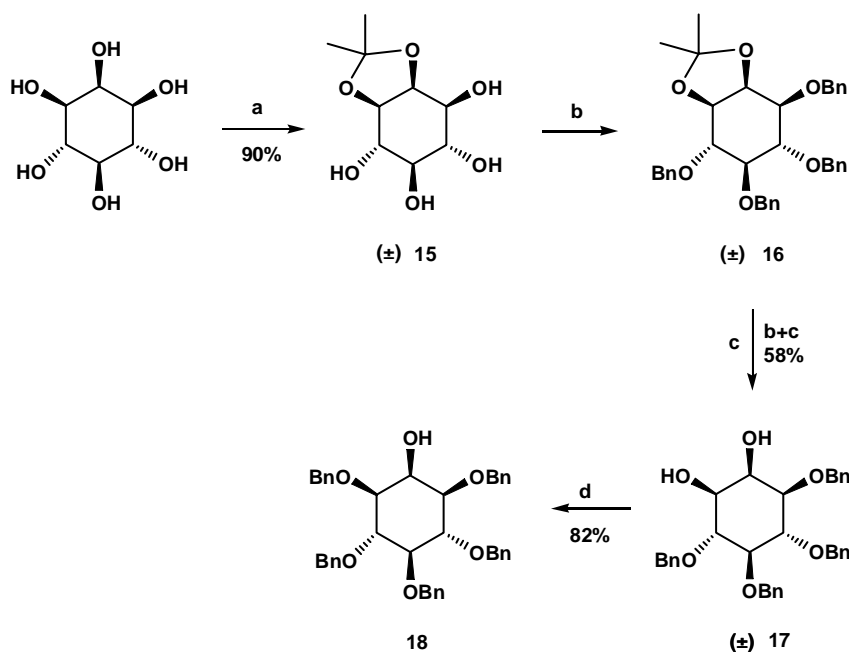


Figure 3.2 Structures of potential competitive inhibitors of IDH.

We considered that inositol analogues **10-13** substituted at 4-position would show inhibition since inositol 4-substituted derivatives are substrates of IDH⁶⁹. 1L-4-*O*-Benzyl-2-deoxy-*myo*-inositol **14** was evaluated as a competitive inhibitor for this purpose.

3.3.2 Synthesis of inhibitors

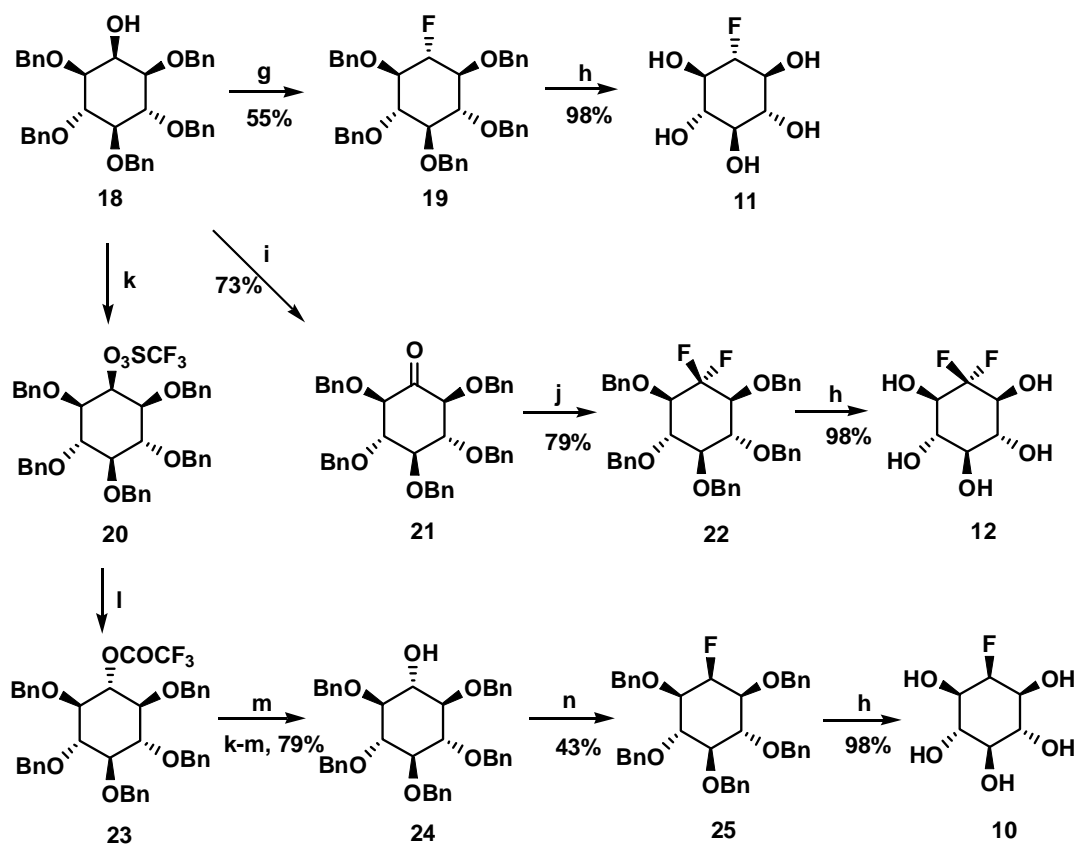
All five compounds **10-14** were synthesized from the same intermediate 1,3,4,5,6-*O*-pentabenzyl-*myo*-inositol **18**. The synthetic route to compound **18** is shown in **Scheme 3.4**. The isopropylidene **15** was obtained in 90% yield by heating *myo*-inositol and dimethoxypropane in DMSO with *p*-toluenesulphonic acid as a catalyst⁹⁴. Perbenzylation of **15** with sodium hydride and benzyl bromide in DMF gave a racemic mixture **16**. The isopropylidene was removed by refluxing **16** in 80% acetic acid for 4 h to produce racemic vicinal *cis*-diol **17**⁹⁵. Diol **17** was regioselectively benzylated by utilizing dibutyltin oxide in the presence of benzyl bromide and tetrabutylammonium bromide in acetonitrile^{96,99}. The desired symmetrical compound **18** was produced after crystallization from methanol in 82% yield. Thus, compound **18** was synthesized from *myo*-inositol in 4 steps with a 43% overall yield.



Scheme 3.4 Chemical synthesis of intermediate **18**. Reagents and conditions: a) 2,2-dimethoxypropane, toluene-*p*-sulfonic acid, DMSO, 90°C, 90%. b) NaH, BnBr, DMF. c) 80 % AcOH, reflux, 58% (b+c). d) BnBr, Bu₂SnO, Bu₄NBr, CH₃CN, reflux, 82%.

The synthetic routes used to make potential inhibitors **10**, **11**, **12** were very similar, as shown in **Scheme 3.5**. Fluorination with DAST generally proceeds with inversion of configuration at the reaction center. Therefore, the hydroxyl at the reaction center has to be of opposite configuration to the desired fluorinated inositol analogue. Treatment of compound **18** with DAST using dichloromethane as a solvent at r.t. gave the 2-deoxy-2-fluoro derivative **19** in 55% yield. Subsequent removal of the benzyl groups by hydrogenolysis using hydrogen gas and Pd-C in THF-H₂O (4:1, v/v) provided compound **11** in an excellent yield (> 95%). Difluoro derivative **12** was synthesized via the ketone **21**, which was prepared by Swern oxidation of compound **18**, and was afforded by following the same procedure as synthesis of compound **11**. In order to obtain the *myo*-configuration retaining compound **10**, in which the stereochemistry of fluoride in 2-deoxy-2-fluoro-*scyllo*-inositol **11** was inverted to the axial orientation, *scyllo*-inositol derivative **24** was synthesized from compound **18** as described in the literature⁹⁹. Esterification of the hydroxyl group with triflic anhydride produced the triflate derivative **20**, and then S_N2 displacement of the triflate group by trifluoroacetate formed the trifluoroacetic ester **23**. This reaction was followed by an ester exchange reaction in methanol with Na₂CO₃. Thus, compound **24** was easily obtained by these three steps without the need of column chromatography, and compound **24** was crystallized from methanol in an overall yield of 79%. Our initial attempt at the fluorination of compound **24** with DAST was carried out at room temperature and yielded only a small amount of compound **19** instead of the desired compound **25**. More than 70% of the starting material **24** was recovered. Compound **24** was then fluorinated with DAST in the presence of 4-(dimethylamino)pyridine (DMAP) in toluene at 80°C¹⁰², which produced 1,3,4,5,6-*O*-pentabenzyl-2-deoxy-2-fluoro-*scyllo*-inositol **19** and 1,3,4,5,6-*O*-pentabenzyl-2-deoxy-2-fluoro-*myo*-inositol **25** in 18% and 43% yield, respectively. The protective benzyl groups of compound **25** were cleaved by hydrogenolysis catalyzed by Pd-C in the solvent

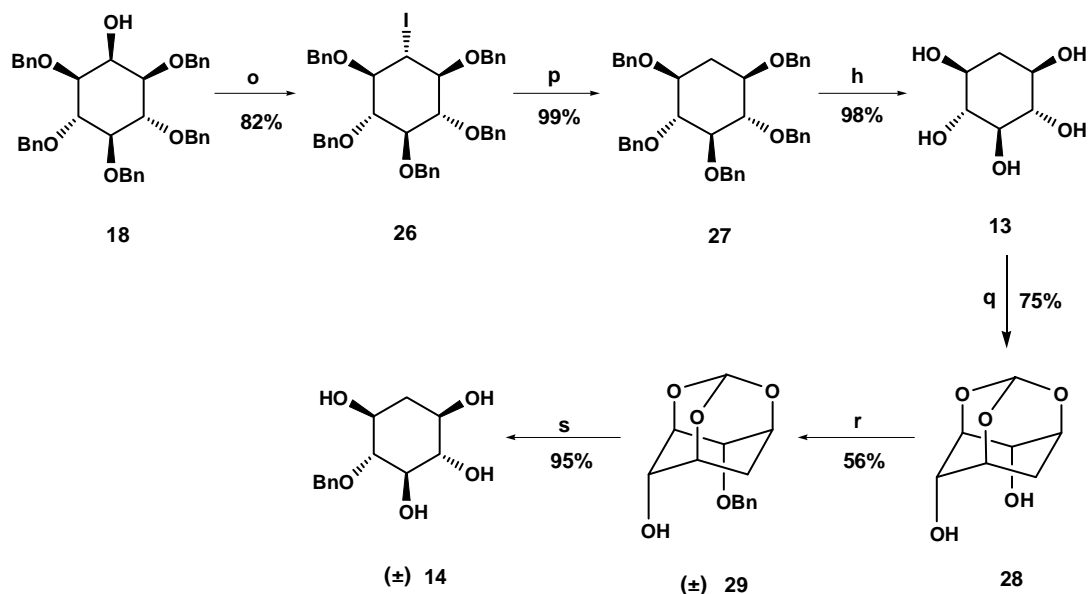
system of THF-H₂O (4:1, v/v) to afford compound **10**. Therefore, potential inhibitors **10**, **11**, and **12** were synthesized from compound **18** in the corresponding overall yields of 33%, 54%, and 57%.



Scheme 3.5 Chemical syntheses of potential inhibitors **10**, **11**, **12** from intermediate **18**. **Reagents and conditions:** g) DAST, CH₂Cl₂, r. t., 55 %. h) 10% Pd-C, THF-H₂O (4:1, v/v), r. t., 98 %. i) DMSO, oxalyl chloride, Et₃N, CH₂Cl₂, -78°C, 73%. j) DAST, CH₂Cl₂, r. t., 79 %. k) Tf₂O, pyridine, CH₂Cl₂, -63 °C to r. t. l) NaOCCF₃, DMF, r. t. m) Na₂CO₃, MeOH, 79 % (overall yield of steps k, l and m). n) DAST, DMAP, toluene, 80°C, 43 %.

Deoxy inositol analogues **13** and **14** were also synthesized from compound **18** (**Scheme 3.6**). Deoxygenation of secondary alcohols was usually carried out by the Barton-McCombie method¹²⁵, in which alcohol is first converted to a thiocarbonyl derivative, followed by radical reduction using tributyltin hydride (Bu_3SnH)¹²⁶⁻¹²⁹. Our initial attempt at deoxygenation involved generating the thiocarbonyl derivative, derived from compound **18** by reacting with *O*-phenyl chlorothionoformate in the presence of sodium hydride in DMF. However, treatment of the resulting thiocarbonyl derivative with tributyltin hydride initiated by AIBN failed to react and thus an alternative procedure was sought. Previously, tributyltin hydride was reported to reduce halide to produce the corresponding alkane in good yield¹³⁰, therefore, this method was applied to deoxygenation of compound **18**. Treatment of compound **18** with iodine in the presence of triphenylphosphine and imidazole in refluxing toluene, gave 1L-1,3,4,5,6-*O*-pentabenzyl-2-deoxy-2-iodo-*scyllo*-inositol **26** in 82% yield¹⁰⁵. The radical dehalogenation of compound **26** into the 2-deoxy analogue **27** proceeded in quantitative yield. Subsequent removal of benzyl protective groups of compound **27** provided the 2-deoxy-*myo*-inositol **13**.

The strategy to prepare 1L-4-*O*-benzyl-2-deoxy-*myo*-inositol **14** is the same as that for the synthesis of substrate analogues shown in **Scheme 3.2**. The pentol **13** was treated with triethylorthoformate in DMF in the presence of *p*-toluenesulfonic acid to afford orthoformate **28** in 75% yield. Benzylation of **28** using 1.1 equivalent of benzyl bromide in DMF in the presence of sodium hydride gave the intermediate **29** in 56% yield. Acidic treatment of **29** with Dowex 50X8 (H^+ form) in methanol removed the orthoformate protective group leading to the potential inhibitor **14** in 95% yield. Therefore, compounds **13** and **14** were synthesized from compound **18** in overall yields of 80% and 32%, respectively.



Scheme 3.6 Chemical syntheses of potential inhibitors 13, 14. Reagents and conditions: o) Ph_3P , imidazole, I_2 , toluene, 82%. p) Bu_3SnH , AIBN, toluene, 99%. q) triethyl orthoformate, toluene-*p*-sulfonic acid, DMF, 120°C-130°C, 75%. r) NaH, BnBr, DMF, 56%. s) Dowex 50X8 (H^+ form), MeOH, 95%.

3.3.3 IC_{50} measurement and inhibitory properties

The synthesized inositol mimics were tested for their ability to inhibit IDH enzymatic activity. Low solubility of the fluorinated inositol analogues in aqueous buffer prevented very high concentrations of inhibitor from being used, but an IC_{50} value could be determined. All the experiments were performed under the methods described in 2.8.4. IC_{50} was obtained by plotting the reciprocal of inhibitory activity (v_0/v_i) against concentrations of inhibitors (the plots are shown in Appendix 3). The inhibition constant (K_i) was calculated using the Cheng and Prusoff equation⁸⁹, **Equation 2.1**, and the results are shown in **Table 3.3**.

Table 3.3 Kinetic constants of compounds 10-14 as potential competitive inhibitors of IDH.

Compounds	10	11	12	13	(±) 14
IC ₅₀ (mM)*	77 ± 2	No inhibition	82 ± 2	107 ± 3	74 ± 2
K _i (mM)	37 ± 5	No inhibition	39 ± 5	51 ± 5	35 ± 5

*IC₅₀ was measured when [myo-inositol] = 20 mM. Conditions: 100 mM Tris-HCl, pH 9.0, 25°C.

According to the kinetic results, compound **11** is neither an inhibitor nor a substrate of IDH and compounds **12**, **10**, **13**, and **14** are inhibitors. These inhibitors were designed as competitive inhibitors; this mode of inhibition was observed using α -D-glucosyl fluoride with IDH¹⁰⁸.

No inhibition of enzymatic activity was observed for compound **11**, and this result is in agreement with the fact that *scyllo*-inositol is neither a substrate nor an inhibitor for IDH⁶⁵. It implies that the active site of IDH might preferentially bind inositol analogues with an axial electronegative group at the 2-position. The K_i value of **10** is the smallest of the inhibitors tests. This might be attributed to the fact that **10** is the one that most closely mimics *myo*-inositol. Compound **12** is a competitive inhibitor and the inhibition property is close to **10**. These phenomena reveal that the presence of an electronegative equatorial substituent at C2 has little effect on the binding affinity when an axial electronegative group is present. Compound **13** is a competitive inhibitor with a higher K_i compared to **10**, whereas **11** is not an inhibitor, suggesting that deoxy inositol analogues still can bind to the active site when no electronegative group at 2-position but binding affinity is weaker. In addition, considering the dipole moments, compound **10** is consistent with the substrate of IDH, *myo*-inositol, and compound **12** is consistent with the product of IDH, 2-keto-*myo*-inositol. This might be the reason that these two

compounds can bind in the active site, whereas compound **11** can not, since it demonstrates a different direction of dipole moment.

As expected, compound **14** is a competitive inhibitor and is the best one (recall that because **14** is racemic, the true K_i is equal to half the observed value). This result is in good accordance with previous hypothesis that there is a nonpolar cavity near the active site⁶⁹. Unfortunately, there is no obvious hydrophobic cavity apparent in the *apo*-IDH and *holo*-IDH crystal structures solved recently. It is still not clear how IDH accommodates the benzyl group. If a high-resolution crystal structure of IDH-inhibitor complex, especially IDH complexed with **14**, can be obtained, it will be very helpful to prove the roles of the active-site residues and the binding pocket for 4-substituent groups.

In summary, inositol analogues, 2-deoxy-2-fluoro-*myo*-inositol **10**, 2-deoxy-2,2-difluoro-*myo*-inositol **12**, 2-deoxy-*myo*-inositol **13**, and 1L-4-*O*-benzyl-2-deoxy-*myo*-inositol **14**, are competitive inhibitors of IDH, while 2-deoxy-2-fluoro-*myo*-inositol **10** is neither an inhibitor nor a substrate for IDH. Since IDH catalyzes the first step of the *myo*-inositol catabolism pathway in bacteria as mentioned in **1.2.2**, inhibiting dehydrogenase activity becomes an effective way to prevent the decomposition of *myo*-inositol.

3.4 Mutagenic studies

IDH catalyzes the oxidation-reduction reaction by binding and orienting the coenzyme NAD and *myo*-inositol/2-keto-*myo*-inositol in the binding sites formed with many amino acid residues that bind them with a combination of hydrogen bonds, electrostatic

interacion, hydrophobic effects, van der Waals and other interactions. The substrate specificity is due to the size, shape, and chemical property of the active sites defined by these interactions. Site-directed mutagenesis, substituting targeted amino acid residue with selected amino acid, is a useful tool for studying the participation of an amino acid residue in catalysis. Each site-directed substitution provides a new mutated IDH that are compared with the wild-type IDH, and the difference could be assigned to the contributions of the two residues. However, such kind of study is an estimation of the importance of a residue. The change in activity should not be the only criterion for assessing the significance of a residue for catalysis. Any substitution possesses the potential to alter the structure of the enzyme and affect activity by steric and chemical effects¹³¹.

3.4.1 Overview of IDH crystal structure

The catalytic dyad of IDH was proposed in 2007 and the substrate specificity was also explored as mentioned in **1.4** and **3.2**. However, further structural and mechanistic data were required to substantiate the previous hypotheses and elucidate substrate specificity. Fortunately, the X-ray structure of *apo*-IDH was solved shortly after. Just a few months prior to this thesis, the binary structure complexed with NADH (*holo*-IDH), and ternary structure complexed with NADH and *myo*-inositol were solved. However, the ternary complex was obtained by soaking binary crystals in *myo*-inositol, and *myo*-inositol binds in a non-productive mode. Nonetheless, some useful information can still be derived.

An active IDH exists as a tetramer (**Figure 3.3**), and NAD and inositol/inosose bind in each monomer. The monomer is made up of two structural domains as shown in

Figure 3.4. The N-terminal domain (1-123 residues) is a Rossmann fold domain, a typical dinucleotide binding domain with a central β -sheet surrounded by α -helices. The C-terminal domain (124-344 residues) displays overall characteristic to enzymes that belong to glyceraldehyde-3-phosphate dehydrogenase-like protein family in the Structural Classification of Proteins (SCOP) database^{85,132}. The C-terminal domain is the *myo*-inositol binding domain consisting of six helices, an antiparallel oriented six-stranded β -sheet, and an antiparallel oriented two-stranded short β -sheet which extends out to form a tetramer with the other three monomers.

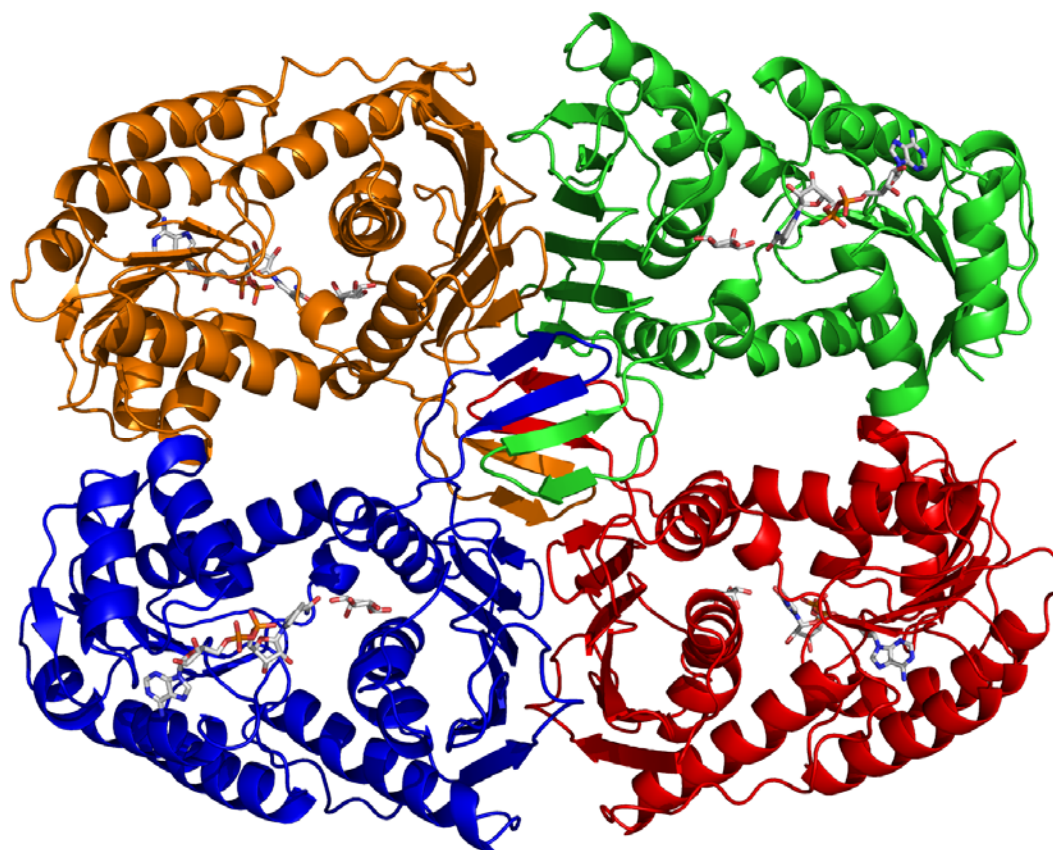


Figure 3.3 The model of a tetrameric IDH. Each color represents one monomer, respectively. The dinucleotide NADH and *myo*-inositol are shown in sticks. Atoms are shown in standard colors: grey for carbon, blue for nitrogen, orange for phosphorus, red for oxygen. *myo*-Inositol binds in a non-productive binding mode in each monomer. Image was generated using PyMOL⁶⁸.

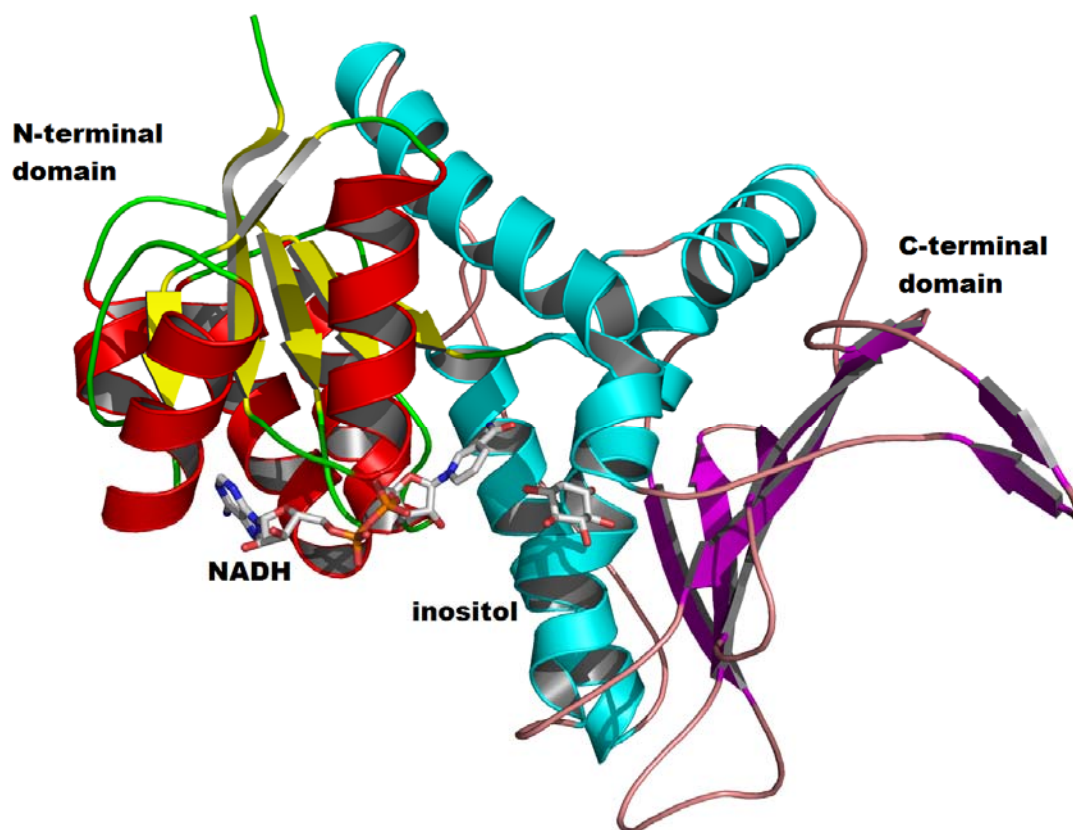
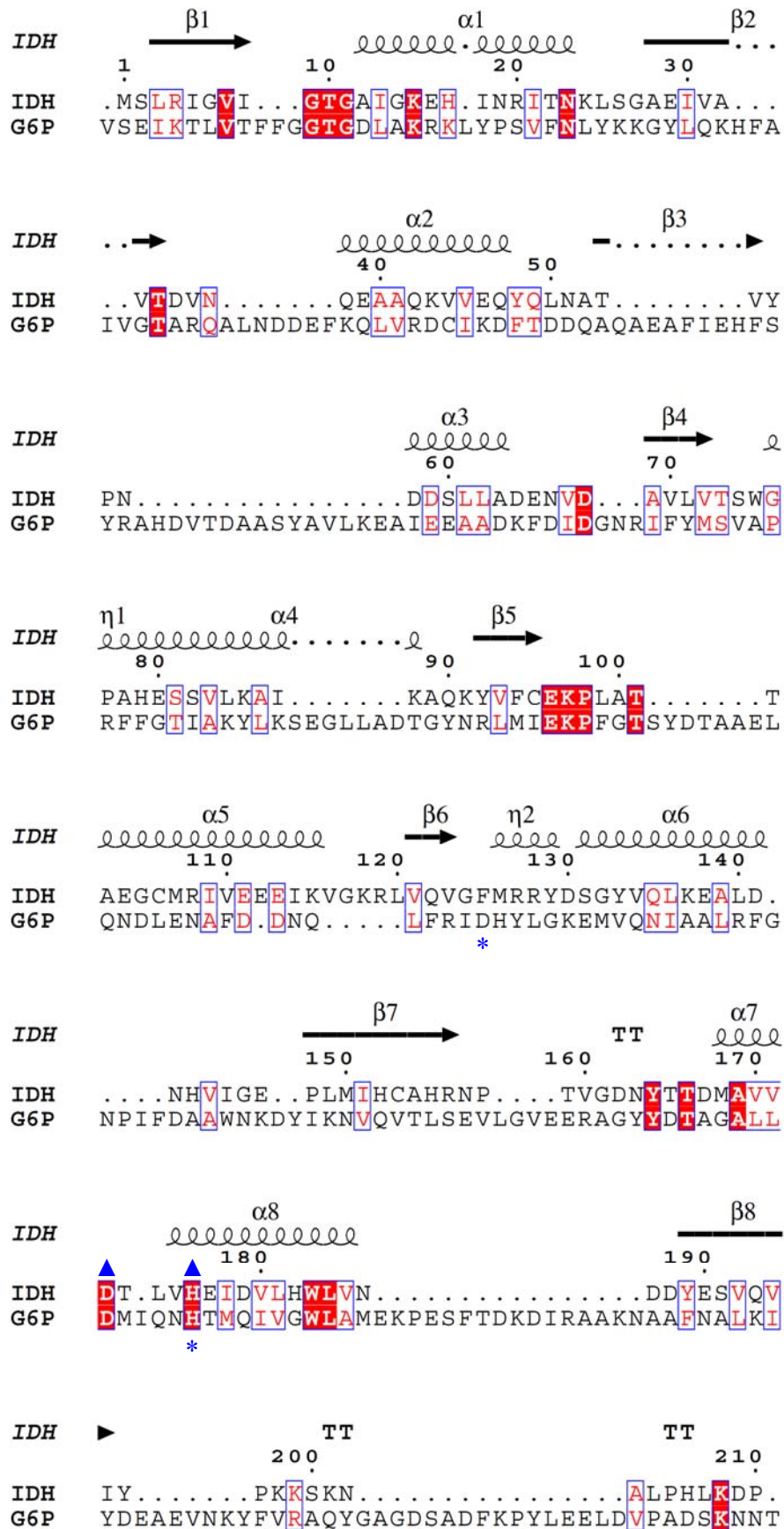


Figure 3.4 The model of one IDH monomer. One IDH monomer consists of two structural domains, they are N-terminal domain (residues1-123, α -helices colored red and β -strands colored yellow) and C-terminal domain (residues124-344, α -helices colored cyans and β -strands colored magenta). NADH and *myo*-inositol are given in stick representation. Atoms are shown in standard colors: grey for carbon, blue for nitrogen, orange for phosphorus, red for oxygen. Image was generated using PyMOL⁶⁸.

3.4.2 Structure alignment and implications

Comparisons of the primary structure of IDH from *B. subtilis* with those of SDRs and MDRs reveal that IDH is not a member of either superfamily although IDH is made up of 344 residues which is in the range of MDRs. However, IDH demonstrates 11% sequence identity with glucose 6-phosphate dehydrogenase (GPDH) from *Leuconostoc mesenteroides* that is claimed to belong to LDRs^{40,56}. Structure alignment (**Figure 3.5** and **3.6**) shows that 279 out of 344 amino acid residues of IDH can be superimposed onto corresponding residues in GPDH with root mean square (RMS) deviation difference in C α atomic positions of 3.3 Å. Furthermore, it was reported that GPDH employs a His-Asp catalytic dyad mechanism (His240 and Asp177)¹³³, and general base His240 is structurally aligned precisely with His176 in IDH. It implicates that IDH might be a member of LDRs. Unfortunately, the secondary residue, Asp172 of IDH, can not be aligned with Asp177 of GPDH (**Figure 3.5**).



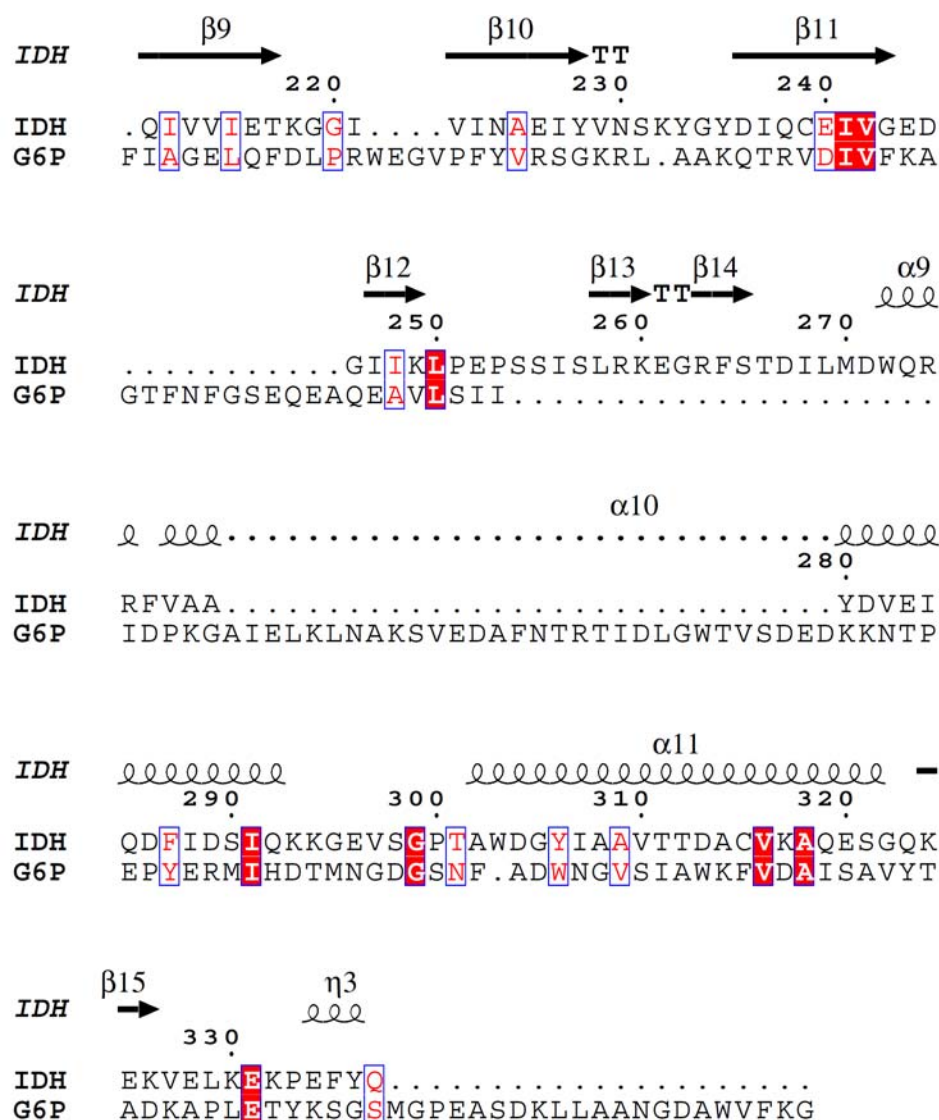


Figure 3.5 Structure alignment of IDH from *B. subtilis* and GPDH from *L. mesenteroides*. GPDH is labeled as G6P. Red highlighted residues are identical residues; the residues written in red are similar residues. Residues His240 and Asp177 of GPDH are indicated with *, Asp172 and His176 of IDH are indicated with ▲. The structure alignment was performed by SEQUOIA¹³⁴, and generated using ESPrpt 2.2⁷⁷.



Figure 3.6 The structure alignment of the crystal structures of GPDH from *L. mesenteroides* (PDB code: 1DPG, blue) and IDH from *B. subtilis* (red). Structures are superimposed using Dali server, and the image was generated using PyMOL⁶⁸.

A fold similarity search of the protein data bank (PDB) using the Dali server revealed the structures homologous to IDH¹³⁵, and the results were sorted by Z-score. The top eight structures and GPDH were chosen for comparison with IDH. The information of these nine enzymes is listed in **Table 3.4**, in which, only glucose-fructose oxidoreductase (GFOR) from *Zymomonas mobilis* and glucose 6-phosphate dehydrogenase (GPDH) from *Leuconostoc mesenteroides* have been characterized in terms of structure-function relationships.

Table 3.4 Nine of IDH homologous enzymes. These enzymes are obtained by searching with Dali server in RCSB protein data bank and are sorted by Z score.

	PDB code	Z score	RMSD	aligned amino acids	identity%	annotation and deposit year
1	3EC7	48	0.9	336/336	49	NAD-dependent putative dehydrogenase from <i>Salmonella typhimurium</i> , 2008
2	3EZY	38	1.9	319/334	30	putative dehydrogenase from <i>Thermotoga maritima</i> , 2008
3	3CEA	36	2.6	323/342	23	NAD-dependent <i>myo</i> -inositol 2-dehydrogenase (IolG) from <i>Lactobacillus plantarum</i> WCFS1, 2008
4	2GLX	32	2.7	301/332	23	NADP-dependent 1,5-anhydro-D-fructose reductase from <i>Sinorhizobium morelense</i> , 2006
5	3EUW	36	2.2	317/333	24	<i>myo</i> -inositol dehydrogenase from <i>Corynebacterium glutamicum</i> , 2008
6	3DB2	33	2.5	301/347	17	putative NADP-dependent oxidoreductase from <i>Desulfitobacterium hafniense</i> , 2008
7	1OFG	30	3.0	303/381	15	NADP-dependent glucose-fructose oxidoreductase from <i>Zymomonas mobilis</i> , 1996
8	1ZH8	30	3.2	295/325	23	NADP-dependent oxidoreductase from <i>Thermotoga maritima</i> , 2005
9	1DPG	18	3.3	279/485	11	NADP-dependent glucose 6-phosphate dehydrogenase from <i>Leuconostoc mesenteroides</i> , 1994

The multiple structure alignment of IDH and the top eight enzymes is shown in **Figure 3.8**. From this comparison, several conserved regions are identified. First, a characteristic glycine rich motif GXGXXG(A), which is thought to be part of coenzyme binding site, is found in the β 1-L1- α 1 region of Rossmann fold of these enzymes¹³⁶. IDH contains the consensus sequence GXGXXG and they are numbered 9-14. The first Gly residue is important for a sharp turn of the loop between β 1 and α 1. The second Gly residue allows a close contact between the protein back bone and the diphosphate of the coenzyme. The third Gly residue is replaced by Ala when the coenzyme is NADP instead of NAD, and Hanukoglu *et al.* postulated GX₁₋₂GX₁₋₂A as a consensus motif for NADP binding proteins¹³⁷. This Ala in place of the third glycine residue along with the larger hydrophobic residues in the contact area between α 1 and β 1 are proposed to widen the coenzyme binding pocket and make more space to accommodate the additional 2'-phosphate group of NADP¹³⁸.

Second, an Asp/Ser is located 19 or 20 residues downstream of the glycine motif, GXGXXGX₁₉₋₂₀D(S). Asp35 (numbered from IDH), on the loop between β 2 and α 2 of Rossmann fold, may act as the direct coenzyme specificity determinant, which discriminates NAD from NADP by forming hydrogen bonds with the 2'- and 3'-hydroxyl groups of the adenosine ribose of NAD and repelling phosphate at the 2'-position of the adenosine ribose of NADP, as reported previously^{139,140}. Some enzymes possess dual specificity, binding both NAD and NADP. In these cases, normally Ser occupies that position (Asp/Ser), which can form hydrogen bonds with either coenzyme. Therefore, it is likely that *LpIolG1*, containing Ala at the corresponding Asp35 position, is a dual specificity enzyme although the protein contains NAD⁺ as a tight binding coenzyme since purification.

Third, motif EKP (residues 96-98, numbered from IDH) is strictly conserved in all these sequences, which indicates it might have some critical structural or functional role(s). Wiegert *et al* reported this motif as a putative fingerprint for a novel class of sugar dehydrogenases that are able to react with substrates structurally similar to glucose⁷⁵. Examination of the crystal structures of these homologous enzymes shows the EKP motif is close to the oxidation-reduction reaction center. In addition, Lys is a frequently utilized catalytic center in dehydrogenases, especially in short chain dehydrogenases^{50,141}. As a consequence, it is possible that the Lys residue of EKP is involved in the catalytic mechanism. The structural orientations of EKP in five homologous enzymes in **Table 3.4** (PDB code: 1OFG, 3EC7, 3CEA, 2GLX and 1ZH8) that complexed with coenzymes NAD/NADP and IDH complexed with NAD have been compared. The coenzymes demonstrate very similar orientation at the nicotinamide end (**Figure 3.7**). However, the adenosine monophosphate (AMP) moieties of GFOR (yellow carbon) and AFR (green carbon) display different orientations from the others. The well conserved motif EKP is proposed to interact with nicotinamide to guide the binding orientation. The Glu residue forms a hydrogen bond with the carbonyl amide group of the nicotinamide ring. A peptide bond between Lys and Pro displays a *cis* conformation that might be important for the correct binding mode of the nicotinamide ring and the substrate⁷¹. The Lys residue is close to the nicotinamide ring and is believed to form a cation- π interaction¹⁴². And the Lys residue also can form hydrogen bonds with 2'-, 3'- hydroxyl of the nicotinamide ribose.

Fourth, it was reported that GFOR employed the catalytic dyad mechanism in which the Asp265 residue deprotonates Tyr269, allowing Tyr269 to abstract a proton from the substrate⁷⁴. This Tyr269 aligns precisely with a His residue in the rest of the sequences, and this His may act as an acid-base catalytic residue. On the other hand, Asp265 is conserved through these nine sequences. Therefore, the catalytic dyad, Asp

and His (Asp172, His176, numbered from IDH, indicated with ▲ in **Figure 3.8**), is highly conserved, which is consistent with the theory that a similar mechanism is utilized by homologous enzymes. However, on the basis of IDH ternary complex structure (non-productive mode), the distance between His176 and Asp172 has been found to be too far away to form a hydrogen bond (~ 7.8 Å). Indeed, the strengthening of this hydrogen bond interaction is regarded as an important structural aspect of catalytic dyad mechanism.

Finally, three Gly residues (Gly147, Gly220, Gly243, numbered from IDH) are strictly conserved in the C-terminal domain of these nine enzymes, in which there is no significant sequence identity, perhaps due to the substrate diversity.

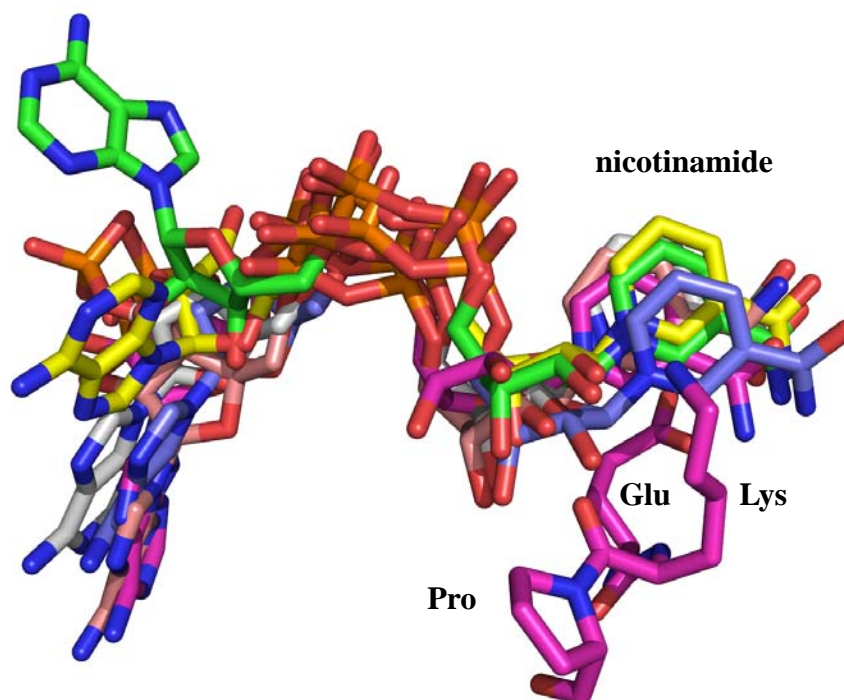


Figure 3.7 Comparison of coenzyme (NAD or NADP) binding mode in IDH (magenta carbon), GFOR from *Z. mobilis* (PDB code: 1OFG, yellow carbon), AFR from *S. morelense* (PDB code: 2GLX, green carbon), and a putative oxidoreductase from *T. maritima* (PDB code: 1ZH8, grey carbon), putative dehydrogenase from *S. typhimurium* (PDB code: 3EC7, cyan carbon), IolG1 from *L. plantarum* (PDB code: 3CEA, purple carbon) by superimposing the backbones of complexed structures. The molecules of NAD/NADP are indicated in sticks (nitrogen colored blue; oxygen colored red; phosphorus colored orange). In order to show a clear picture, only motif EKP of IDH is shown. Image was generated using PyMOL⁶⁸.

β1 →

IDH

		1	10
		.	*.*
<i>IDH</i>MS	LRI	GVI
<i>3EC7</i>MT	LKA	GIV
<i>3EZY</i>S	LRI	GVI
<i>3CEA</i>TRKP	LRA	AI
<i>2GLX</i>NRW	G	LI
<i>3EUW</i>LT	LRI	AL
<i>3DB2</i>MYNP	VG	VA
<i>1OFG</i>	ATLPAGASQVPTTPAGRMPYAIRPMPEDRRFGYA	IV	GL
<i>1ZH8</i>LRK	IRL	GIV

α1 β2 α2

IDH

	000000000000	30	40	50
	*		*	
<i>IDH</i>	AIGKEHINRITNKL.SGAEIVAVTDVNQEA	AQKVVEQYQ	L	
<i>3EC7</i>	MIGSDHLRRLANTV.SGVEVVAVCDIVAGRA	QAALDKYA	I	
<i>3EZY</i>	RIGTIHAENLK.MI.DDAILYAISDVREDRL	REMKEKLG	V	
<i>3CEA</i>	RLGERHARHLVNKI.QGVKLVAA	CALDSNQ	LEWAKNELG	V
<i>2GLX</i>	TIAREWVIGAIRAT..GGEVVSMMSTSAERGA	AAYATENG	I	
<i>3EUW</i>	RIGHVHAANIA.AN.PDLELVVIADPFIEGA	AQRLAEANG	A	
<i>3DB2</i>	RWAYVMADAYT.KS.EKCLKLVTCYSRTEDKRE	KFGKRYNC		
<i>1OFG</i>	KYALNQILPGFAGC.QHSRIEALVSGNAEK	AKIVAAEYG	V	
<i>1ZH8</i>	IAARELHLPALKNLSHLFEITAVTSRTRSH	AEEFAKMVG.		

β3 α3 β4 η1 α4

IDH

	60	70	80
<i>IDH</i>	NAT.VYP..NDDSLLADENVDAVLVTSWGP	HAESSVLKAI	
<i>3EC7</i>	EAK.DYN..DYHDLINDKDVVVIIITASNEA	HADVAVAAAL	
<i>3EZY</i>	E.K.AYK..DPHELIEDPNVDAVLVCCSSTNT	HSELVIAC	
<i>3CEA</i>	E.T.TYT..NYKDMIDTENIDAFIVAPT	TPFHPEMTIYAM	
<i>2GLX</i>	G.K.SVT..SVEELVGDPDVDAVYVSTTNEL	HREQTLAAI	
<i>3EUW</i>	..E.AVA..SPDEVFARDDIDGIVIGSP	TSTHVDLITRAV	
<i>3DB2</i>	..A.GDA..TMEAALLAREDVEMVITV	NDKHAEVIEQCA	
<i>1OFG</i>	DPRKIYDYSNFDKIAKDPKIDAVYIILP	NSLHAEFAIRAF	
<i>1ZH8</i>	NPA.VFD..SYEELL	ESGLVDAVDLTLPVELNL	LPFIEKAL

β5 α5 β6 η2

IDH

	90	100	110	120
		***		*
<i>IDH</i>	KAQKYVFCEKPLATTAE	GC	MRIV	EEEEIKVGKRLVQVGF
<i>3EC7</i>	NANKYVFCEKPLAVTA	ADCQR	VI	EAEQKNGKRMVQIG
<i>3EZY</i>	KAKKHVFCEKPLSLN	LADVDR	MI	EETKKADV.I
<i>3CEA</i>	NAGLNVFCEKPLGLD	FNEVDE	MA	KVIKSHPNQIFQSG
<i>2GLX</i>	RAGKHVLCEKPLAMT	LEDARE	MV	VAAREAGV.V
<i>3EUW</i>	ERGIPALCEKPI	DL	I	EMVRACK
<i>3DB2</i>	RSGKHIYVEKPI	SVSL	DHAQR	IDQVIKETGV.K
<i>1OFG</i>	KAGKHVMCEKPM	ATS	V	ADCQR
<i>1ZH8</i>	RKGVHVI	CEKPI	STD	VETGKKVV

$\alpha 6$ $\beta 7$
IDH 130 140 150 160 T
 IDH RYDSGYVQ LKEALDNHVI GEPLM IHCAHRNP..TV...GD
 3EC7 RYDKGYVQ LKN IIDS GEIGQPLMVHGRHYNA..ST...VP
 3EZY RFDRNFKK LKEAVENGTIGKPHVLRITSRDP..APP..PL
 3CEA RYDDSYRY AKKIVDNGDIGKIIYMRGYGIDP..ISG..ME
 2GLX RNAAAHRAMRD AIAEGRIGRPIAARVFAVYLPPHL..QG
 3EUW RFDPSFAA INARVANQEIGNLEQLVIIISRDPA..APA..PK
 3DB2 RRLGALRK MKEMIDTKEIGEVSSI EAVFSNERGLEL..KK
 1OFG HYDPMNRA AVKLI RENQLGKLGMVTTDNSDVMQNDPAQQ
 1ZH8 RHVPFAFWK AKELVESGAIGDPVFMNWQIWVGMDENNKYVH

$\alpha 7$ $\alpha 8$ $\beta 8$
IDH T 170 180 190
 IDH NYT....TDM..AVVDTLVHEIDVLHHLVND DYESVQVI
 3EC7 EYK....TPQ..AIYETL IHEIDVMHWLLNEDYKTVKVY
 3EZY DYI....RVS GGIFLDMT IHD FDMARYIMGEVEEVFAD
 3CEA SFTKFATEADS GGIFVDMN IHDIDLIRWFTGQDPVQAYGL
 2GLX WRLERP..EAG GGIVLDITVHDADTLRFVLND DPAAEVAI
 3EUW DYI....AGS GGIFRDMT IHD LDMARFFVP.NIVEVTAT
 3DB2 GNWRGEPATAP GGPLTQLGVHQIDNLQFLLG.PVARVFNF
 1OFG WRLR..RELAG GGSLMDIGIYGLNGTRYLLGE EPIEVRAY
 1ZH8 T.DWRKKPKHV GGFLSDGGVHHAAAMRLILG.EIEWISAV

$\beta 9$ $\beta 10$
IDH TT T...T 200 210 220 230
 IDH YPKKSKNALP...HLKDPQIVV IETKG GIVINAEIYVNSK
 3EC7 FPRQSSLVT...TLRDPQLVVMETTSGINIVVEVFVNCQ
 3EZY G.SVLVDEEIGKAGDVDTAVVVLRFKSGALGVIDNSRRAV
 3CEA T.SNIAAPQLADIGEFETGVAQLKMSDGV IATLIGGRHAA
 2GLX S.HSAGMGK...EGVEDGVMGVLRFQSGVIAQFHDAFTTK
 3EUW G.ANVFSQEIAEFNDYDQVIVTLRGSKGELINIVNSRHCS
 3DB2 G.KPMYTEV...ENITVNQTLLEFEDGKQAYLGTNWACP
 1OFG T.YSDPNDERF.VEVEDRIIWQMRFRSGALSHGASSYSTT
 1ZH8 A.KDLSPLL...GGMDFLSSIFEFEFGTVGNYSYSYSLK

$\beta 11$ $\beta 12$ $\beta 13$ $\beta 14$
IDH 240 250 260 TT
 IDH YGYDIQC EIVGEDGI IKL.PEPSS..ISLRKEGRF.ST.D
 3EC7 YGYDIHC DVTGEKGMAEL.PTVAS..AAVRKAAKY.ST.D
 3EZY YGYDQRI EVFGSKGRIFA.DNVRETTVVLTDQGD.RGSR
 3CEA HGNQVEL EVMGSNGWVRI GEHPDLNRVTVFNDQGV.VR.P
 2GLX F.AETGF EVHGTGSLIG.RN.....
 3EUW YGYDQRL EAFGSKGMLAA.DNIRPTTVRKHNAESTEQAADP
 3DB2 ..GVFSINVYGTKANLFYQLD.....
 1OFG ..TTSRFSVQGDKAVLLMDPATG.....
 1ZH8 G..NERF EITGTKGKISISWD.....

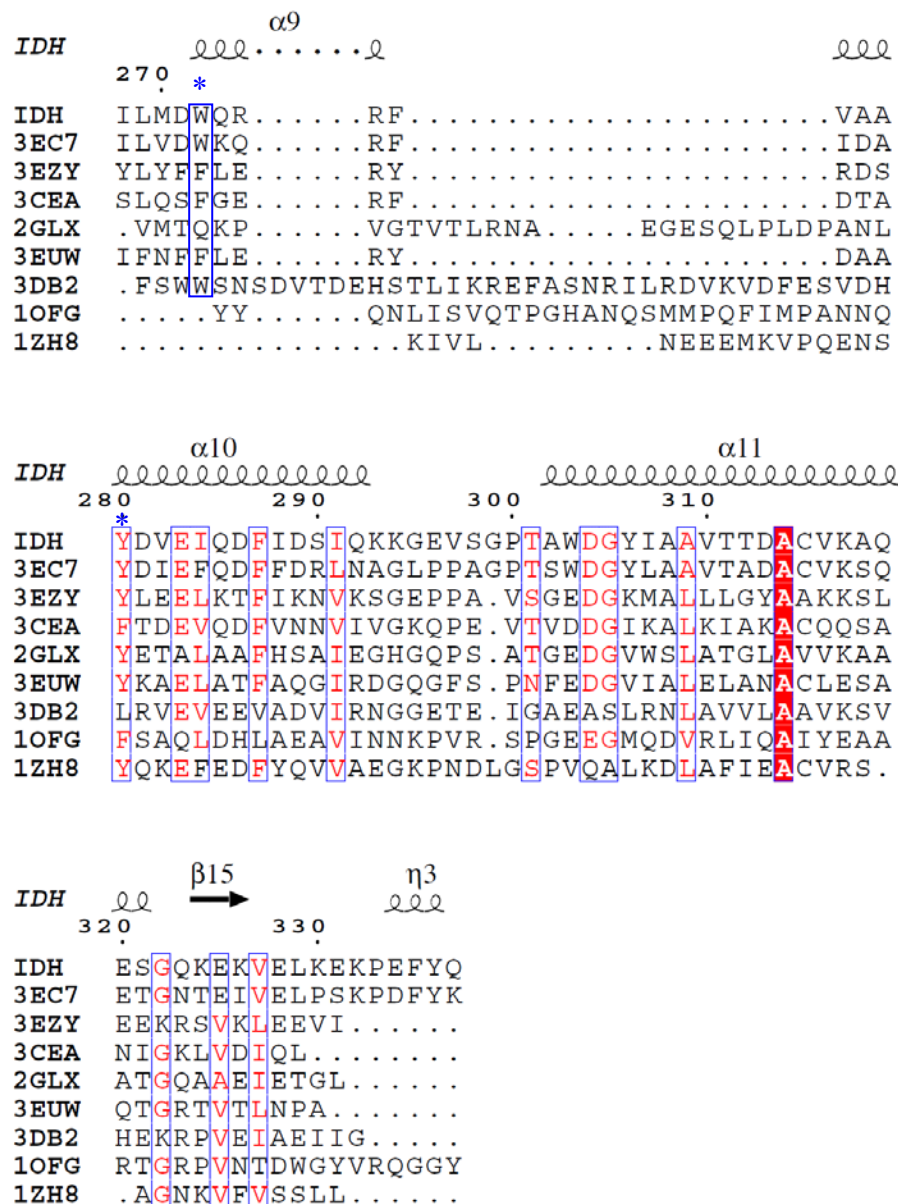


Figure 3.8 Multiple structure-based sequence alignment of IDH from *B. subtilis* and its homologs.

IDH: *myo*-inositol 2-dehydrogenase from *B. subtilis*; 3EC7: dehydrogenase from *S. typhimurium*; 3EZY: dehydrogenase from *T. maritima*; 3CEA: *myo*-inositol 2-dehydrogenase (IolG1) from *L. plantarum*; 3EUW: *myo*-inositol dehydrogenase from *C. glutamicum*; 3DB2: oxidoreductase from *D. Hafniense*; 2GLX: 1,5-anhydro-D-fructose reductase from *S. morelense*; 1OFG: glucose-fructose oxidoreductase from *Z. mobilis*; 1ZH8: oxidoreductase from *T. maritima*. The structure alignment was performed by SEQUOIA¹³⁴, and generated using ESPrnt 2.2⁷⁷. Red highlighted residues are identical residues; the residues written in red are similar residues. The other important residues are indicated with *.

3.4.3 Alteration of coenzyme specificity

3.4.3.1 Overview of alteration of coenzyme specificity

NADP differs structurally from NAD only by an additional phosphate group esterified to the 2'-hydroxyl group of adenosine (**Figure 1.5**). As a consequence, the discrimination between NAD and NADP is an impressive example of the power of substrate recognition with enzymes. Since a large number of complex structures of NAD/NADP-dependent dehydrogenase are known, it provides a significant amount of structural data to analyze the discrimination. A better understanding of the protein-coenzyme interactions will contribute interesting results for protein engineering and redesign studies. Recently, the usage of enzymes as catalysts to synthesize chemicals has brought many challenges, such as developmental costs of biocatalysts as enzymes often require one or more costly cofactors. For example, NADP-dependent 2,5-diketo-D-gluconic acid reductase is a valuable catalyst for vitamin C production, but NADP is too expensive (nearly \$500/mmol) to use in industry. Researchers tried to engineer this enzyme to NAD-dependent, which is more stable and less expensive (nearly \$100/mmol)¹⁴³. Regeneration of NADP/NAD thus became a challenge to allow addition of catalytic amount. So far, engineered formate dehydrogenase is the most successful example for this regeneration system¹⁴⁰.

A lot of work has been done to investigate the coenzyme specificity-determining region in dehydrogenase^{39,139,144}. These studies have provided some common features of NAD- or NADP-dependent enzymes. Both NAD and NADP generally bind to enzymes that have domains folded in a Rossmann-type fold. In these binding domains, the N-terminal half involved in binding the adenosine diphosphate (ADP) moiety is less variable than the C-terminal half that binds nicotinamide moiety since the residues

around nicotinamide are substrate-dependent³⁹. It was reported that the negatively charged Asp or Glu residue at the consensus motif GXGXXGX₁₇₋₁₈D(E) is thought to play a significant role in coenzyme specificity for NAD by forming hydrogen bonds to both of the 2'- and 3'-hydroxyls of the adenosine ribose, whereas NADP-specific dehydrogenases typically have a positively charged residue Arg whose side chain faces the adenine plane to interact with 2'-phosphate by electrostatic interaction and hydrogen bonding, and also form cation- π stacking interactions with the adenine ring¹⁴⁰. The Asp or Glu residue is therefore the fingerprint to discriminate NAD and NADP recognition. The Arg residue can help stabilize NADP but it is not a necessary residue. In many cases, Arg is substituted by other residues, such as Ser or His, and the interaction with NADP is mediated by water molecules¹⁴⁴. Despite many attempts in mutagenic and structural analysis, alteration of coenzyme specificity remains a challenge since there is no clear recipe for completely switching specificity. To my knowledge, 15-hydroxyprostaglandin dehydrogenase (15-PGDH) is the only enzyme reported whose coenzyme specificity switched strictly from NAD to NADP¹⁴⁵. *myo*-Inositol 2-dehydrogenase (IDH) from *B. subtilis* is highly specific to NAD and fails to catalyze the reaction with NADP as the coenzyme. In order to learn more about coenzyme recognition, the wild-type IDH is engineered in an attempt to improve its ability to use NADP as the coenzyme by means of site-directed mutagenesis.

3.4.3.2 Alteration of specificity on the basis of sequence alignment

Gly14, Asp35

To identify amino acid residues that account for the coenzyme specificity of IDH, in the beginning, the choice of the mutations to be introduced into IDH was based on the sequence alignment with GFOR, a well characterized homolog at the time this work

was initiated. GFOR, which shares 18% sequence identity with IDH, is a strictly NADP-dependent enzyme. It was reported that the single mutation of Ser116 to Asp converted the strict NADP specificity of wild-type GFOR to a dual NAD/NADP specificity enzyme⁷⁵. Examination of the complex structure of S116D shows that Asp116 is the residue which forms hydrogen bonds with 2'-, 3'- hydroxyls of ribose at the adenine end is found in many NAD-dependent enzymes⁷⁰.

Sequence alignment of GFOR and IDH (**Figure 1.11**) revealed the two residues Gly14 and Asp35 in IDH which are corresponding residues of Ala95 and Ser116 could account for the observed coenzyme specificity of IDH⁷⁵. The $\beta\alpha\beta$ dinucleotide-binding fold fingerprint sequence GXGXXA in the NADP binding region of GFOR is changed to GXGXXG in the NAD binding region of IDH. Gly14 is the last residue in the GXGXXG fingerprint in IDH. Hanukoglu *et al* postulated GXGXXA as a consensus motif for NADP binding proteins¹³⁷. This Ala residue along with the larger hydrophobic residues in the contact area between $\alpha 1$ and $\beta 1$ are proposed to widen the coenzyme binding pocket and make more space to accommodate the additional 2'-phosphate group of NADP¹³⁸. It has been reported that a single mutation Ala13 to Gly of 1,5-anhydro-D-fructose reductase (AFR) exhibited dual coenzyme specificity to both NAD and NADP while wild-type AFR is strictly NADP-dependent⁸⁵. Ser116 of GFOR, located 21 residues downstream from the end of the fingerprint sequence GXGXXA, is displaced in NAD-binding enzyme IDH with Asp (numbered 35 in IDH). The Asp35 residue probably prevents NADP binding either by charge repulsion interaction or by steric hindrance with the adenosyl 2'-phosphate group.

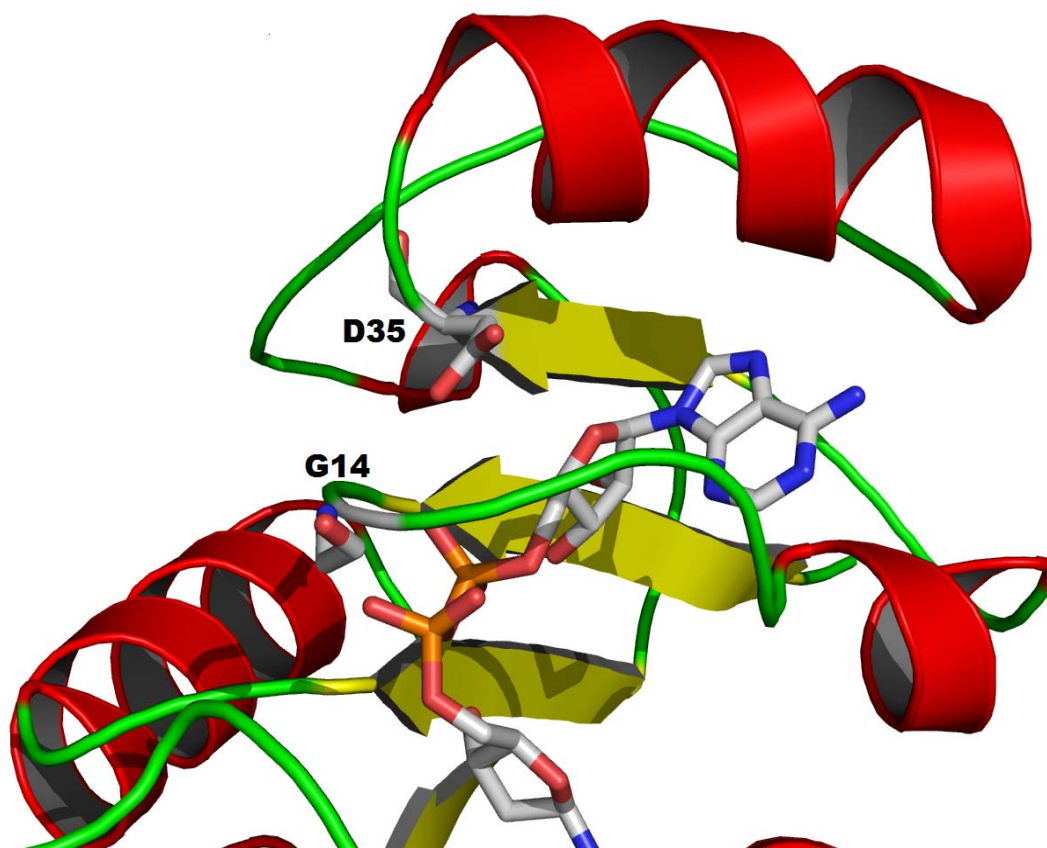


Figure 3.9 The model of N-terminal of IDH homology model with Gly14 and Asp35. Amino acid residue Gly14 and Asp35, and part of coenzyme NADH are indicated in sticks (oxygen in red, nitrogen in blue, phosphorus in orange, carbon in grey). Image was generated using PyMOL⁶⁸.

The relative position of the two residues Gly14 and Asp35 in the IDH homology model (**Figure 3.9**), in which NADH was docked manually, is consistent with the above hypotheses. Therefore, site-directed mutagenesis studies on the residues Gly14 and Asp35 were carried out to generate single and double mutants (G14A, D35S, and G14A/D35S) and the ability of these mutants for utilizing both NAD^+ and NADP^+ as their coenzyme were measured, and the results are shown in **Table 3.5**. A single mutation Asp35 to Ser, substituted with a relatively small and uncharged side-chain,

alters the strict NAD coenzyme specificity of wild-type IDH to dual specificity for either NAD or NADP, suggesting that Asp35 might be the fingerprint which can discriminate NAD from NADP as a coenzyme. The mutant G14A is almost inactive with coenzyme NADP^+ , and the double mutant G14A/D35S presents worse activity with either NAD^+ or NADP^+ as a coenzyme than the single mutant D35S. Therefore, replacement of Gly14 leads no coenzyme alteration and this result is not consistent with the corresponding studies on GFOR and AFR^{75,85}. Interestingly, mutant D35S demonstrates positive cooperativity (Hill constant $h = 2$) with NADP^+ , and no positive cooperativity ($h = 1$) with NAD^+ was observed. Double mutant G14A/D35S demonstrates positive cooperativity ($h = 2$) with both NAD^+ and NADP^+ . In this situation, when the coenzyme binds to one monomer of an active tetramer, the other monomer is stimulated, allowing the second coenzyme to bind more easily (D35S and G14A/D35S are assumed to follow compulsory ordered Bi Bi mechanism as wild type IDH since random ordered Bi Bi mechanism could demonstrate sigmoidal curve. The sigmoidal plots of D35S with NADP^+ and G14A/D35S with NAD^+ and NADP^+ are shown in Appendix 4).

The IDH-NADH complexed structure was solved thereafter, which let us revise some of our predictions. Examination of the complex structure reveals that the AMP moiety in IDH displays different orientation from those in GFOR and AFR. However, Asp35 is located near the adenosine ribose and is able to chelate the diol of the ribose near the adenine as previously proposed (**Figure 3.10**). It thus can be concluded that Asp35 is the key residue to discriminate NAD and NADP. On the other hand, Gly14 is not on the loop between $\beta 1$ and $\alpha 1$ as predicted by homology model, this residue exists in the $\alpha 1$ -helix instead. It is therefore not surprising that the substitution of Gly14 is not able to affect the coenzyme specificity.

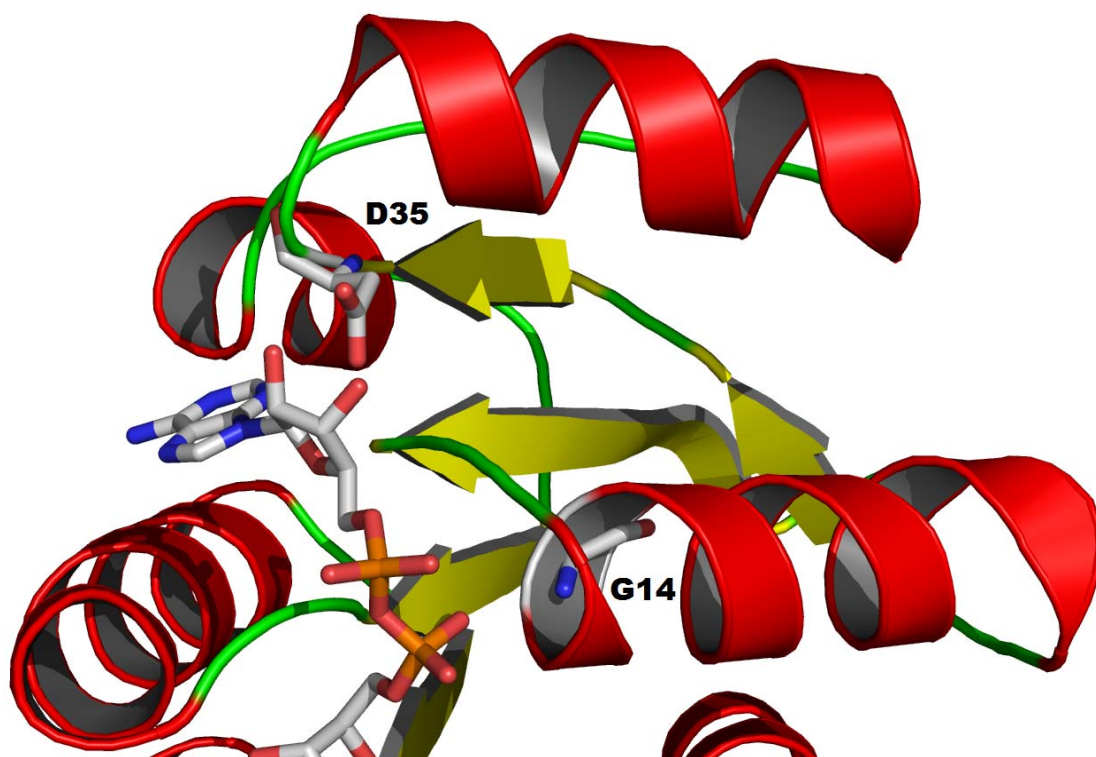


Figure 3.10 The model of N-terminal NADH-IDH complex structure with Gly14 and Asp35. Amino acid residue Gly14 and Asp35, and part of coenzyme NADH are indicated in sticks (oxygen in red, nitrogen in blue, phosphorus in orange, carbon in grey). Image was generated using PyMOL⁶⁸.

Table 3.5 Kinetic constants for the mutants D35S, G14A, and G14A/D35S.

Enzymes		$K_m(\text{NAD(P)}^+)$ (mM)	$K_m(\text{inositol})$ (mM)	V_{\max} ($\mu\text{mol} \cdot \text{min}^{-1} \cdot \text{mg}^{-1}$)	k_{cat} (s^{-1})	$k_{\text{cat}}/K_m^{\text{NAD(P)}^+}$ ($\text{s}^{-1} \cdot \text{mM}^{-1}$)	$\frac{k_{\text{cat}}/K_m^{\text{NAD(P)}^+}}{k_{\text{cat}}/K_m^{\text{NAD}^+}}$
wild-type IDH		0.08 ± 0.01	4.4 ± 0.5	62 ± 2	42 ± 2	525	0
D35S	NAD^+	1.7 ± 0.1	22 ± 7	223 ± 6	150 ± 4	89	0.6
	NADP^+	2.3 ± 1.0	809 ± 261	170 ± 43	114 ± 29	50	
G14A	NAD^+	0.15 ± 0.02	4.7 ± 0.9	45 ± 1	30 ± 1	200	-
	NADP^+	trace activity					
G14A/D35S	NAD^+	3.4 ± 2.9	259 ± 71	47 ± 6	32 ± 4	10	0.1
	NADP^+	30 ± 16	190 ± 90	39 ± 17	26 ± 11	0.9	

Conditions: 100 mM Tris-HCl, pH 9.0, 25°C.

3.4.3.3 Alteration of specificity on the basis of crystal structure

Gly11, Ala12, and Val36

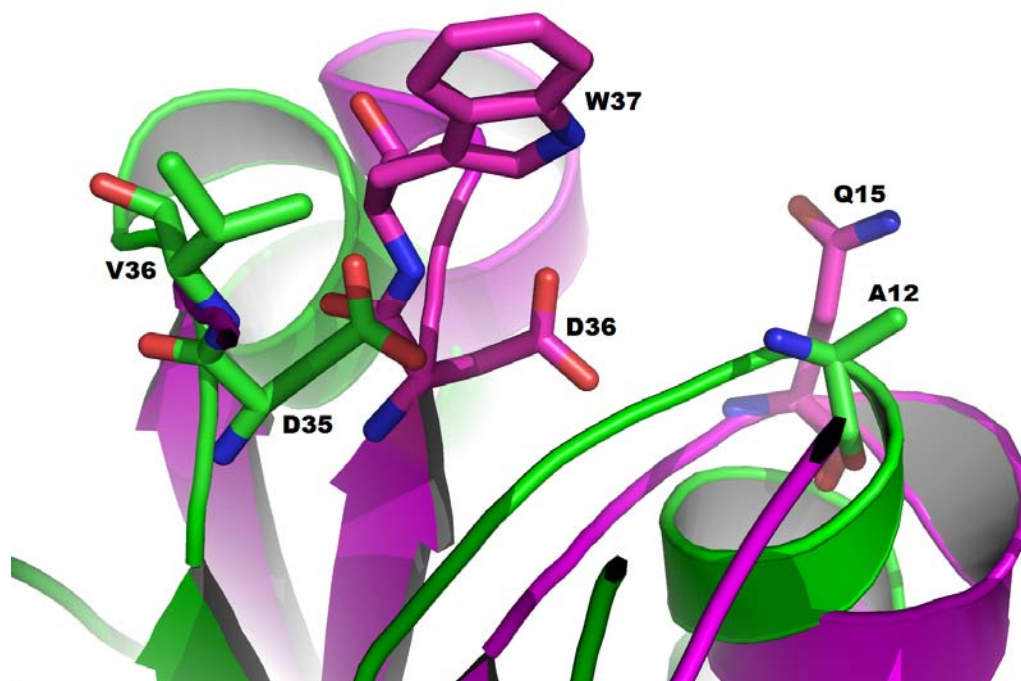


Figure 3.11 Structure alignment of *apo*-IDH from *B. subtilis* and human 15-PGDH. IDH is indicated in green; 15-PGDH is indicated in magentas. The selected amino acid residues, Gln15, Asp36, and Trp37 of 15-PGDH corresponding to Ala12, Asp35, Val36 of IDH, are indicated in sticks. Image was generated using PyMOL⁶⁸.

15-Hydroxyprostaglandin dehydrogenase (15-PGDH)¹⁴⁵, a strictly NAD-dependent short chain dehydrogenase, is the only enzyme reported to have its coenzyme specificity switched completely to NADP. Although 15-PGDH is a member of SDRs, the Rossmann fold is well-conserved throughout dehydrogenases. 15-PGDH provides therefore an interesting model for investigating conversion of coenzyme specificity for dehydrogenases. This complete alteration was accomplished by a triple mutant Q15K/D36S/W37R in which hydrogen bonding, cation- π , and electrostatic interactions were introduced to establish potential interactions with NADP¹⁴⁵. As the crystal

structure of 15-PGDH was deposited in the protein data bank and *apo*-IDH structure was solved at that time, structure alignment with *apo*-IDH and 15-PGDH (PDB code: 2GDZ) was employed to predict the crucial residues which could convert the coenzyme specificity (**Figure 3.11**). On the basis of this structure alignment, the corresponding residues Ala12, Asp35, and Val36 in IDH were postulated to play the same roles as Gln15, Asp36, and Trp37 in 15-PGDH. Furthermore, Gln15 and Ala12 exit at the beginning of α 1 and Asp36, Trp37, Asp35, and Val36 exit on the loop between β 2 and α 2 of both Rossmann fold domains of 15-PGDH and IDH, respectively. Therefore, similar mutants, A12K/D35S, D35S/V36R, and A12K/D35S/V36R of IDH, were constructed. In addition, Gly11 of IDH, instead of Ala12, also could be aligned with Gln15 of 15-PGDH. Thus, Lys was introduced at this site and the corresponding mutants G11K/D35S and G11K/D35S/V36R were generated. Subsequently, the coenzyme specificities of these five mutants were measured and the kinetic constants are shown in **Table 3.6**.

The mutants G11K/D35S and G11K/D35S/V36R lose all dehydrogenase activity with both NAD^+ and NADP^+ . One reason might be that the substitution at site 11 in these two mutants ruins the fingerprint motif GXGXXG and further disturbs the Rossmann fold. Another possibility is that the longer side chain of Lys11 blocked NAD or NADP from binding since examination of the IDH-NADH complex structure shows the sidechain of Gly11 is pointing towards the diphosphate of NAD.

When Ala12, which is on the loop between β 1 and α 1 of IDH, was mutated to a positively charged residue Lys, the K_m values for both NAD^+ and NADP^+ decreased (the kinetic data shown in **Table 3.5** and **Table 3.6**, D35S/V36R vs A12K/D35S/V36R, D35S vs A12K/D35S). It suggests that the long and positively charged side-chain of Lys might establish an ionic interaction with the diphosphate that stabilizes

NAD/NADP and thus the binding affinity increases. Introduction of Lys or Arg at site 12 is therefore likely to favourably modify electronic interaction in this region. By contrast, the structure alignment shows the residue Arg or Lys located in the corresponding Ala12 position of IDH in five other homologs (**Figure 3.8**, 3EZY, 3CEA, 3EUW, 3DB2, and 1OFG).

Removal of the negatively charged Asp35 by replacement with a Ser residue makes the K_m value for NAD^+ increase, but this mutant can recognize NADP^+ as a coenzyme. Consequently, amino acid residue Asp35 is identified as the direct coenzyme specificity determinant. Further substitution of Val36 to Arg (D35S/V36R) decreases the K_m value of NADP^+ from 2.3 mM to 0.16 mM, and increases the 7-fold preference for NADP^+ compared to the single mutant D35S [$[(k_{\text{cat}}/K_m)^{\text{NADP}^+}]_{\text{D35S/V36R}} / [(k_{\text{cat}}/K_m)^{\text{NADP}^+}]_{\text{D35S}} = 7$], indicating that further stabilization of NADP^+ by Arg was needed to increase the NADP specificity. Arg36 in mutant D35S/V36R is thus proposed as the typical residue whose side chain faces the adenine plane to interact with 2'-phosphate of NADP^+ , and whose guanidinium group forms a cation- π interaction with the adenine moiety of NADP as observed in other dehydrogenases¹⁴⁴.

Of the double/triple mutants, A12K/D35S/V36R demonstrates the lowest K_m value with NADP^+ , which is comparable to the K_m value of NAD^+ with wild-type IDH. A12K/D35S displays equal specificity with NAD^+ and NADP^+ [$(k_{\text{cat}}/K_m)^{\text{NADP}^+} / (k_{\text{cat}}/K_m)^{\text{NAD}^+} = 1.0$], and D35S/V36R and A12K/D35S/V36R display more preference for NADP^+ than NAD^+ [$(k_{\text{cat}}/K_m)^{\text{NADP}^+} / (k_{\text{cat}}/K_m)^{\text{NAD}^+} > 1.0$]. These mutants are obviously more successful in specificity alteration than that of the single mutant D35S [$(k_{\text{cat}}/K_m)^{\text{NADP}^+} / (k_{\text{cat}}/K_m)^{\text{NAD}^+} = 0.6$]. Particularly, the mutant D35S/V36R switches the coenzyme specificity of IDH from entirely NAD-dependent to a 6-fold preference for NADP^+ over NAD^+ [$(k_{\text{cat}}/K_m)^{\text{NADP}^+} / (k_{\text{cat}}/K_m)^{\text{NAD}^+} = 5.7$].

Table 3.6 Kinetic constants for the mutants G11K/D35S, G11K/D35S/V36R, D35S/V36R, A12K/D35S, and A12K/D35S/V36R.

Enzymes		$K_m(\text{NAD(P)}^+)$ (mM)	$K_m(\text{inositol})$ (mM)	V_{\max} ($\mu\text{mol} \cdot \text{min}^{-1} \cdot \text{mg}^{-1}$)	k_{cat} (s^{-1})	$k_{\text{cat}}/K_m^{\text{NAD(P)}^+}$ ($\text{s}^{-1} \cdot \text{mM}^{-1}$)	$\frac{k_{\text{cat}}/K_m^{\text{NAD(P)}^+}}{k_{\text{cat}}/K_m^{\text{NAD}^+}}$
wild-type IDH		0.08 ± 0.01	4.4 ± 0.5	62 ± 2	42 ± 2	525	0
G11K/D35S	NAD^+	no activity					
	NADP^+	no activity					
G11K/D35S/ V36R	NAD^+	no activity					
	NADP^+	no activity					
D35S/V36R	NAD^+	1.8 ± 0.2	7.4 ± 5.6	176 ± 15	118 ± 10	65	5.7
	NADP^+	0.16 ± 0.02	35 ± 4	88 ± 2	59 ± 2	369	
A12K/D35S	NAD^+	1.9 ± 0.3	16 ± 7	262 ± 7	176 ± 7	95	1.0
	NADP^+	1.7 ± 0.8	185 ± 91	227 ± 31	153 ± 21	93	
A12K/D35S/ V36R	NAD^+	1.2 ± 0.2	4.2 ± 0.6	206 ± 10	139 ± 7	116	4.9
	NADP^+	0.06 ± 0.01	24 ± 2	50 ± 2	34 ± 2	567	

Conditions: 100 mM Tris-HCl, pH 9.0, 25°C.

Ala40

Subsequently, the *holo*-IDH structure was solved. Examination of the structure found that Ala40 on $\alpha 2$, among the residues around the 2'-hydroxyl group of ribose of NAD, was another putative site with the potential to interact with 2'-phosphate of NADP (**Figure 3.12**). Thus, introducing a residue with a positively charged side-chain at this position was thought to be able to establish a potentially stabilizing ionic interaction with the nearby phosphate of NADP. The structure alignment in **Figure 3.8** shows that the residue Arg or Lys located at the corresponding Ala40 position in four homologs (1OFG, 3DB2, 2GLX, and 1ZH8) identified as NADP-dependent enzymes. The replacements of Ala40 with Lys and Arg were therefore carried out by means of site-directed mutagenesis, resulting in one double mutant D35S/A40K and two triple mutants D35S/V36R/A40K and D35S/V36R/A40R. Their ability to utilize NADP^+ and NAD^+ was measured and the results are presented in **Table 3.7**.

Steady-state kinetic analysis revealed a noticeable decrease of the K_m values of mutants D35S/A40K, D35S/V36R/A40K, and D35S/V36R/A40R for NADP^+ , compared to that of the parent mutants D35S and D35S/V36R. In particular, the mutant D35S/V36R/A40K displayed the lowest K_m value for NADP^+ (0.04 ± 0.01 mM). Therefore, a further stabilization of NADP may be achieved by replacing Ala with Lys/Arg. However, this mutant also showed the lowest k_{cat} for NADP^+ (14 s^{-1}). As a consequence, despite the fact that Lys with a long and charged side-chain might be an ideal amino acid for position 40 to bind NADP^+ , this substitution leads to a less productive binding of NADP^+ and thus results in a poor catalytic efficiency with NADP^+ .

Further analysis of kinetic constants showed that the three mutants (D35S/A40K, D35S/V36R/A40K, and D35S/V36R/A40R) displayed clear preference for NADP^+

over NAD^+ as their coenzyme [$2 < (k_{\text{cat}}/K_{\text{m}})^{\text{NADP}^+}/(k_{\text{cat}}/K_{\text{m}})^{\text{NAD}^+} < 4$]. The double mutant D35S/A40K displays a shift in its coenzyme specificity towards NADP^+ compared to the parent mutant D35S ($[(k_{\text{cat}}/K_{\text{m}})^{\text{NADP}^+}/(k_{\text{cat}}/K_{\text{m}})^{\text{NAD}^+}]_{\text{D35S/A40K}}/[(k_{\text{cat}}/K_{\text{m}})^{\text{NADP}^+}/(k_{\text{cat}}/K_{\text{m}})^{\text{NAD}^+}]_{\text{wt}} = 4$), whereas, the triple mutants D35S/V36R/A40K and D35S/V36R/A40R display less NADP^+ specificity than their parent mutant ($[(k_{\text{cat}}/K_{\text{m}})^{\text{NADP}^+}/(k_{\text{cat}}/K_{\text{m}})^{\text{NAD}^+}]_{\text{triple mutant}}/[(k_{\text{cat}}/K_{\text{m}})^{\text{NADP}^+}/(k_{\text{cat}}/K_{\text{m}})^{\text{NAD}^+}]_{\text{D35S/V36R}} = 0.6$).

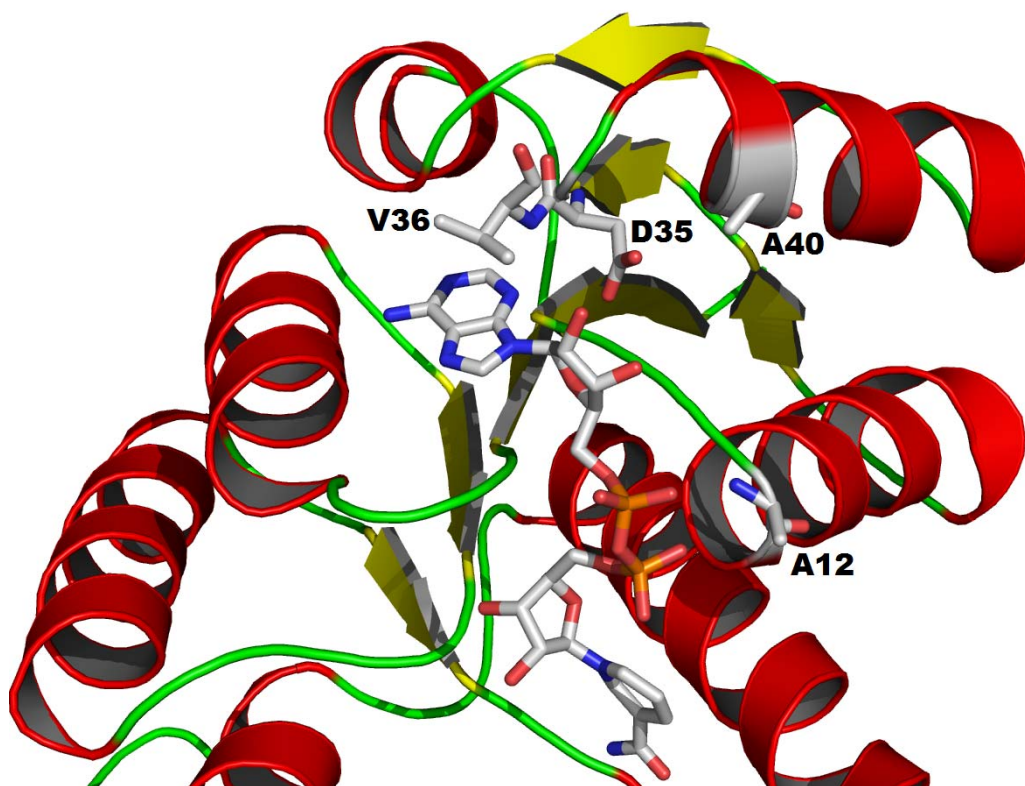


Figure 3.12 The model of N-terminal domain of *holo*-IDH structure. The residues Ala12, Asp35, Val36, Ala40, and the coenzyme NADH are indicated in sticks (oxygen in red, nitrogen in blue, phosphorus in orange, carbon in grey). Image was generated using PyMOL⁶⁸.

Table 3.7 Kinetic constants for the mutants D35S/A40K, D35S/V36R/A40R, and D35S/V36R/A40K.

Enzymes		$K_m(\text{NAD(P)}^+)$ (mM)	$K_m(\text{inositol})$ (mM)	V_{\max} ($\mu\text{mol}\cdot\text{min}^{-1}\cdot\text{mg}^{-1}$)	k_{cat} (s^{-1})	$k_{\text{cat}}/K_m^{\text{NAD(P)}^+}$ ($\text{s}^{-1}\cdot\text{mM}^{-1}$)	$\frac{k_{\text{cat}}/K_m^{\text{NADP}^+}}{k_{\text{cat}}/K_m^{\text{NAD}^+}}$
wild-type IDH		0.08 ± 0.01	4.4 ± 0.5	62 ± 2	42 ± 2	525	0
D35S/A40K	NAD^+	2.8 ± 0.8	9.0 ± 2.0	273 ± 16	184 ± 11	66	2.3
	NADP^+	0.9 ± 0.2	41 ± 18	217 ± 12	146 ± 8	155	
D35S/V36R/ A40R	NAD^+	1.0 ± 0.1	43 ± 7	93 ± 4	63 ± 3	63	3.7
	NADP^+	0.06 ± 0.01	8.4 ± 1.0	21 ± 1	14 ± 1	233	
D35S/V36R/ A40K	NAD^+	0.9 ± 0.1	25 ± 5	125 ± 9	84 ± 6	93	3.8
	NADP^+	0.04 ± 0.01	8.5 ± 1.3	21 ± 1	14 ± 1	350	

Conditions: 100 mM Tris-HCl, pH 9.0, 25°C.

3.4.3.4 Summary

Six amino acid residues (Gly11, Ala12, Ala14, Asp35, Val36, and Ala40) of wild-type IDH, which, according to sequence alignment, structure comparison, and structure analysis, could be important determinants of coenzyme specificity, were mutated in an attempt to accommodate NADP. Eleven IDH mutants bearing single, double, or triple mutations were produced and eight of them can utilize NADP⁺ as a coenzyme, but they are not entirely NADP⁺ specific. From these mutational analyses, it has been noticed that the regions of NAD- and NADP-binding sites differ to some extent and the difference is essential in determining the coenzyme specificity. Four regions around the coenzyme are identified in this work. First, Asp35 is identified as the discriminator that only chelates the diol of the ribose near adenine of NAD via hydrogen bonds. The single mutation (Asp35 to Ser) alters wild-type IDH, a strictly NAD-dependent dehydrogenase, to an enzyme with dual coenzyme specificity. Second, the successive residue Val36, its sidechain directed towards the plane of adenine, seems to play an important role in discriminating NAD and NADP. Replacement of this residue with Arg (mutant D35S/V36R) exhibits the highest ratio of specificity constants $[(k_{\text{cat}}/K_{\text{m}})^{\text{NADP}^+}/(k_{\text{cat}}/K_{\text{m}})^{\text{NAD}^+} = 5.7]$ among all the mutants. The double mutant D35S/V36R therefore is the most successful one for alteration of the coenzyme preference of IDH. The mutagenic results demonstrate that the combined steric factor and electrostatic interaction might comprise the main determinants responsible for coenzyme specificity. Third, structure-guided mutation of residue Ala40 on $\alpha 2$ increases the ratio of specificity constants for mutant D35S/A40K compared to its parent mutant D35S and decreases the ratio of the specificity constants for mutants D35S/V36R/A40K and D35S/V36R/A40R compared to their parent mutant D35S/V36R. However, all of the three mutants display lower K_{m} values than that of their parent mutants. Fifth, the loop between $\beta 1$ and $\alpha 1$ of wild-type IDH fix the

diphosphate group of NAD through hydrogen bonding interactions. Mutations of residue Ala12 (A12K/D35S and A12K/D35S/V36R) on this loop exhibit lower K_m values and little effect on the ratio of specificity constants, compared to their corresponding parent mutants (D35S and D35S/V36R).

Although only the NAD binding pocket of IDH was modified and the mutated sites were far away from *myo*-inositol-binding site, the kinetic analyses revealed that the values of K_m for *myo*-inositol of almost all mutants increased and the catalytic efficiency decreased compared to that of wild-type IDH. This can be explained by the compulsory Bi Bi mechanism that IDH obeys, which requires coenzyme binds first in order to accommodate the substrate *myo*-inositol. The mutants are not able to adopt the same active conformation as wild-type IDH after binding with coenzymes NAD/NADP, leading to non-optimal protein-coenzyme conformations. As a result, the binding property of *myo*-inositol is impaired to some extent. Therefore, the K_m values of *myo*-inositol increases. It is proposed that the subtle change of protein-coenzyme conformation might bring the significant difference in substrate binding affinity/ K_m values. This phenomenon has also been observed in the case of formate dehydrogenase¹⁴⁰.

Alteration of IDH to a NADP-specific enzyme may require further structural modification. In this regard, a 7-fold mutation was utilized to convert isocitrate dehydrogenase coenzyme specificity from 7000-fold preference for NADP⁺ to a 200-fold preference for NAD⁺, and the enzymatic activity is comparable to that of wild-type isocitrate dehydrogenase¹⁴⁶. These 7 residues include not only the ones which interact with the coenzyme directly but also the second-layer residue (Val351) which interacts with first-layer residues by steric packing. It is a challenge to find the second-layer residues which play critical roles in controlling specificity, but would be

interesting to try such mutations in IDH to increase the binding affinity and catalytic activity with NADP as a coenzyme.

3.4.4 Alteration of substrate specificity from *myo*-inositol to *myo*-inositol 4-*O*-phosphate

IDH demonstrates a broad range of substrate spectrum including 4-substituted *myo*-inositol and glucose derivatives as mentioned in **1.4.3**. However, IDH can not utilize 1L-*myo*-inositol-4-*O*-phosphate as a substrate. As IDH selectively reacts with 1L-4-substituted-*myo*-inositol, it could be used to develop a method to resolve racemic mixture of negatively charged inositol derivatives, such as (\pm) 1L-*myo*-inositol-4-*O*-phosphate⁶⁹. Thus, several attempts have been made to engineer IDH to an enzyme that is able to recognize 1L-*myo*-inositol-4-*O*-phosphate as a substrate.

During the time that no IDH structure was available, Tyr233, Gly234 and Tyr235 were proposed to be the basis of the hydrophobic pocket according to the homology model⁷⁸ (**Figure 1.13**). Introduction of Arg or Lys at sites 233 and 235 was therefore likely to modify electrostatic interaction in this region. The mutants Y233R and Y235R were postulated to be able to recognize a negatively charged group at the 4-position of *myo*-inositol such as 1L-*myo*-inositol-4-*O*-phosphate as a substrate. Unfortunately, both mutants Y233R and Y235R completely lose activity with *myo*-inositol and demonstrated no activity with 1L-*myo*-inositol-4-*O*-phosphate while mutants Y233F and Y235F demonstrated comparable activity with wild-type IDH (see **Table 3.8**).

When the crystal structure of IDH was solved, it was found that the homology model predicted IDH structure poorly, especially for inositol-binding domain. There is no obvious hydrophobic cavity in the crystal structure. However, it was identified in the structure alignment (**Figure 3.8**) that this YGY motif is conserved in the other three IDH homologs: dehydrogenase from *Salmonella typhimurium* (3EC7), dehydrogenase from *Thermotoga maritima* (3EZY), and *myo*-inositol dehydrogenase from *Corynebacterium glutamicum* (2EUW), suggesting that the motif YGY may play some structural or functional role in these dehydrogenases.

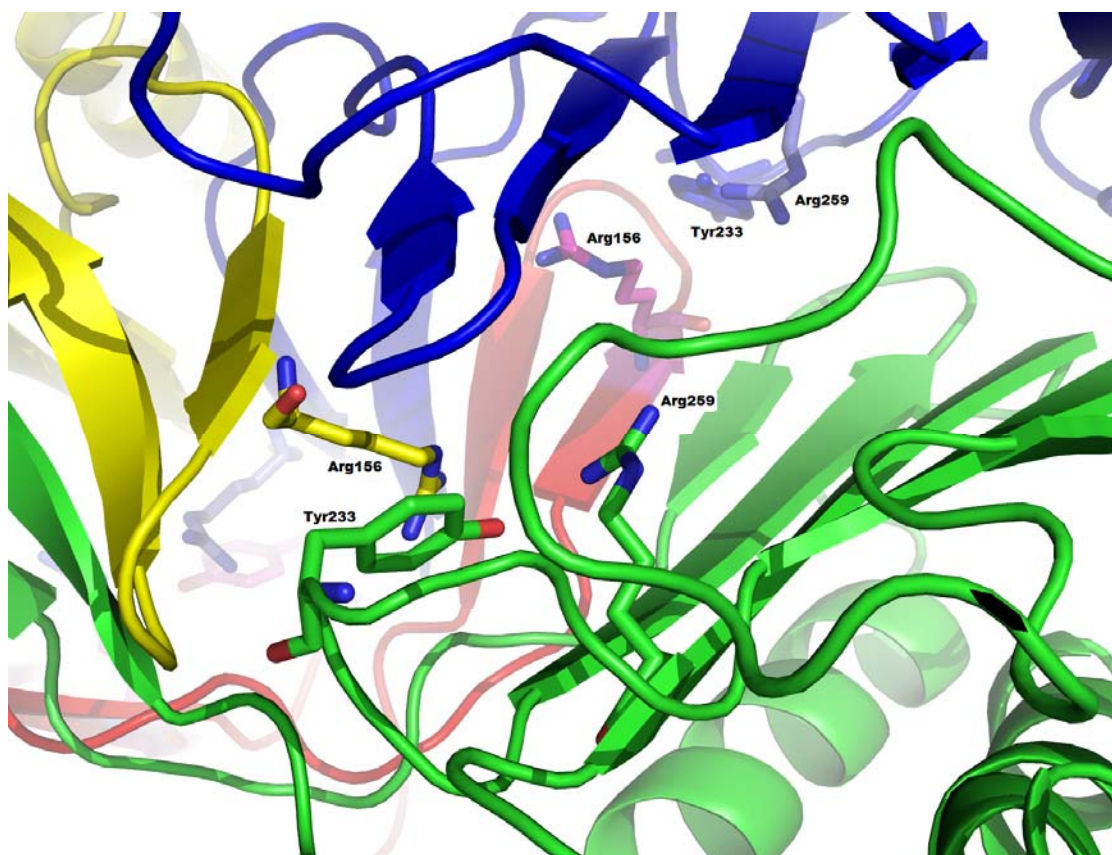


Figure 3.13 The model of interface of IDH tetramer. Yellow, green, red, and blue are indicated the four monomers that consist of a tetramer. The amino acid residues Tyr233, Arg156, and Arg259 are indicated in sticks. Image was generated using PyMOL⁶⁸.

Examination of the crystal structure of IDH shows that residue Tyr235, pointing into the putative inositol binding site, may interact with the substrate *myo*-inositol, whereas, Tyr233 is present in the interface of monomer and monomer. In the vicinity of sidechain of Tyr233, there are two amino acid residues, bearing positively charged sidechain, arginines Arg156' (' indicates Arg residue from another monomer) and Arg259 (**Figure 3.13**). The replacement of Tyr233 with Arg introduces positive charge-repelling interactions in this region, and the unfavourable interaction is likely to force the tetramer to fall apart to dimers/monomers, and mutant Y233R therefore is inactive. To obtain more evidence to support this hypothesis, double mutants or triple mutants were designed to recover the activity by removing a positive sidechain on Arg156 and Arg259. At first, single mutations were tried on these two residues. The mutant R156Q lost all the dehydrogenase activity. Mutants R259Q, R259A, and R259Y showed similar Michaelis constants with NAD^+ and *myo*-inositol to wild-type IDH, but the values of k_{cat} dropped compared to wild-type IDH. On the basis of these results, double mutations at Tyr233 and Arg259, mutants Y233R/R259A, Y233R/R259E, Y233R/R259Q, and Y233R/R259Y, were carried out. Unfortunately, no obvious activity of these double mutants was observed. By examining the tetrameric IDH structure, there are three negatively charged residues (Glu240", Asp236, and Glu252) around Arg156' and Arg259. It seems difficult to get positive and negative charges balanced in this area, and more mutants may be necessary to rescue the enzymatic activity.

On the basis of the *apo*-IDH crystal structure, Asn157 was proposed as the putative site that had the potential to interact with phosphate group of 1L-*myo*-inositol-4-*O*-phosphate. Therefore, the site-directed mutagenesis of Asn157 to a positively charged arginine was constructed to establish the ionic interaction. The kinetic data revealed that the activity of mutant N157R with *myo*-inositol decreased

7-fold and the specificity constant $k_{\text{cat}}/K_{\text{m}}(\text{inositol})$ decreased more than 30-fold (**Table 3.8**). Unfortunately, mutant N157R can not recognize either 1L-*myo*-inositol-4-*O*-phosphate or 1L-4-*O*-benzyl-*myo*-inositol as the substrate.

Inspection of the *apo*-IDH structure and homology model reveals that, even though this model was thought to be of good quality, it could not be used for identifying the residues determining the coenzyme specificity and the inositol-binding site (**Figure 3.14**). The superposition of the two structures demonstrates that 286 out of 344 amino acid residues can be aligned with the RMS deviation of 3.5 Å. In particular, the extended conformations of binding NADs are different, especially in the adenine diphosphate (ADP) moiety. When the X-ray structures of *apo*- and *holo*-IDH are available, it is still quite difficult to predict which amino acid residues are important for *myo*-inositol binding. In fact, if the crystal structure of IDH was known at the time I started this project, we would probably never have found that the site Tyr233 is a critical residue for tetrameric formation by rational design.

In the course of this mutational study on the alteration of substrate specificity, amino acid residues Tyr233, Tyr235, and Asn157 were postulated on the basis of IDH homology model and crystal structure, respectively. However, none of the mutants substituted on the targeted sites could alter substrate specificity.

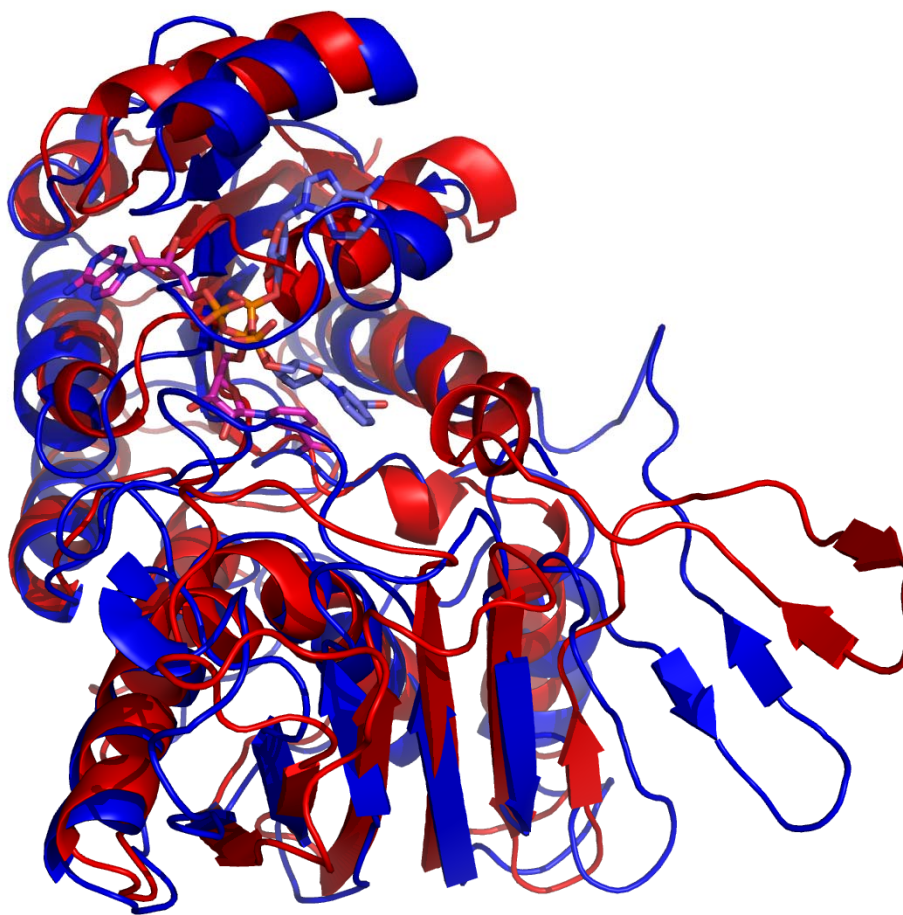


Figure 3.14 Superpositioned models of the crystal structure of IDH (red) from *B. subtilis* and the homology model of IDH (blue). Two molecules of NADH are shown in sticks (carbon in magenta belongs to crystal structure, carbon in light blue belongs to homology model, oxygen in red, nitrogen in blue, phosphorus in orange). Image was generated using PyMOL⁶⁸.

Table 3.8 Kinetic constants for the mutants at the sites of Asn157, Tyr233, Tyr235, Arg259, and Arg156.

Enzymes	$K_m(\text{NAD}^+)$ (mM)	K_m (<i>myo</i>-inositol) (mM)	V_{\max} ($\mu\text{mol}\cdot\text{min}^{-1}\cdot\text{mg}^{-1}$)	k_{cat} (s^{-1})
wild-type IDH	0.08 ± 0.01	4.4 ± 0.5	62 ± 2	42 ± 2
N157R	0.24 ± 0.05	356 ± 62	8.7 ± 1.3	6 ± 1
Y233F	0.07 ± 0.01	4.0 ± 0.4	55 ± 3	37 ± 2
Y235F	0.11 ± 0.02	39 ± 4	36 ± 5	24 ± 4
Y233F/Y235F	0.12 ± 0.04	56 ± 6	37 ± 3	25 ± 2
Y233R			No activity	
Y235R			No activity	
R259Q	0.05 ± 0.02	5.6 ± 1.1	24 ± 1	16 ± 1
R156Q			No activity	
R259A	0.07 ± 0.01	3.4 ± 0.3	50 ± 1	34 ± 1
R259Y	0.06 ± 0.01	3.5 ± 0.4	46 ± 1	31 ± 1
Y233R/R259A			trace activity	
Y233R/R259E			trace activity	
Y233R/R259Q			trace activity	
Y233R/R259Y			trace activity	

Conditions: 100 mM Tris-HCl, pH 9.0, 25°C.

3.4.5 Mutagenic study of the inositol-binding site

3.4.5.1 Overview of the inositol-binding pocket

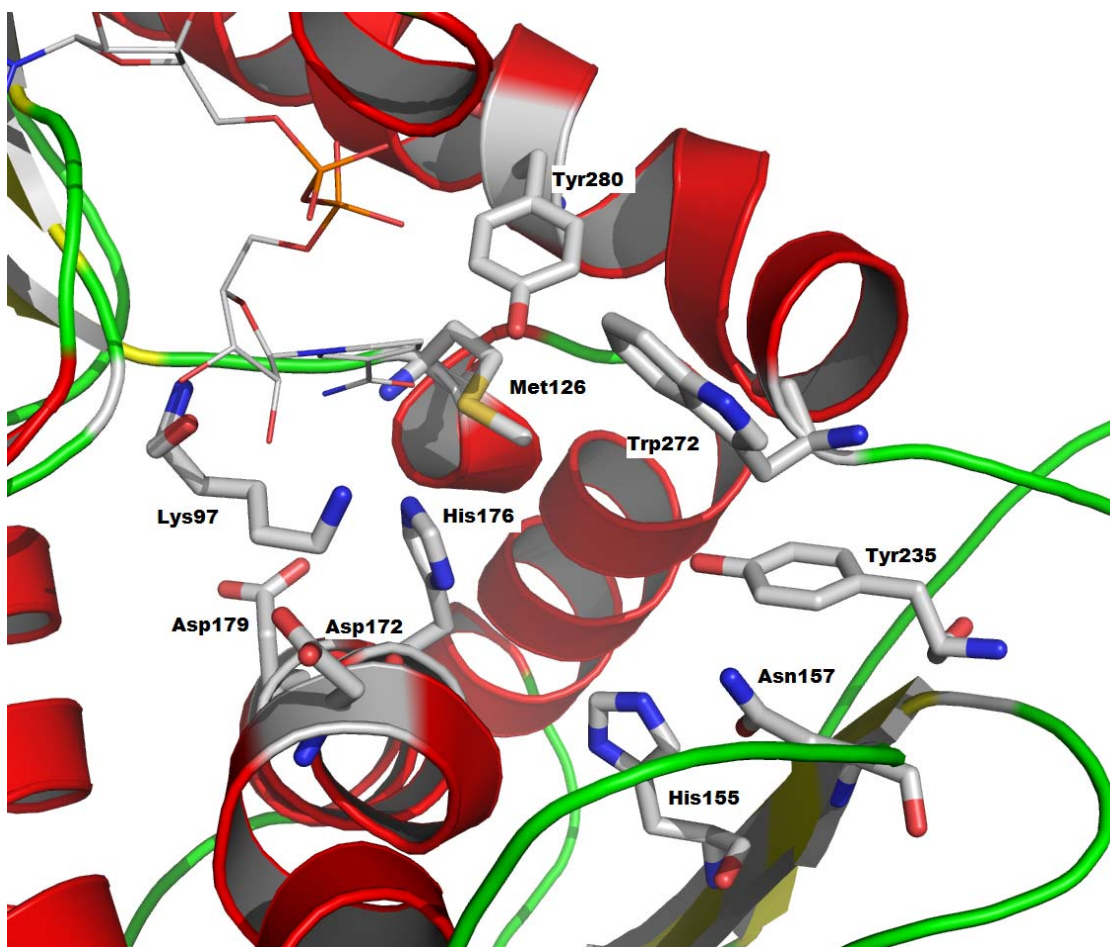


Figure 3.15 Proposed inositol-binding pocket. Proposed inositol binding residues are represented in sticks and NADH is represented in lines (oxygen in red, nitrogen in blue, phosphorus in orange, carbon in grey). Image was generated using PyMOL⁶⁸.

The oxidation-reduction reaction catalyzed by IDH is a hydride transfer between the nicotinamide ring of the coenzyme NAD^+ and the substrate *myo*-inositol. The *myo*-inositol binding site is thus located near the nicotinamide moiety, which is in the cleft between the N-terminal domain and the C-terminal domain according to the *apo*-

and *holo*-IDH crystal structures. Since His176 and Asp172 have been identified as catalytically important residues previously⁷⁸, the inositol-binding pocket is easily identified (**Figure 3.15**). To gain insight into substrate binding, a series of site-specific mutations in the IDH gene at sites corresponding to Tyr280, Trp272, Lys97, Asn157, His155, Tyr235, Met126, and Asp179 were performed.

3.4.5.2 Mutagenic studies of putative *myo*-inositol binding residues

Lys 97

Motif EKP is highly conserved among IDH homologs, and these Lys sidechains point toward substrate-binding pockets according to the crystal structures known. However, the role of Lys has not been identified yet. This intriguing lysine residue, Lys97 in IDH, is adjacent to the face of nicotinamide ring (~ 3.5 Å distant) in the *holo*-IDH structure, and a favorable cation- π interaction is formed. It suggests that this conformation may be influenced by the oxidation state of NAD, and the orientation of Lys97 sidechain might rearrange during the oxidation-reduction reaction. To understand the effect of Lys97, this residue was mutated to Arg, whose sidechain is more likely than that of Lys to be in a cation- π interaction¹⁴². However, the longer sidechain of Arg could cause the distortion of local geometry and thus decrease the activity. Comparing the kinetic parameters between K97R and wild-type IDH, the replacement not only decreased the K_m value for both NAD^+ and *myo*-inositol (**Table 3.9**), suggesting they bound with mutant K97R tighter than wild-type IDH, but also decreased the turnover number k_{cat} 600 fold. This result is consistent with the previous conclusion that product release is the rate-limiting step in IDH catalyzed reaction. Thus there are three possibilities: first, the conformation of K97R remains as wild-type IDH,

and Arg97 introduces stronger interactions with both coenzyme and *myo*-inositol than does Lys97; second, the conformation of the N-terminal domain remains as wild-type IDH, and Lys97 is not involved in *myo*-inositol binding, and the tighter binding NAD^+ triggers C-terminal conformation change; third, replacement with Arg affects the conformation of both the N-terminal domain and C-terminal domain.

The other mutation, Lys97Q, was meant to remove the charge and keep the $-\text{NH}_2$ group that would allow the formation of a hydrogen bond. This replacement abolished the enzymatic activity completely, suggesting that charge might be a necessary factor for the enzymatic activity.

N-Acetylgalactosaminidase (PDB code: 2IXB)¹⁴⁷, a hydrolase belongs to the GH4 family, and shares 18% sequence identity with IDH. Comparing structures of N-acetylgalactosaminidase and IDH, 307 out of 344 amino acid residues of IDH can be aligned to this glycosidase with the RMS deviation of 2.9 Å. In addition, the catalytic residue His176 of IDH is well aligned with His228, which is the catalytic acid/base in N-acetylgalactosaminidase^{147,148}. This N-acetylgalactosaminidase demonstrates a very similar NAD binding mode to IDH, but the motif EKP is substituted with EVS. On the basis of this evidence, Lys97 was replaced with Val, in which both the charge and hydrogen bonding property were removed. K97V also lost all the activity. It was found that the *apo*-K97V structure (Karin E. Van Straaten, unpublished result) is identical to *apo*-IDH, with RMS difference in $\text{C}\alpha$ atomic positions of 0.4 Å after superposition (**Figure 3.16**). Apparently, this substitution does not change the IDH conformation. Clearly Lys97 plays a critical role in enzymatic function.

In summary, three mutants K97R, K97Q, and K97V were made to investigate the role of Lys97. On the basis of kinetic results, Lys97 was identified to relate to the binding properties of both coenzyme and substrate. Since Lys could also facilitate proton transfer by hydrogen bonding to the adjacent residue or act as catalytic acid/base directly, further elucidation of the exact role of Lys97 is necessary.

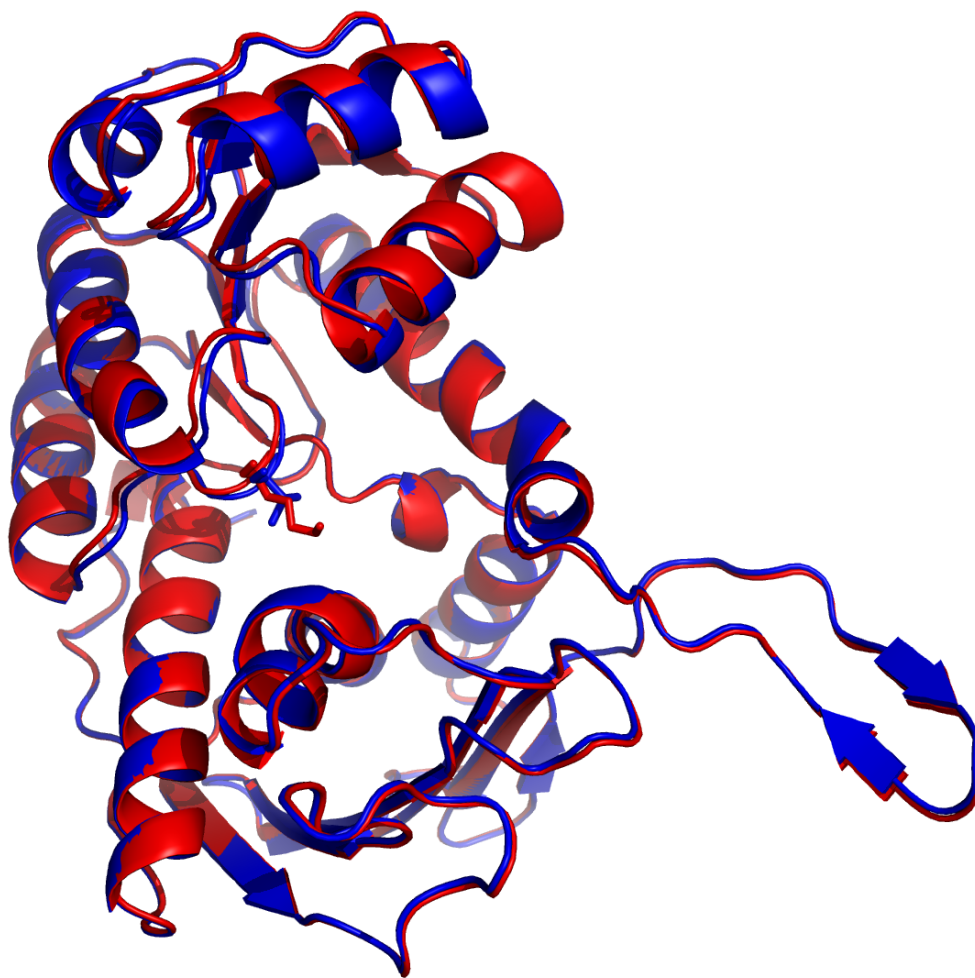


Figure 3.16 Superpositioned models of *apo*-IDH and *apo*-K97V. *apo*-IDH colored in red; *apo*-K97V colored in blue. Amino acid residues Lys97 and Val97 are indicated in sticks. Image was generated using PyMOL⁶⁸.

Table 3.9 Kinetic constants of mutants generated from the sites Lys97, Tyr280, Tyr235, and Trp272 in the proposed inositol-binding pocket.

Enzymes	$K_m(\text{NAD}^+)$ (mM)	K_m (inositol) (mM)	V_{\max} ($\mu\text{mol}\cdot\text{min}^{-1}\cdot\text{mg}^{-1}$)	k_{cat} (s^{-1})	$k_{\text{cat}}/K_m(\text{inositol})$ ($\text{s}^{-1}\text{ mM}^{-1}$)
wild-type IDH	0.08 ± 0.01	4.4 ± 0.5	62 ± 2	42 ± 2	9.55
K97R	0.03 ± 0.01	0.8 ± 0.2	0.11 ± 0.01	0.07 ± 0.01	0.09
K97Q		No activity			
K97V		No activity			
Y280F	0.07 ± 0.01	7.9 ± 1.4	37 ± 4	25 ± 3	3.16
Y235F	0.11 ± 0.02	39 ± 4	36 ± 5	24 ± 4	0.62
Y233F/Y235F	0.12 ± 0.04	56 ± 6	37 ± 3	25 ± 2	0.45
W272A	0.59 ± 0.07	351 ± 32	74 ± 7	50 ± 5	0.14
W272H	0.70 ± 0.10	204 ± 32	92 ± 4	62 ± 3	0.30

Conditions: 100 mM Tris-HCl, pH 9.0, 25°C.

Tyr280

The sidechain of Tyr280 is adjacent to the carbonyl group of the nicotinamide ring of NAD^+ ($\sim 3.0 \text{ \AA}$) in the *holo*-IDH structure. It is likely that a hydrogen bond is formed between them. Among IDH homologs, this Tyr280 position is filled with Tyr or Phe (**Figure 3.8**), but it is still not clear what role the residue Tyr/Phe plays. Since the hydroxyl group of Tyr280 also could form a hydrogen bond with *myo*-inositol, Tyr280 was replaced with Phe, which keeps the aromatic ring but is incapable of forming a hydrogen bond, to investigate the role of the hydroxyl group. Kinetic studies revealed that the K_m value of NAD^+ did not change after the replacement, but the K_m value of *myo*-inositol was doubled (**Table 3.9**), suggesting Tyr280 was probably hydrogen bonding to *myo*-inositol, not NAD^+ . In addition, the *apo*-Y280F structure is identical to *apo*-IDH (**Figure 3.17**). All amino acid residues of Y280F can be superimposed onto corresponding residues of wild-type IDH with RMS difference in $\text{C}\alpha$ atomic positions of 0.3 \AA . Moreover, the aromatic rings of Tyr280 and Phe280 are oriented in the same direction. It therefore can be concluded that the substitution at site 280 does not alter the structure of the enzyme.

Tyr235

Tyr235 is the other Tyr residue in the substrate-binding pocket that could interact with *myo*-inositol directly. Like Tyr280, Tyr235 was substituted with Phe. The K_m value of NAD^+ of Y235F was comparable to that of wild-type IDH; however, K_m value of *myo*-inositol was almost ten-fold of that of wild-type IDH. Also, this replacement decreased the turnover number to half of that of wild-type IDH. The double mutant Y233F/Y235F demonstrated similar properties with single mutant Y235F according to the measured kinetic constants (**Table 3.9**).

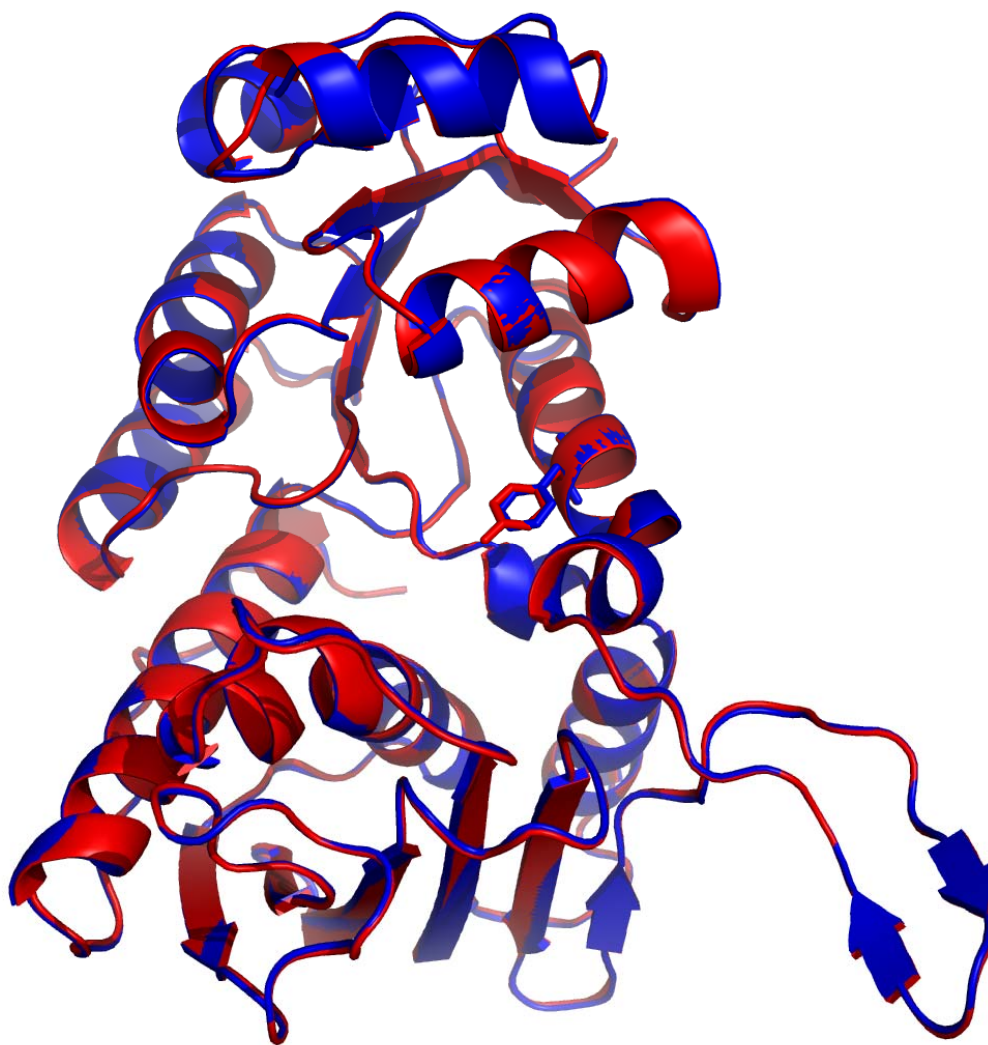


Figure 3.17 Superpositioned models of *apo*-IDH and *apo*-Y280F. *apo*-IDH colored in red; *apo*-Y280F colored in blue. Amino acid residues Tyr280 and Phe280 are indicated in sticks. Image was generated using PyMOL⁶⁸.

Trp272

On the basis of the structure of the ternary complex, which is believed to be a non-productive complex, Trp272 is expected to play important roles in substrate binding (**Figure 3.18**). Actually, Trp272 is not well conserved among IDH homologs (**Figure 3.8**), and Phe is usually present at this position. A bulky sidechain of Trp272 was postulated to provide an important region for making the inositol binding pocket. In addition, The -NH- group might interact with *myo*-inositol by hydrogen bonding (~ 3.3 Å). Considering this information, Trp272 was mutated to His and Ala, respectively. A smaller sidechain of His maintains aromaticity and the pattern of hydrogen-bonding interaction. Whereas, the accompanying change of the sidechain size is expected to alter the contacts with substrate. Replacing Trp272 with Ala was a large change in size and property, effectively removing all the functionality of the Trp sidechain. Surprisingly, kinetic results indicated this single mutation in the substrate-binding domain affected Michaelis constants of both coenzyme and substrate. Compared to wild-type IDH, the K_m values of W272H and W272A for NAD^+ increased almost ten times, and the K_m values for *myo*-inositol increased fifty and eighty times respectively (**Table 3.9**). The increase in the K_m values for both NAD^+ and inositol could thus indicate that a single replacement of Trp272 in the vicinity of *myo*-inositol not only affects *myo*-inositol binding site, but also affects NAD^+ binding site. It is likely that the change results from a disturbance of protein conformation by replacement on Trp272. Unfortunately, structures of these mutants have not been solved.

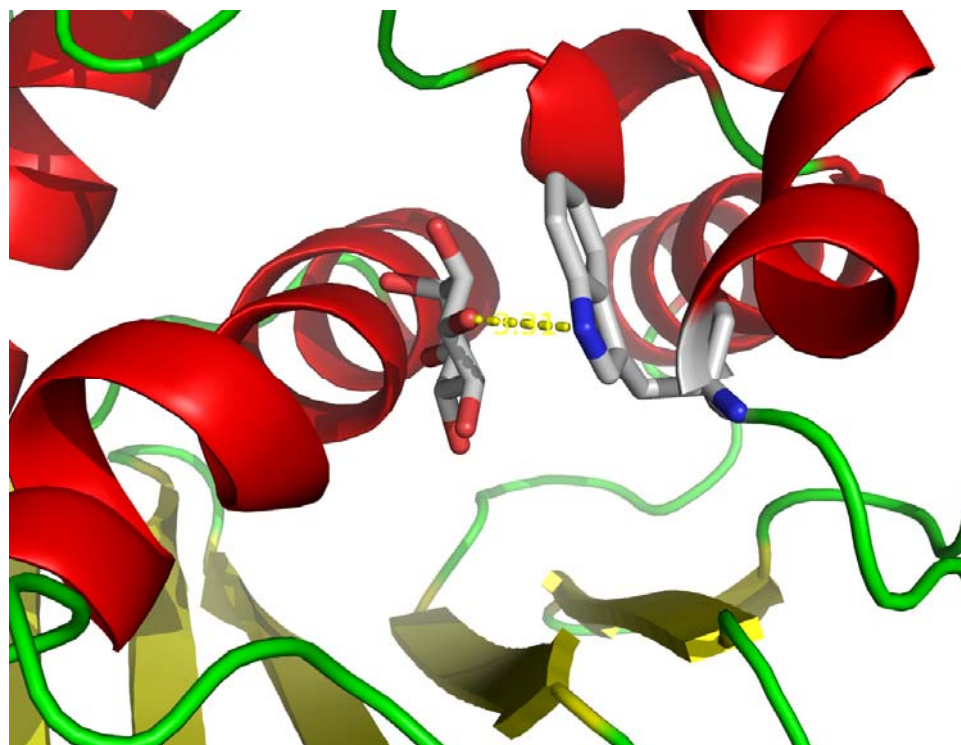


Figure 3.18 Proximity of bound *myo*-inositol and Trp272 in non-productive IDH ternary complex. *myo*-Inositol and Trp272 are indicated in sticks (oxygen in red, nitrogen in blue, and carbon in grey). Image was generated using PyMOL⁶⁸.

Asp179

Asp179 is a conserved residue among IDH homologs (**Figure 3.8**), and could possibly participate in the catalytic dyad with His176 (Asp179 is ~ 6.8 Å away from His176 in *holo*-IDH). Based on this hypothesis, Asp179 was replaced isosterically with Asn, which can retain hydrogen-bonding ability. The substitution increased the K_m values for both NAD^+ and *myo*-inositol moderately, and increased turnover number slightly. It is apparent that Asp179 is not involved in the catalytic dyad. Although Asp179 is not in the first layer of residues interacting with substrate or coenzyme, this conserved Asp residue is still important since a single substitution changed the Michaelis constant and catalytic efficiency. A small increase in turnover number might result from the decrease substrate binding affinity as product release is the rate limiting step for IDH catalyzed reaction.

Table 3.10 Kinetic constants of mutants generated from the sites Asp179, Asn157, Met126, and His155 in the proposed inositol-binding pocket.

Enzymes	$K_m(\text{NAD}^+)$ (mM)	K_m (<i>myo</i>-inositol) (mM)	V_{\max} ($\mu\text{mol}\cdot\text{min}^{-1}\cdot\text{mg}^{-1}$)	k_{cat} (s^{-1})	k_{cat}/K_m (<i>myo</i>-inositol) ($\text{s}^{-1}\text{ mM}^{-1}$)
wild-type IDH	0.08 ± 0.01	4.4 ± 0.5	62 ± 2	42 ± 2	9.55
D179N	0.35 ± 0.04	28 ± 5	79 ± 3	53 ± 2	1.90
N157R	0.24 ± 0.05	356 ± 62	8.7 ± 1.3	6 ± 1	0.02
N157S	0.08 ± 0.01	14 ± 3	33 ± 2	22 ± 2	1.57
M126A	2.3 ± 2.2	> 1000	-	-	-
M126S	5.7 ± 1.5	> 1000	-	-	-
H155F			No activity		
H155K	> 5	> 1000	-	-	-

Conditions: 100 mM Tris-HCl, pH 9.0, 25°C.

Asn157

Examination of the ternary complex structure suggests that Asn157 likely interacts with *myo*-inositol (~ 3.0 Å to C5 hydroxyl). It was thus hypothesized that the Asn157 sidechain forms a hydrogen bond with *myo*-inositol. Therefore, this residue was substituted by Ser. This replacement was meant to keep the hydrogen bond donor/acceptor that would allow the formation the hydrogen bond, however, the shorter side chain of Ser could make the bond strength weaker. Kinetic studies showed that the substitution of Asn157 did not affect the K_m value of NAD^+ , but moderately increased the K_m value of *myo*-inositol, and decreased turnover number (**Table 3.10**). Recently, structure of *apo*-N157S was solved, and it is quite similar to *apo*-IDH. All amino acid residues of N157S can be superimposed onto corresponding residues of wild-type IDH with RMS difference in C α atomic positions of 0.4 Å (**Figure 3.19**). Moreover, the sidechains of Asn157 and Ser157 are pointing in the same direction. It can be therefore concluded that the proper formation and strength of the hydrogen bond between *myo*-inositol and Asn157 is related to the catalytic efficiency.

N157R was made for the substrate specificity alteration mentioned in **3.4.4**. The charged longer sidechain of Arg apparently disturbed the conformation of both coenzyme binding domain and substrate binding domain since the values of K_m for both NAD^+ and *myo*-inositol increased.

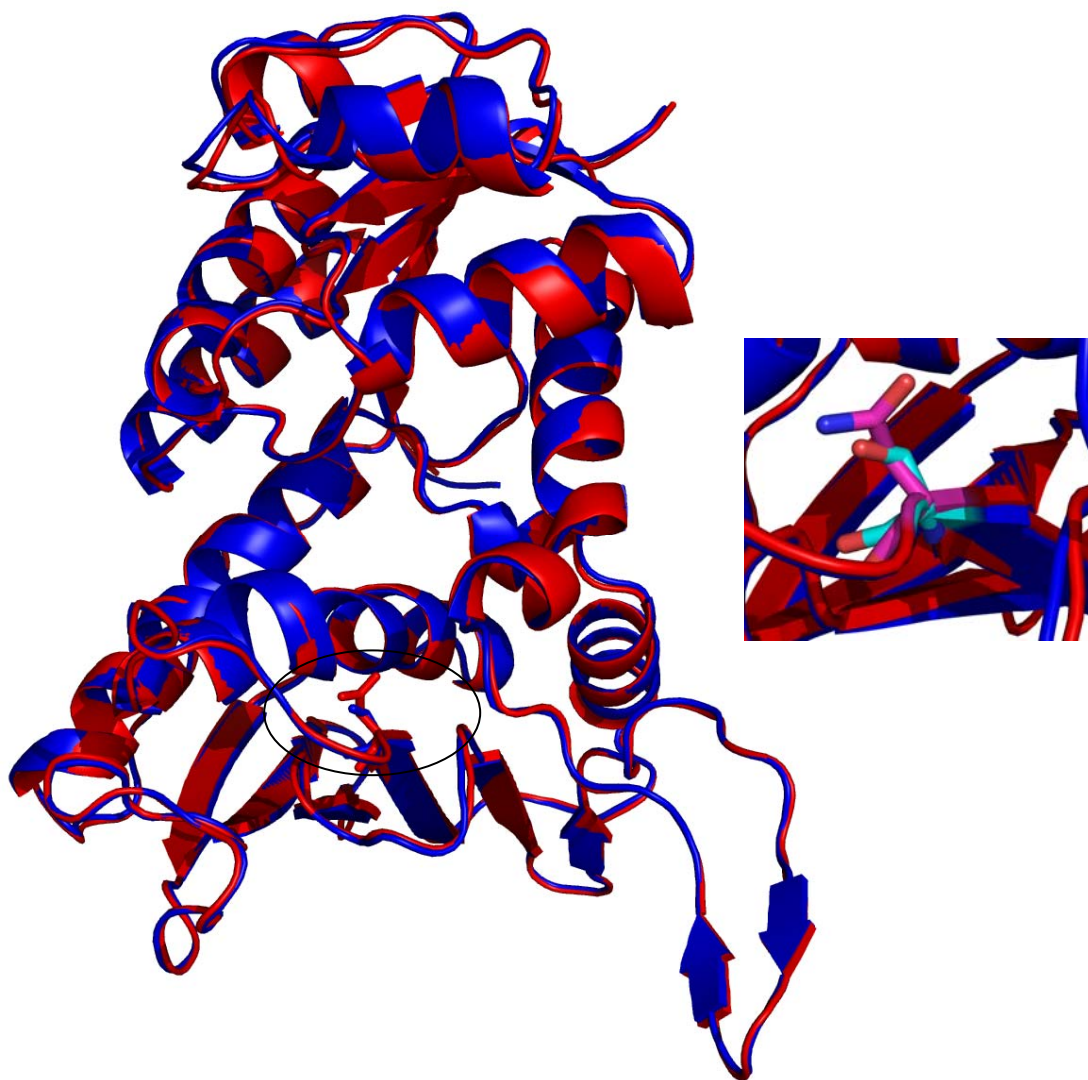


Figure 3.19 Superpositioned models of *apo*-IDH and *apo*-N157S. *apo*-IDH colored in red; *apo*-N157S colored in blue. Image was generated using PyMOL⁶⁸.

Met126

Met126 is not well conserved among IDH homologs (**Figure 3.8**), but the motif GFMRRYD, located between N-terminal domain and C-terminal domain, is conserved in dehydrogenase from *Salmonella typhimurium* and IolG1 from *Lactobacillus plantarum*. Within this motif, Met is the only residue whose sidechain might be involved in the first layer of inositol-binding pocket. This suggests that Met126 possibly interacts with *myo*-inositol directly. Residue Met126 was therefore substituted by short chain residues Ala and Ser, respectively. The single mutations, M126A and M126S, were expected to change *myo*-inositol binding affinity. However, kinetic results (**Table 3.10**) showed both the K_m values of NAD^+ and the K_m values of *myo*-inositol were affected by replacement on site 126, especially the K_m values of *myo*-inositol since they are too high to be measured accurately due to the solubility limit of *myo*-inositol. It thus indicated that Met126 is a key residue for substrate binding. Fortunately, the structure of *apo*-M126A was solved, and it demonstrates a more open conformation in the N-terminal domain than that of wild-type IDH (**Figure 3.20**). Thus, M126A undergoes conformational changes upon removal of sidechain of Met, which appears to be a key feature for maintaining the structure. We therefore reasoned that the C-terminal conformation of binary complex NAD-M126A was different from that of wild-type IDH, and this difference resulted in the higher Michaelis constant of *myo*-inositol with M126A than that of wild-type IDH.

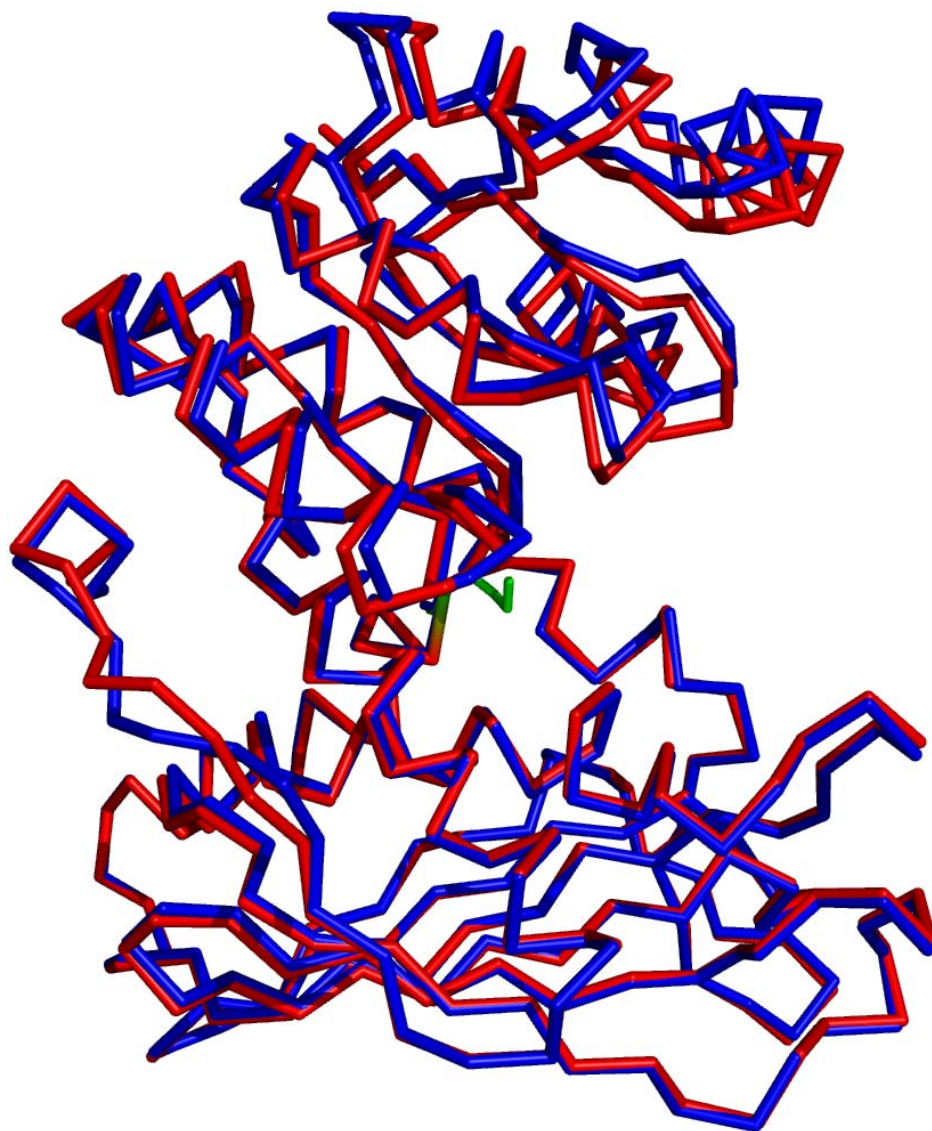


Figure 3.20 Superpositioned backbones of *apo*-IDH and *apo*-M126A. *apo*-IDH colored in red; *apo*-M126A colored in blue; amino acid residue Met126 is indicated in stick colored in green. Image was generated using PyMOL⁶⁸.

His155

Although His155 is not a conserved residue among the sequence of IDH homologs (**Figure 3.8**), it is believed to bind with *myo*-inositol since it is 2.5 Å away from C6 hydroxyl of *myo*-inositol in the non-productive IDH ternary structure. Surprisingly, the replacement of His155 with Phe gave an enzyme with no activity. However, the replacement with Lys, which maintained the charge and allowed the formation of hydrogen bonds, resulted in an enzyme with activity. Unfortunately, no precise kinetic data was measured for H155K because the value of K_m is too high to attain saturated conditions. The long sidechain of Lys could cause the distortion of the local geometry and thus decrease *myo*-inositol binding affinity. Therefore, His155 might be a key residue for substrate binding or structure maintaining.

3.4.5.3 Summary

In summary, we have chosen eight amino acid residues (Tyr280, Trp272, Lys97, Asn157, His155, Tyr235, Met126, and Asp179), which, according to current theories based on sequence alignment and crystal structures, could be important residues involved in *myo*-inositol binding. In the course of mutational and kinetic studies, it was found that the replacements of these residues affected the K_m values of *myo*-inositol more or less, three of them (K97Q, K97V, and H155F) even lost dehydrogenase activity. Out of eight targeted residues, the substitutions on the sites of Trp272, Lys97, Asn157, His155, Met126, and Asp179 affected the K_m values for both NAD^+ and *myo*-inositol. In particular, mutants M126S, M126A, and H155K increased the K_m values of both NAD^+ and *myo*-inositol dramatically.

The structures of *apo*-Y280F, *apo*-K97V, and *apo*-N157S were solved and found to be quite similar with the structure of wild-type *apo*-IDH. Whereas, it was found that the M126A mutant undergoes a conformation change upon replacement of Met residue, which appears to be the key feature for maintaining the IDH structure and activity.

4. SUMMARY AND FUTURE DIRECTIONS

This dissertation describes mechanistic, inhibitory, and mutagenic studies of *myo*-inositol 2-dehydrogenase (IDH) from *Bacillus subtilis*. As reported in 1979, this enzyme catalyzes the reversible interconversion of *myo*-inositol and 2-keto-*myo*-inositol with transformation of NAD^+ and NADH concomitantly⁶⁵. When I started this project in 2004, no structural information was available about IDH. Our initial interest in IDH was the catalytic mechanism, including the chemical mechanism and the kinetic mechanism. It was discovered that His176 acted as a base/acid to catalyze the oxidation-reduction reaction. During the catalysis, IDH obeys compulsory Bi Bi mechanism like the other dehydrogenases, in which NAD^+ binds first and NADH releases last after chemical reaction⁶⁵. Since the chemical step is not the rate-limiting step for many of dehydrogenases, ^2H kinetic isotope effect was utilized to explore whether IDH employs the same process. It turned out that no kinetic isotope effect was observed, and consequently the chemical step of the reaction IDH catalyzed was not rate-limiting. This evidence, as well as previously determined rate constants, suggests that the breakdown of ternary complex and liberation of NADH constituted the rate-limiting step.

The previous work in this laboratory regarding the substrate spectrum gave insight into the features of the IDH substrates⁶⁹, which are 4-substituted *myo*-inositol analogues or 6-substituted α -D-glucose analogues. It appears that the substrate binding site demonstrates a large range in size accommodating substituted groups, but it is sensitive to the charges born by the substituted groups. On the basis of this information, four compounds with new shapes, 4-*O*-(2-benzothiazolylmethyl)-*myo*-inositol **1**, 4-*O*-(4-*tert*-butylbenzyl)-*myo*-inositol **2**, 4-*O*-propargyl-*myo*-inositol **3**, and 4-*O*-(1-allyl-4-methylene-1,2,3-triazol)-*myo*-inositol **4**, were synthesized, and the steady-state kinetic parameters for these compounds with IDH were determined. It was found they were all substrates of IDH, in particular, compound **1** demonstrated lower K_m^{app} than that of natural substrate *myo*-inositol. It is interesting to note that compound **1** differs from *myo*-inositol by such a large group. Therefore it was proposed that the additional group introduced more favourable interaction with IDH active site. However, how IDH accommodates this 4-substituted group is still unknown, even though crystal structures of *apo*- and *holo*-IDH have been obtained recently.

By applying the knowledge gained from substrates exploring, five compounds, 2-deoxy-2-fluoro-*myo*-inositol **10**, 2-deoxy-2-fluoro-*scyllo*-inositol **11**, 2-deoxy-2,2-difluoro-*myo*-inositol **12**, 2-deoxy-*myo*-inositol **13**, and 4-*O*-benzyl-2-deoxy-*myo*-inositol **14**, were designed, synthesized, and tested as potential inhibitors of IDH. As shown by our data, compound **11**, mimicking *scyllo*-inositol, is neither a substrate nor an inhibitor, and compounds **10**, **12**, **13**, and **14**, mimicking *myo*-inositol, are competitive inhibitors of IDH. It is likely that IDH can only bind compounds that demonstrate similar dipole moments as *myo*-inositol or 2-keto-*myo*-inositol. As a consequence, competitive inhibitors are discovered for inhibiting IDH dehydrogenase activity, as well as providing additional support evidence for the substrate recognition.

Since a large number of dehydrogenase-NAD/NADP complex structures are available, how a dehydrogenase discriminates NAD and NADP as its coenzyme has been a hot topic in the past decades. In addition, many enzymes as biocatalysts in industry are NAD/NADP-dependent. A lot of attempts have been carried out to try to convert the coenzyme specificity, and some of the successful ones have been already applied in enzymatic synthesis. However, no clear recipe is available to switch coenzyme specificity strictly so far. The previous accumulated knowledge about coenzyme specificity sheds light on our IDH coenzyme specificity. In the past few years, sequence alignment with glucose-fructose oxidoreductase (when no structure information was available), structure alignment with 15-hydroxyprostaglandin dehydrogenase (when the structure of *apo*-IDH was available), and structure-based engineering (when the structure of *holo*-IDH was available) were utilized to predict the residues that are crucial to discriminate NAD and NADP. During the course of the mutagenic study, six amino acid residues (Gly11, Ala12, Ala14, Asp35, Val36, and Ala40) were selected to modify, producing 11 mutated IDHs bearing single, double, or triple mutations. It is found that Asp35 is the crucial site to discriminate NAD and NADP, and the sites of Val36 and Ala40 are important for coenzyme binding affinity. Among the constructed mutants, mutant D35S/V36R is the most successful one, which converting coenzyme specificity from entirely NAD^+ -dependent to 6-fold preference for NADP^+ over NAD^+ . So far, we have not yet obtained the engineered IDH that switches the coenzyme specificity completely.

It was found that IDH catalyzes the oxidation-reduction reaction employed His176-Asp172, similar to catalytic dyad of His-Asp that was reported in glucose-fructose oxidoreductase (GFOR). Examination of the structure of IDH indicated that residues Tyr280, Trp272, Lys97, Asn157, His155, Tyr235, Met126, and

Asp179, apart from catalytic residues His176 and Asp172, could have direct interactions with *myo*-inositol. Therefore, modifications of these residues were carried out to determine their contributions, and the activities of the engineered IDH were measured. According to our kinetic results, the replacements of these residues led to enzymes with increased K_m values of *myo*-inositol. Although the modifications were made at the C-terminal domain (substrate-binding domain), it also resulted in the increase of K_m values of NAD^+ which is bound at the N-terminal domain. In particular, M126A suffers from considerable conformation change compared to the structure of wild-type IDH. Thus, a single substitution can affect not only the local feature but also affect the global enzyme conformation, and further affect the dehydrogenase activity.

Although a lot of work has been done on IDH, many questions concerning catalysis by IDH remain to be answered. One of the most interesting concerns would be how the 1L-4-substituted *myo*-inositol is bound as a substrate and is oxidized. Further investigation to examine the structure-function relationships of IDH might need to concentrate on X-ray crystallography, solving structures of wild-type IDH and its mutants that complexed with synthesized substrates and inhibitors.

I hope this work will provide a basis for exploring the other unknown aspects of IDH. Current and future studies on this enzyme will help elucidate the other putative inositol dehydrogenases, such as *myo*-inositol 2-dehydrogenase (IolG1) from *Lactobacillus plantarum*, *myo*-inositol dehydrogenase from *Corynebacterium glutamicum*, dehydrogenase from *Salmonella typhimurium*, and dehydrogenase from *Thermotoga maritima*.

REFERENCES

1. Fisher, S. K., Novak, J. E., and Agranoff, B. W. (2002) Inositol and Higher Inositol Phosphates in Neural Tissues: Homeostasis, Metabolism and Functional Significance. *J. Neurochem.* 82, 736-754. (License Number for Figure 1: 2394380085507)
2. Kindl, H., Scholda, R., and Hoffmann-Ostenhof, O. (1966) The Biosynthesis of Cyclitols. *Angew. Chem. Int. Ed.* 5, 165-173.
3. Kersting, M. C., Boyette, M., Massey, J. H., and Ryals, P. E. (2003) Identification of the Inositol Isomers Present in *Tetrahymena*. *J. Eukaryot. Microbiol.* 50, 164-168.
4. Yoshida, K., Aoyama, D., Ishio, I., Shibayama, T., and Fujita, Y. (1997) Organization and Transcription of the *myo*-Inositol Operon, *iol*, of *Bacillus subtilis*. *J. Bacteriol.* 179, 4591-4598.
5. Vidal-Leiria, M., and Van Uden, N. (1973) Inositol Dehydrogenase from the Yeast *Cryptococcus melibiosum*. *Biochim. Biophys. Acta, Enzymol.* 293, 295-303.
6. Berman, T., and Magasanik, B. (1966) The Pathway of *myo*-Inositol Degradation in *Aerobacter aerogenes*. Dehydrogenation and Dehydration. *J. Biol. Chem.* 241, 800-806.
7. Poole, P. S., Blyth, A., Reid, C. J., and Walters, K. (1994) *myo*-Inositol Catabolism and Catabolite Regulation in *Rhizobium Leguminosarum* Bv. *Viciae*. *Microbiology*, 140, 2787-2795.

8. Galbraith, M. P., Feng, S. F., Borneman, J., Triplett, E. W., De Bruijn, F. J., and Rossbach, S. (1998) A Functional *myo*-Inositol Catabolism Pathway is Essential for Rhizopine Utilization by *Sinorhizobium Meliloti*. *Microbiology*, 144, 2915-2924.
9. Jiang, G., Krishnan, A. H., Kim, Y., Wacek, T. J., and Krishnan, H. B. (2001) A Functional *myo*-Inositol Dehydrogenase Gene is Required for Efficient Nitrogen Fixation and Competitiveness of *Sinorhizobium Fredii* USDA191 to Nodulate Soybean (*Glycine Max* [L.] Merr.). *J. Bacteriol.* 183, 2595-2604.
10. Krings, E., Krumbach, K., Bathe, B., Kelle, R., Wendisch, V. F., Sahm, H., and Eggeling, L. (2006) Characterization of *myo*-Inositol Utilization by *Corynebacterium glutamicum*: The Stimulon, Identification of Transporters, and Influence on L-Lysine Formation. *J. Bacteriol.* 188, 8054-8061.
11. Yebra, M. J., Zuniga, M., Beaufils, S., Perez-Martinez, G., Deutscher, J., and Monedero, V. (2007) Identification of a Gene Cluster Enabling *Lactobacillus Casei* BL23 to Utilize *myo*-Inositol. *Appl. Environ. Microbiol.* 73, 3850-3858.
12. (1989) Numbering of Atoms in *myo*-Inositol. Recommendations 1988. *Biochem. J.* 258, 1-2.
13. (1976) IUPAC Commission on the Nomenclature of Organic Chemistry (CNO) and IUPAC-IUB Commission on Biochemical Nomenclature (CBN). Nomenclature of Cyclitols. Recommendations, 1973. *Biochem. J.* 153, 23-31.
14. Michell, R. H. (2008) Inositol Derivatives: Evolution and Functions. *Nat. Rev. Mol. Cell Biol.* 9, 151-161.
15. Loewus, F. A., and Loewus, M. W. (1983) *myo*-Inositol: Its Biosynthesis and Metabolism. *Annu. Rev. Plant Physiol.* 34, 137-161.
16. Loewus, M. W., Wright, R. W., Jr, Bondioli, K. R., Bedgar, D. L., and Karl, A. (1983) Activity of *myo*-Inositol-1-Phosphate Synthase in the Epididymal Spermatozoa of Rams. *J. Reprod. Fertil.* 69, 215-220.
17. Berridge, M. J., and Irvine, R. F. (1984) Inositol Trisphosphate, a Novel Second Messenger in Cellular Signal Transduction. *Nature.* 312, 315-321.
18. Hokin, L. E. (1985) Receptors and Phosphoinositide-Generated Second Messengers. *Annu. Rev. Biochem.* 54, 205-235.

19. Berridge, M. J. (1993) Inositol Trisphosphate and Calcium Signalling. *Nature*. 361, 315-325.
20. Munnik, T., Irvine, R. F., and Musgrave, A. (1998) Phospholipid Signalling in Plants. *Biochim. Biophys. Acta, Lipids Lipid Metab.* 1389, 222-272.
21. York, J. D., Odom, A. R., Murphy, R., Ives, E. B., and Wentz, S. R. (1999) A Phospholipase C-Dependent Inositol Polyphosphate Kinase Pathway Required for Efficient Messenger RNA Export. *Science*. 285, 96-100.
22. Stevenson, J. M., Perera, I. Y., Heilmann, I., Persson, S., and Boss, W. F. (2000) Inositol Signaling and Plant Growth. *Trends Plant Sci.* 5, 252-258.
23. York, J. D., Guo, S., Odom, A. R., Spiegelberg, B. D., and Stolz, L. E. (2001) An Expanded View of Inositol Signaling. *Adv. Enzyme Regul.* 41, 57-71.
24. Cockcroft, S. (2006) The Latest Phospholipase C, PLCh, is Implicated in Neuronal Function. *Trends Biochem. Sci.* 31, 4-7.
25. Krauss, M., and Haucke, V. (2007) Phosphoinositides: Regulators of Membrane Traffic and Protein Function. *FEBS Lett.* 581, 2105-2111.
26. Molina, Y., Ramos, S. E., Douglass, T., and Klig, L. S. (1999) Inositol Synthesis and Catabolism in *Cryptococcus Neoformans*. *Yeast*. 15, 1657-1667.
27. Charalampous, F. C., and Lyras, C. (1957) Biochemical Studies on Inositol. IV. Conversion of Inositol to Glucuronic Acid by Rat-Kidney Extracts. *J. Biol. Chem.* 228, 1-13.
28. Naber, N. I., Swan, J. S., and Hamilton, G. A. (1986) L-*myo*-Inosose-1 as a Probable Intermediate in the Reaction Catalyzed by *myo*-Inositol Oxygenase. *Biochem.* 25, 7201-7207.
29. Xing, G., Hoffart, L. M., Diao, Y., Prabhu, K. S., Arner, R. J., Reddy, C. C., Krebs, C., and Bollinger, J. M., Jr. (2006) A Coupled Dinuclear Iron Cluster that is Perturbed by Substrate Binding in *myo*-Inositol Oxygenase. *Biochem.* 45, 5393-5401.
30. Goode, D., Lewis, M. E., and Crabbe, M. J. C. (1996) Accumulation of Xylitol in the Mammalian Lens is Related to Glucuronate Metabolism. *FEBS Lett.* 395, 174-178.
31. Hanks, L. V., Politzer, W. M., Touster, O., and Anderson, L. (1969) *myo*-Inositol Catabolism in Human Pentosurics: The Predominant Role of the

Glucuronate-Xylulose-Pentose Phosphate Pathway. *Ann. N. Y. Acad. Sci.* 165, 564-576.

32. Loewus, F. A., and Murthy, P. P. N. (2000) *myo*-Inositol Metabolism in Plants. *Plant Sci.* 150, 1-9.

33. Anderson, W. A., and Magasanik, B. (1971) Pathway of *myo*-Inositol Degradation in *Aerobacter aerogenes*. Conversion of 2-Deoxy-5-Keto-D-Gluconic Acid to Glycolytic Intermediates. *J. Biol. Chem.* 246, 5662-5675.

34. Yoshida, K., Yamaguchi, M., Morinaga, T., Kinehara, M., Ikeuchi, M., Ashida, H., and Fujita, Y. (2008) *myo*-Inositol Catabolism in *Bacillus subtilis*. *J. Biol. Chem.* 283, 10415-10424.

35. Fujita, Y., Shindo, K., Miwa, Y., and Yoshida, K. (1991) *Bacillus subtilis* Inositol Dehydrogenase-Encoding Gene (*idh*): Sequence and Expression in *Escherichia coli*. *Gene.* 108, 121-125.

36. Yoshida, K., Yamaguchi, M., Ikeda, H., Omae, K., Tsurusaki, K., and Fujita, Y. (2004) The Fifth Gene of the *iol* Operon of *Bacillus subtilis*, *iolE*, Encodes 2-Keto-*myo*-Inositol Dehydratase. *Microbiology.* 150, 571-580.

37. Stines-chaumeil, C., Talfournier, F., and Branlant, G. (2006) Mechanistic Characterization of the MSDH (Methylmalonate Semialdehyde Dehydrogenase) from *Bacillus subtilis*. *Biochem. J.* 395, 107-115.

38. Kallberg, Y., and Persson, B. (2006) Prediction of Coenzyme Specificity in Dehydrogenases/Reductases. A Hidden Markov Model-Based Method and its Application on Complete Genomes. *FEBS J.* 273, 1177-1184.

39. Carugo, O., and Argos, P. (1997) NADP-Dependent Enzymes. II: Evolution of the Mono-and Dinucleotide Binding Domains. *Proteins.* 28, 29-40.

40. Persson, B., Jeffery, J., and Hoernvall, H. (1991) Different Segment Similarities in Long-Chain Dehydrogenases. *Biochem. Biophys. Res. Commun.* 177, 218-223.

41. Joernvall, H., Persson, B., Krook, M., Atrian, S., Gonzalez-Duarte, R., Jeffery, J., and Ghosh, D. (1995) Short-Chain Dehydrogenases/Reductases (SDR). *Biochem.* 34, 6003-6013.

42. Nordling, E., Jornvall, H., and Persson, B. (2002) Medium-Chain Dehydrogenases/Reductases (MDR). Family Characterizations Including Genome Comparisons and Active Site Modelling. *Eur. J. Biochem.* 269, 4267-4276.
43. Joernvall, H., Persson, M., and Jeffery, J. (1981) Alcohol and Polyol Dehydrogenases are both Divided into Two Protein Types, and Structural Properties Cross-Relate the Different Enzyme Activities within Each Type. *Proc. Natl. Acad. Sci. U. S. A.* 78, 4226-4230.
44. White, J. L., Hackert, M. L., Buehner, M., Adams, M. J., Ford, G. C., Lentz, P. J., Jr., Smiley, I. E., Steindel, S. J., and Rossmann, M. G. (1976) A Comparison of the Structures of *Apo*-Dogfish M4 Lactate Dehydrogenase and its Ternary Complexes. *J. Mol. Biol.* 102, 759-779.
45. Persson, B., Kallberg, Y., Bray, J. E., Bruford, E., Dellaporta, S. L., Favia, A. D., Duarte, R. G., Joernvall, H., Kavanagh, K. L., Kedishvili, N., Kisiela, M., Maser, E., Mindnich, R., Orchard, S., Penning, T. M., Thornton, J. M., Adamski, J., and Oppermann, U. (2009) The SDR (Short-Chain Dehydrogenase/Reductase and Related Enzymes) Nomenclature Initiative. *Chem. Biol. Interact.* 178, 94-98.
46. Bray, J. E., Marsden, B. D., and Oppermann, U. (2009) The Human Short-Chain Dehydrogenase/Reductase (SDR) Superfamily: A Bioinformatics Summary. *Chem. Biol. Interact.* 178, 99-109.
47. Oppermann, U. C. T., Filling, C., and Jornvall, H. (2001) Forms and Functions of Human SDR Enzymes. *Chem. Biol. Interact.* 130-132, 699-705.
48. Kallberg, Y., Oppermann, U., Jornvall, H., and Persson, B. (2002) Short-Chain Dehydrogenases/Reductases (SDRs). Coenzyme-Based Functional Assignments in Completed Genomes. *Eur. J. Biochem.* 269, 4409-4417.
49. Filling, C., Berndt, K. D., Benach, J., Knapp, S., Prozorovski, T., Nordling, E., Ladenstein, R., Jornvall, H., and Oppermann, U. (2002) Critical Residues for Structure and Catalysis in Short-Chain Dehydrogenases/Reductases. *J. Biol. Chem.* 277, 25677-25684.
50. Kavanagh, K. L., Jörnvall, H., Persson, B., and Oppermann, U. (2008) The SDR Superfamily: Functional and Structural Diversity within a Family of Metabolic and Regulatory Enzymes. *Cell. Mol. Life Sci.* 65, 3895-3906.

51. Knoll, M., and Pleiss, J. (2008) The Medium-Chain Dehydrogenase/Reductase Engineering Database: A Systematic Analysis of a Diverse Protein Family to Understand Sequence-Structure-Function Relationship. *Protein Sci.* 17, 1689-1697.
52. Jornvall, H., Hoog, J., and Persson, B. (1999) SDR and MDR: Completed Genome Sequences Show these Protein Families to be Large, of Old Origin, and of Complex Nature. *FEBS Lett.* 445, 261-264.
53. Jornvall, H., Nordling, E., and Persson, B. (2003) Multiplicity of Eukaryotic ADH and Other MDR Forms. *Chem. Biol. Interact.* 143-144, 255-261.
54. Klimacek, M., Kavanagh, K. L., Wilson, D. K., and Nidetzky, B. (2003) *Pseudomonas fluorescens* Mannitol 2-Dehydrogenase and the Family of Polyol-Specific Long-Chain Dehydrogenases/Reductases: Sequence-Based Classification and Analysis of Structure-Function Relationships. *Chem. Biol. Interact.* 143-144, 559-582.
55. Klimacek, M., and Nidetzky, B. (2002) A Catalytic Consensus Motif for D-Mannitol 2-Dehydrogenase, a Member of a Polyol-Specific Long-Chain Dehydrogenase Family, Revealed by Kinetic Characterization of Site-Directed Mutants of the Enzyme from *Pseudomonas fluorescens*. *Biochem. J.* 367, 13-18.
56. Rowland, P., Basak, A. K., Gover, S., Levy, H. R., and Adams, M. J. (1994) The Three-dimensional Structure of Glucose 6-Phosphate Dehydrogenase from *Leuconostoc mesenteroides* Refined at 2.0 Å Resolution. *Structure.* 2, 1073-1087.
57. Dean, A. M., and Koshland, D. E., Jr. (1993) Kinetic Mechanism of *Escherichia coli* Isocitrate Dehydrogenase. *Biochem.* 32, 9302-9309.
58. Pirrung, M. C., Han, H., and Nunn, D. S. (1994) Kinetic Mechanism and Reaction Pathway of *Thermus thermophilus* Isopropylmalate Dehydrogenase. *J. Org. Chem.* 59, 2423-2429.
59. Karsten, W. E., Tipton, P. A., and Cook, P. F. (2002) Tartrate Dehydrogenase Catalyzes the Stepwise Oxidative Decarboxylation of D-Malate with both NAD and Thio-NAD. *Biochem.* 41, 12193-12199.
60. Liu, D., Karsten, W. E., and Cook, P. F. (2000) Lysine 199 is the General Acid in the NAD-Malic Enzyme Reaction. *Biochem.* 39, 11955-11960.
61. Adams, M. J., Ellis, G. H., Gover, S., Naylor, C. E., and Phillips, C. (1994) Crystallographic Study of Coenzyme, Coenzyme Analogue and Substrate Binding in

6-Phosphogluconate Dehydrogenase: Implications for NADP Specificity and the Enzyme Mechanism. *Structure*. 2, 651-668.

62. Campbell, R. E., Mosimann, S. C., Van de Rijn, I., Tanner, M. E., and Strynadka, N. C. J. (2000) The First Structure of UDP-Glucose Dehydrogenase Reveals the Catalytic Residues Necessary for the Two-Fold Oxidation. *Biochem*. 39, 7012-7023.

63. Ruzheinikov, S. N., Burke, J., Sedelnikova, S., Baker, P. J., Taylor, R., Bullough, P. A., Muir, N. M., Gore, M. G., and Rice, D. W. (2001) Glycerol Dehydrogenase Structure, Specificity, and Mechanism of a Family III Polyol Dehydrogenase. *Structure*. 9, 789-802.

64. Kavanagh, K. L., Klimacek, M., Nidetzky, B., and Wilson, D. K. (2002) Crystal Structure of *Pseudomonas fluorescens* Mannitol 2-Dehydrogenase Binary and Ternary Complexes. Specificity and Catalytic Mechanism. *J. Biol. Chem*. 277, 43433-43442.

65. Ramaley, R., Fujita, Y., and Freese, E. (1979) Purification and Properties of *Bacillus subtilis* Inositol Dehydrogenase. *J. Biol. Chem*. 254, 7684-7690.

66. Freese, E., and Fujita, Y. (1976) Control of Enzyme Synthesis during Growth and Sporulation. *Microbiology*. 164-184.

67. Fujita, Y., Ramaley, R., and Freese, E. (1977) Location and Properties of Glucose Dehydrogenase in Sporulating Cells and Spores of *Bacillus subtilis*. *J. Bacteriol*. 132, 282-293.

68. DeLano WL. The PyMOL molecular graphics system. San Carlos, CA: DeLano Scientific LLC, 2008.

69. Daniellou, R., Phenix, C. P., Tam, P. H., Laliberte, M. C., and Palmer, D. R. J. (2005) Stereoselective Oxidation of Protected Inositol Derivatives Catalyzed by Inositol Dehydrogenase from *Bacillus subtilis*. *Org. Biomol. Chem*. 3, 401-403.

70. Lott, J. S., Halbig, D., Baker, H. M., Hardman, M. J., Sprenger, G. A., and Baker, E. N. (2000) Crystal Structure of a Truncated Mutant of Glucose-Fructose Oxidoreductase Shows that an N-Terminal Arm Controls Tetramer Formation. *J. Mol. Biol*. 304, 575-584.

71. Kingston, R. L., Scopes, R. K., and Baker, E. N. (1996) The Structure of Glucose-Fructose Oxidoreductase from *Zymomonas mobilis*: An Osmoprotective Periplasmic Enzyme Containing Non-Dissociable NADP. *Structure*. 4, 1413-1428.

72. Zachariou, M., and Scopes, R. (1986) Glucose-Fructose Oxidoreductase, a New Enzyme Isolated from *Zymomonas mobilis* that is Responsible for Sorbitol Production. *J. Bacteriol.* 167, 863-869.
73. Leigh, D., Scopes, R. K., and Rogers, P. L. (1984) A Proposed Pathway for Sorbitol Production of *Zymomonas mobilis*. *Appl. Microbiol. Biotechnol.* 20, 413-415.
74. Nurizzo, D., Halbig, D., Sprenger, G. A., and Baker, E. N. (2001) Crystal Structures of the Precursor Form of Glucose-Fructose Oxidoreductase from *Zymomonas mobilis* and its Complexes with Bound Ligands. *Biochem.* 40, 13857-13867.
75. Wiegert, T., Sahm, H., and Sprenger, G. A. (1997) The Substitution of a Single Amino Acid Residue (Ser-116→Asp) Alters NADP-containing Glucose-Fructose Oxidoreductase of *Zymomonas mobilis* into a Glucose Dehydrogenase with Dual Coenzyme Specificity. *J. Biol. Chem.* 272, 13126-13133.
76. Thompson, J. D., Higgins, D. G., and Gibson, T. J. (1994) CLUSTAL W: Improving the Sensitivity of Progressive Multiple Sequence Alignment through Sequence Weighting, Position-Specific Gap Penalties and Weight Matrix Choice. *Nucleic Acids Res.* 22, 4673-4680.
77. Gouet, P., Courcelle, E., Stuart, D. I., and Metoz, F. (1999) ESPript: Analysis of Multiple Sequence Alignments in PostScript. *Bioinformatics.* 15, 305-308.
78. Daniellou, R., Zheng, H., Langill, D. M., Sanders, D. A. R., and Palmer, D. R. J. (2007) Probing the Promiscuous Active Site of *myo*-Inositol Dehydrogenase using Synthetic Substrates, Homology Modeling, and Active Site Modification. *Biochem.* 46, 7469-7477.
79. Donglu Zhang, Mingshe Zhu, W. Griffith Humphreys. (2008) *Drug Metabolism in Drug Design and Development : Basic Concepts and Practice*. Wiley-Interscience, Hoboken, N.J.
80. H. Gerhard Vogel. (2008) *Drug Discovery and Evaluation: Pharmacological Assays*. Berlin ; New York : Springer.
81. Lehninger, A. L., Nelson, D. L., and Cox, M. M. (2004) *Lehninger Principles of Biochemistry*. 4th Edition, WH Freeman.
82. Robert A. Copeland. (2000) *Enzymes: A Practical Introduction to Structure, Mechanism, and Data Analysis*. 2nd Edition, J. Wiley, New York.

83. Cornish-Bowden, A., and Duggleby, R. G. (1995) *Analysis of Enzyme Kinetic Data*. Oxford University Press.
84. Cosgrove, M. S., Gover, S., Naylor, C. E., Vandeputte-Rutten, L., Adams, M. J., and Levy, H. R. (2000) An Examination of the Role of Asp-177 in the His-Asp Catalytic Dyad of *Leuconostoc mesenteroides* Glucose 6-Phosphate Dehydrogenase: X-Ray Structure and pH Dependence of Kinetic Parameters of the D177N Mutant Enzyme. *Biochem.* 39, 15002-15011.
85. Dambe, T. R., Kuhn, A. M., Brossette, T., Giffhorn, F., and Scheidig, A. J. (2006) Crystal Structure of NADP(H)-Dependent 1,5-Anhydro-D-Fructose Reductase from *Sinorhizobium morelense* at 2.2 Å Resolution: Construction of a NADH-Accepting Mutant and its Application in Rare Sugar Synthesis. *Biochem.* 45, 10030-10042.
86. Alizade, M. A., Gaede, K., and Brendel, K. (1976) Chirality of the Hydrogen Transfer to NAD Catalyzed by *myo*-Inositol Dehydrogenase from *Klebsiella pneumoniae*. *J. Biosci.* 31C, 624-625.
87. Saiki, R. K., Gelfand, D. H., Stoffel, S., Scharf, S. J., Higuchi, R., Horn, G. T., Mullis, K. B., and Erlich, H. A. (1988) Primer-Directed Enzymatic Amplification of DNA with a Thermostable DNA Polymerase. *Science.* 239, 487-491.
88. Laemmli, U. K. (1970) Cleavage of Structural Proteins during the Assembly of the Head of Bacteriophage T4. *Nature.* 227, 680-685.
89. Cheng, Y., and Prusoff, W. H. (1973) Relationship between the Inhibition Constant (K_i) and the Concentration of Inhibitor which Causes 50 Per Cent Inhibition (IC₅₀) of an Enzymatic Reaction. *Biochem. Pharmacol.* 22, 3099-3108.
90. Angyal, S. J. (2000) *myo*-Inositol 4,6-Carbonate: an Easily Prepared Small Molecule with Three syn-axial Hydroxyl Groups. *Carbohydr. Res.* 325, 313-320.
91. Bock, H., and Dammel, R. (1988) Gas-Phase Reactions. 66. Gas-Phase Pyrolyses of Alkyl Azides: Experimental Evidence for Chemical Activation. *J. Am. Chem. Soc.* 110, 5261-5269.
92. Zahradnik, P., and Buffa, R. (2002) Synthesis and Theoretical Study of a New Type of Pentacyclic Bis-Benzothiazolium Compound. *Molecules.* 7, 534-539.
93. Hansen, C. A., Dean, A. B., Draths, K. M., and Frost, J. W. (1999) Synthesis of 1,2,3,4-Tetrahydroxybenzene from D-Glucose: Exploiting *myo*-Inositol as a Precursor to Aromatic Chemicals. *J. Am. Chem. Soc.* 121, 3799-3800.

94. Desai, T., Gigg, J., Gigg, R., Martin-Zamora, E., and Schnetz, N. (1994) The Synthesis and Resolution of (\pm)-1,4-Di-*O*-Benzyl-2,3-*O*-Isopropylidene-*myo*- Inositol. *Carbohydr. Res.* 258, 135-144.
95. Chung, S., Kwon, Y., Chang, Y., Sohn, K., Shin, J., Park, K., Hong, B., and Chung, I. (1999) Synthesis of all Possible Regioisomers of *scyllo*-Inositol Phosphate. *Bioorg. Med. Chem.* 7, 2577-2589.
96. Horne, G., Mills, S. J., and Potter, B. V. L. (2004) First Derivatives of *myo*-Inositol 1,4,6-Trisphosphate Modified at Positions 2 and 3: Structural Analogues of D-*myo*-Inositol 1,4,5-Trisphosphate. *Carbohydr. Res.* 339, 51-65.
97. Koto, S., Hirooka, M., Yoshida, T., Takenaka, K., Asai, C., Nagamitsu, T., Sakuma, H., Sakurai, M., Masuzawa, S., Komiya, M., Sato, T., Zen, S., Yago, K., and Tomonaga, F. (2000) Syntheses of Penta-*O*-benzyl-*myo*-Inositols, *O*- β -L-Arabinosyl-(1 \rightarrow 2)-sn-*myo*-Inositol, *O*- α -D-Galactosyl-(1 \rightarrow 3)-sn-*myo*- Inositol, and *O*- α -D-Galactosyl-(1 \rightarrow 6)-*O*- α -D-Galactosyl-(1 \rightarrow 3)-sn-*myo*-Inositol. *Bull. Chem. Soc. Jpn.* 73, 2521-2529.
98. Sawyer, D. A., and Potter, B. V. L. (1992) Total Synthesis of Fluorinated Analogs of Inositol and Inositol 1,4,5-Trisphosphate. *J. Chem. Soc. Perkin Trans.1*, 923-932.
99. Lowe, G., and McPhee, F. (1991) Synthesis of [^3H]-Labeled and Unlabeled 2-Deoxy-2-fluoro-*myo*-inositol and 1-Deoxy-1-fluoro-*scyllo*-inositol for Use in Studies of the Phosphoinositide Cycle. *J. Chem. Soc. Perkin Trans.1*, 1249-1253.
100. Migaud, M. E., and Frost, J. W. (1996) Elaboration of a General Strategy for Inhibition of *myo*-Inositol 1-phosphate Synthase: Active Site Interactions of Analogs Possessing Oxidized Reaction Centers. *J. Am. Chem. Soc.* 118, 495-501.
101. Alves Benicio, A. A., Da Silva, A. D., De Almeida, M. V., Da Silva, M. M., and Dov Gero, S. (2001) Stereoselective Synthesis of 2,6-Dideoxy; 3,6-Dideoxy; 2,3,6-Trideoxy-inositol 1,4,5-Trisphosphate and 6-Deoxy-inositol 1,3,4,5-Tetrakisphosphate Analogs from 6-Deoxy-D-Inositol Precursors. *Tetrahedron.* 57, 1161-1167.
102. Jiang, C., Schedler, D. J. A., Morris, P. E., Jr., Zayed, A. H. A., and Baker, D. C. (1990) Fluorinated Cyclitols. an Improved Synthesis of 5-Deoxy-5-fluoro-*myo*-Inositol, its Deuterium Labeling, and Synthesis of a 5,5-Gem-Difluoro Analog. *Carbohydr. Res.* 207, 277-285.

103. Yang, S. S., Beattie, T. R., and Shen, T. Y. (1982) Synthesis of Fluorodeoxy-*scyllo*-Inositol and Phosphatidylfluorodeoxy-*scyllo*-Inositol. *Tetrahedron Lett.* 23, 5517-5520.
104. Martin, S. F., Josey, J. A., Wong, Y., and Dean, D. W. (1994) General Method for the Synthesis of Phospholipid Derivatives of 1,2-*O*-Diacyl-*sn*-Glycerols. *J. Org. Chem.* 59, 4805-4820.
105. Garegg, P. J., and Samuelsson, B. (1980) Novel Reagent System for Converting a Hydroxy-Group into an Iodo-Group in Carbohydrates with Inversion of Configuration. Part 2. *J. Chem. Soc. Perkin Trans.1*, 2866-2869.
106. Jiang, C., Moyer, J. D., and Baker, D. C. (1987) Synthesis of Deoxy and Deoxyhalo Analogs of *myo*-Inositol. *J. Carbohydr. Chem.* 6, 319-355.
107. Billington, D. C., Baker, R., Kulagowski, J. J., Mawer, I. M., Vacca, J. P., DeSolms, S. J., and Huff, J. R. (1989) The Total Synthesis of *myo*-Inositol Phosphates via *myo*-Inositol Orthoformate. *J. Chem. Soc. Perkin Trans.1*, 1423-1429.
108. Daniellou, R., Zheng, H., and Palmer, D. R. J. (2006) Kinetics of the Reaction Catalyzed by Inositol Dehydrogenase from *Bacillus subtilis* and Inhibition by Fluorinated Substrate Analogs. *Can. J. Chem.* 84, 522-527.
109. Jonathan Clayden. (2001) *Organic Chemistry*. Oxford University Press, Oxford.
110. L. Melander and W. H. Saunders. (1980) *Reaction Rates of Isotopic Molecules*. A Wiley Interscience publication, New York.
111. Daniel L. Purich. (1996) Isotope Effects: Determination of Enzyme Transition State Structure, *Contemporary Enzyme Kinetics and Mechanism*. 2nd Edition, 407-432, Academic press.
112. Leskovac, V. (2003) *Comprehensive Enzyme Kinetics*. Springer press.
113. Basran, J., Sutcliffe, M. J., and Scrutton, N. S. (2001) Deuterium Isotope Effects during Carbon-Hydrogen Bond Cleavage by Trimethylamine Dehydrogenase. Implications for Mechanism and Vibrationally Assisted Hydrogen Tunneling in Wild-Type and Mutant Enzymes. *J. Biol. Chem.* 276, 24581-24587.
114. Fonseca, I. O., Silva, R. G., Fernandes, C. L., de Souza, O. N., Basso, L. A., and Santos, D. S. (2007) Kinetic and Chemical Mechanisms of Shikimate Dehydrogenase from *Mycobacterium tuberculosis*. *Arch. Biochem. Biophys.* 457, 123-133.

115. Jacques, S. L., Ejim, L. J., and Wright, G. D. (2001) Homoserine Dehydrogenase from *Saccharomyces Cerevisiae*: Kinetic Mechanism and Stereochemistry of Hydride Transfer. *Biochimica et Biophysica Acta*. 1544, 42-54.
116. Grubmeyer, C., and Teng, H. (1999) Mechanism of *Salmonella Typhimurium* Histidinol Dehydrogenase: Kinetic Isotope Effects and pH Profiles. *Biochem.* 38, 7355-7362.
117. Lindstad, R. I., Hermansen, L. F., and McKinley-McKee, J. S. (1992) The Kinetic Mechanism of Sheep Liver Sorbitol Dehydrogenase. *Eur. J. Biochem.* 210, 641-647.
118. Pourmotabbed, T., Shih, M. J., and Creighton, D. J. (1989) Bovine Liver Formaldehyde Dehydrogenase. Kinetic and Molecular Properties. *J. Biol. Chem.* 264, 17384-17388.
119. Ostlund, R. E., Jr., Seemayer, R., Gupta, S., Kimmel, R., Ostlund, E. L., and Sherman, W. R. (1996) A Stereospecific *myo*-inositol/*D-chiro*-Inositol Transporter in HepG2 Liver Cells. Identification with *D-chiro*-[3-³H]-Inositol. *J. Biol. Chem.* 271, 10073-10078.
120. Catelani, G., Corsaro, A., D'Andrea, F., Mariani, M., and Pistara, V. (2002) Intramolecular Aldol Cyclization of *L-lyxo*-Hexos-5-Ulose Derivatives: A New Diastereoselective Synthesis of *D-chiro*-Inositol. *Bioorg. Med. Chem. Lett.* 12, 3313-3315.
121. Devaraj, S., Shashidhar, M. S., and Dixit, S. S. (2005) Chelation Controlled Regiospecific *O*-Substitution of *myo*-Inositol Orthoesters: Convenient Access to Orthogonally Protected *myo*-Inositol Derivatives. *Tetrahedron*. 61, 529-536.
122. Yoshida, K., Yamaguchi, M., Morinaga, T., Ikeuchi, M., Kinehara, M., and Ashida, H. (2006) Genetic Modification of *Bacillus subtilis* for Production of *D-chiro*-Inositol, an Investigational Drug Candidate for Treatment of Type 2 Diabetes and Polycystic Ovary Syndrome. *Appl. Environ. Microbiol.* 72, 1310-1315.
123. Parsch, J., and Engels, J. W. (2002) C-F·····H-C Hydrogen Bonds in Ribonucleic Acids. *J. Am. Chem. Soc.* 124, 5664-5672.
124. Ma, J. A., and Cahard, D. (2004) Asymmetric Fluorination, Trifluoromethylation, and Perfluoroalkylation Reactions. *Chem. Rev.* 104, 6119-6146.

125. Barton, D. H. R., and McCombie, S. W. (1975) A New Method for the Deoxygenation of Secondary Alcohols. *J. Chem. Soc., Perkin Trans.1*, 1975, 1574-1585.
126. Barton, D. H., and Subramanian, R. (1977) Reactions of Relevance to the Chemistry of Aminoglycoside Antibiotics. Part 7. Conversion of Thiocarbonates into Deoxy-Sugars. *J. Chem. Soc. Perkin Trans. 1*, 15, 1718-1723.
127. Robins, M. J., and Wilson, J. S. (1981) Smooth and Efficient Deoxygenation of Secondary Alcohols. A General Procedure for the Conversion of Ribonucleosides to 2'-Deoxynucleosides. *J. Am. Chem. Soc.* 103, 932-933.
128. Robins, M. J., Wilson, J. S., and Hansske, F. (1983) Nucleic Acid Related Compounds. 42. A General Procedure for the Efficient Deoxygenation of Secondary Alcohols. Regiospecific and Stereoselective Conversion of Ribonucleosides to 2'-Deoxynucleosides. *J. Am. Chem. Soc.* 105, 4059-4065.
129. Martin, S. F., Dappen, M. S., Dupre, B., and Murphy, C. J. (1987) A Convergent Total Synthesis of (±)-Phyllanthocin. *J. Org. Chem.* 52, 3706-3708.
130. Horton, D., Priebe, W., and Sznajdman, M. L. (1993) Steric and Conformational Effects in the Dehalogenation of 2-Halo Sugar Derivatives with Tributylstannane. *J. Org. Chem.* 58, 1821-1826.
131. Plapp, B. V. (1995) Site-Directed Mutagenesis: A Tool for Studying Enzyme Catalysis. *Methods Enzymol.* 249, 91-119.
132. Murzin, A. G., Brenner, S. E., Hubbard, T., and Chothia, C. (1995) SCOP: A Structural Classification of Proteins Database for the Investigation of Sequences and Structures. *J. Mol. Biol.* 247, 536-540.
133. Cosgrove, M. S., Naylor, C., Paludan, S., Adams, M. J., and Levy, H. R. (1998) On the Mechanism of the Reaction Catalyzed by Glucose 6-Phosphate Dehydrogenase. *Biochem.* 37, 2759-2767.
134. Bruns, C. M., Hubatsch, I., Ridderström, M., Mannervik, B., and Tainer, J. A. (1999) Human Glutathione Transferase A4-4 Crystal Structures and Mutagenesis Reveal the Basis of High Catalytic Efficiency with Toxic Lipid Peroxidation Products. *J. Mol. Biol.* 288, 427-439.
135. Holm, L., and Sander, C. (1993) Protein Structure Comparison by Alignment of Distance Matrixes. *J. Mol. Biol.* 233, 123-138.

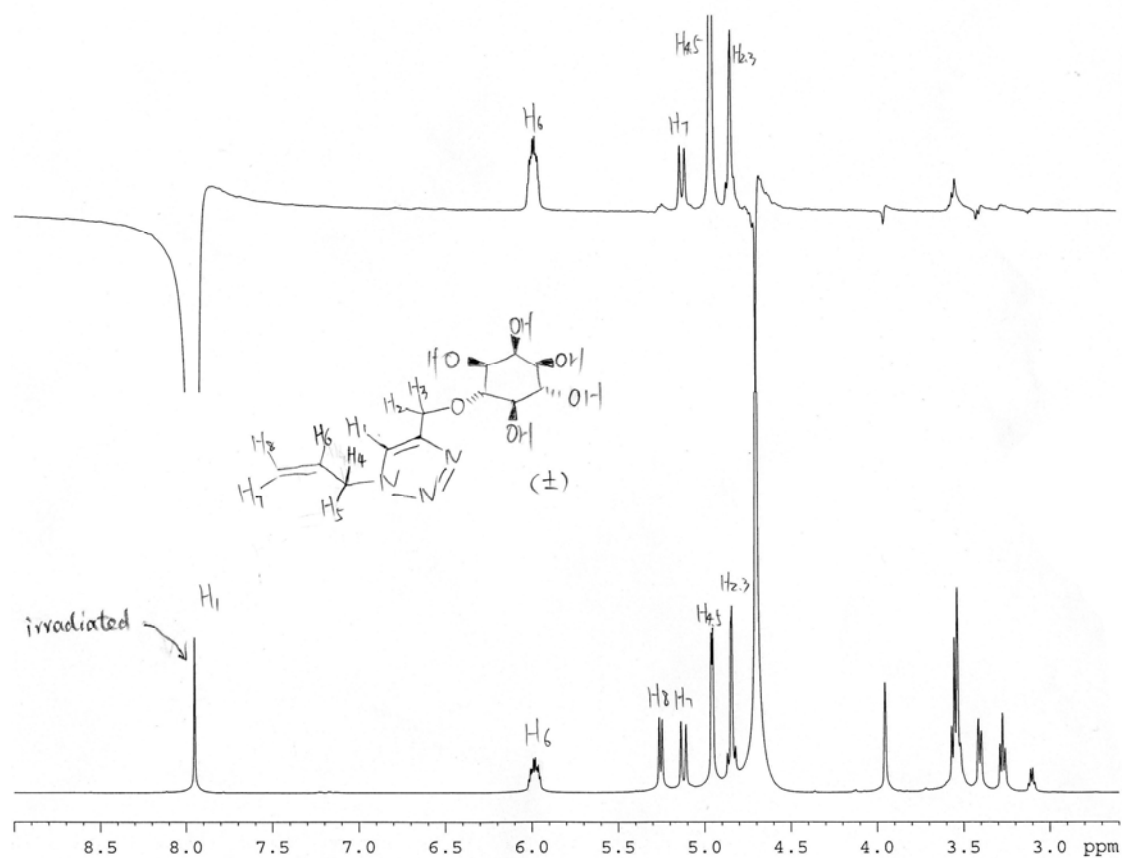
136. Kleiger, G., and Eisenberg, D. (2002) GXXXG and GXXXA Motifs Stabilize FAD and NAD(P)-Binding Rossmann Folds through C α -H \cdots O Hydrogen Bonds and Van Der Waals Interactions. *J. Mol. Biol.* 323, 69-76.
137. Hanukoglu, I., and Gutfinger, T. (1989) cDNA Sequence of Adrenodoxin Reductase. *Eur. J. Biochem.* 180, 479-484.
138. Rao, S. T., and Rossmann, M. G. (1973) Comparison of Super-Secondary Structures in Proteins. *J. Mol. Biol.* 76, 241-256.
139. Woodyer, R., van der Donk, W. A., and Zhao, H. (2003) Relaxing the Nicotinamide Cofactor Specificity of Phosphite Dehydrogenase by Rational Design. *Biochem.* 42, 11604-11614.
140. Andreadeli, A., Platis, D., Tishkov, V., Popov, V., and Labrou, N. E. (2008) Structure-Guided Alteration of Coenzyme Specificity of Formate Dehydrogenase by Saturation Mutagenesis to Enable Efficient Utilization of NADP⁺. *FEBS J.* 275, 3859-3869.
141. Ghosh, D., Pletnev, V. Z., Zhu, D. W., Wawrzak, Z., Duax, W. L., Pangborn, W., Labrie, F., and Lin, S. X. (1995) Structure of Human Estrogenic 17 β -Hydroxysteroid Dehydrogenase at 2.20 Å Resolution. *Structure.* 3, 503-513.
142. Gallivan, J. P., and Dougherty, D. A. (1999) Cation- π Interactions in Structural Biology. *Proc. Natl. Acad. Sci. U.S.A.* 96, 9459.
143. Banta, S., Swanson, B. A., Wu, S., Jarnagin, A., and Anderson, S. (2002) Alteration of the Specificity of the Cofactor-Binding Pocket of *Corynebacterium* 2,5-Diketo-D-Gluconic Acid Reductase A. *Protein Engineering.* 15(2), 131-140.
144. Carugo, O., and Argos, P. (1997) NADP-Dependent Enzymes. I: Conserved Stereochemistry of Cofactor Binding. *Proteins: Structure, Function, and Bioinformatics.* 28, 10-28.
145. Cho, H., Oliveira, M. A., and Tai, H. H. (2003) Critical Residues for the Coenzyme Specificity of NAD-Dependent 15-Hydroxyprostaglandin Dehydrogenase. *Arch. Biochem. Biophys.* 419, 139-146.
146. Hurley, J. H., Chen, R., and Dean, A. M. (1996) Determinants of Cofactor Specificity in Isocitrate Dehydrogenase: Structure of an Engineered NADP⁺→NAD⁺ Specificity-Reversal Mutant. *Biochem.* 35, 5670-5678.

147. Liu, Q. P., Sulzenbacher, G., Yuan, H., Bennett, E. P., Pietz, G., Saunders, K., Spence, J., Nudelman, E., Levery, S. B., White, T., Neveu, J. M., Lane, W. S., Bourne, Y., Olsson, M. L., Henrissat, B., and Clausen, H. (2007) Bacterial Glycosidases for the Production of Universal Red Blood Cells. *Nat. Biotechnol.* 25, 454-464.
148. Yip, V. L. Y., Varrot, A., Davies, G. J., Rajan, S. S., Yang, X., Thompson, J., Anderson, W. F., and Withers, S. G. (2004) An Unusual Mechanism of Glycoside Hydrolysis Involving Redox and Elimination Steps by a Family 4 β -Glycosidase from *Thermotoga Maritima*. *J. Am. Chem. Soc.* 126, 8354-8355.
149. Porte, S., Valencia, E., Yakovtseva, E.A., Borrás, E., Shafqat, N., Debreczeny, J. E., Pike, A. C. W., Oppermann, U., Farres, J., Fita, I., Pares, X. (2009) Three-Dimensional Structure and Enzymatic Function of Proapoptotic Human P53-Inducible Quinone Oxidoreductase Pig3. *J. Biol. Chem.* 284, 17194-17205.
150. Dagert, M., Ehrlich, S. D. (1979) Prolonged incubation in calcium chloride improves the competence of *Escherichia coli* cells. *Gene* 6(1), 23-28.

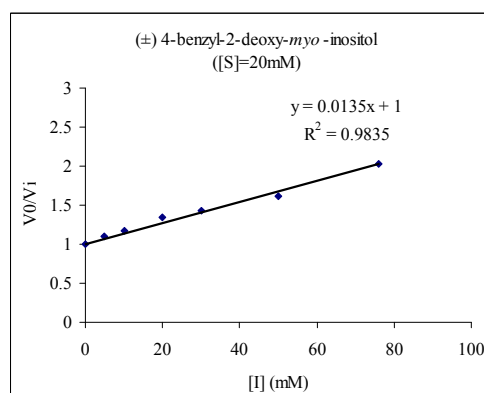
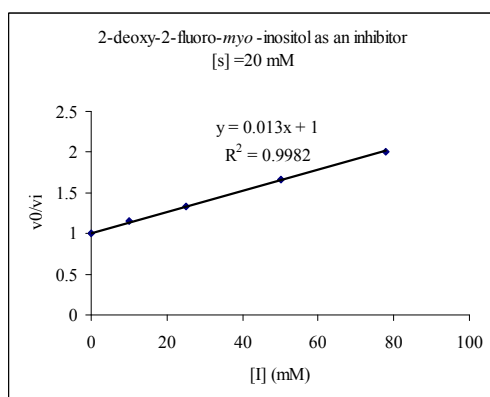
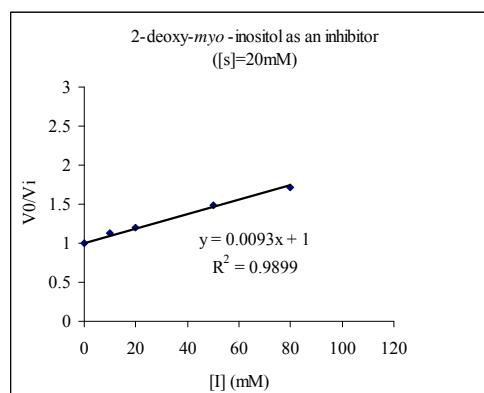
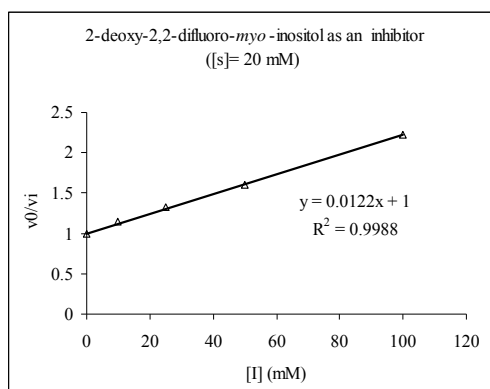
Appendix 1. Restriction digestions fractions after treated with corresponding digest enzymes. wt: wild-type.

plasmids	DNA pieces (bp)	Restriction enzyme
Y233F	4324+2077	Hpa1
wt IDH	6401	
Y235F	4324+2077	Hpa1
wt IDH	6401	
Y233R	4324+2077	Hpa1
wt IDH	6401	
Y235R	3738+1234+895+402+132	Eae1
wt IDH	3738+1297+1234+132	
M126A	3680+1940+781	ECoN1
wt IDH	2721+3680	
M126S	3680+1940+781	ECoN1
wt IDH	2721+3680	
D35S	1498 + 4903	Hpa1
wt IDH	6401	
D179N	2361, 1366, 1188, 1082, 394	Acl1
wt IDH	2326, 2269, 1386, 394	
G14A	4217+2180	ASiS1
wt IDH	6399	
G14A/D35S	4217+2180	ASiS1
wt IDH	6399	

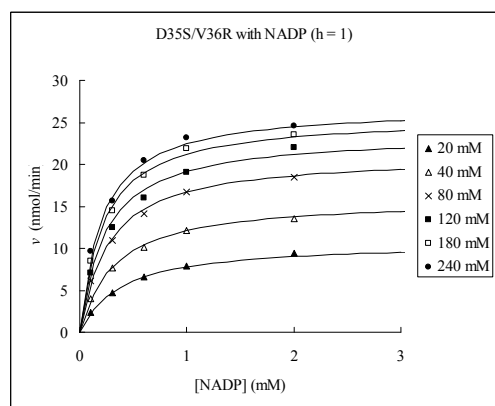
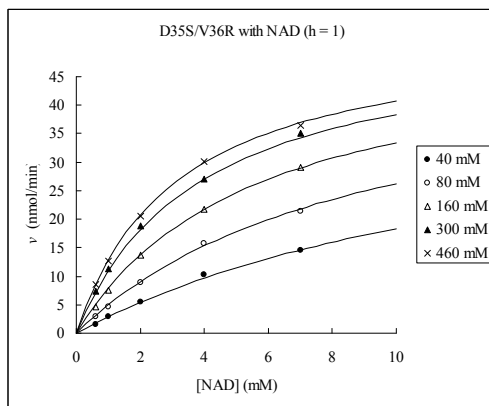
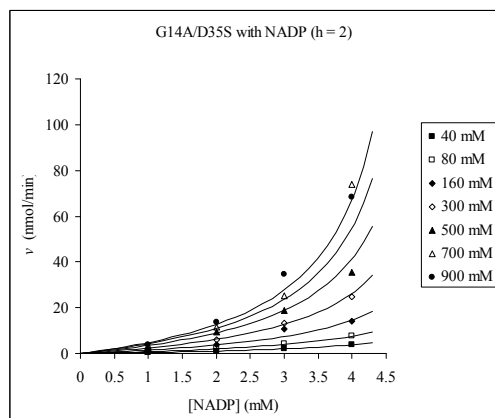
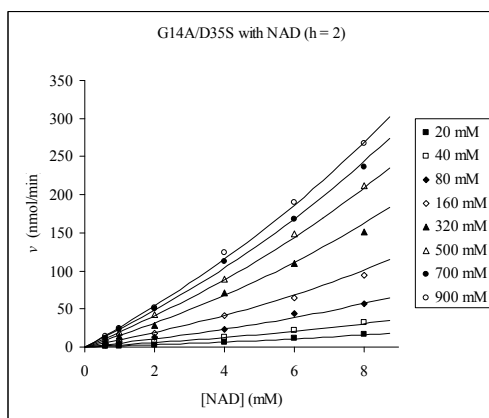
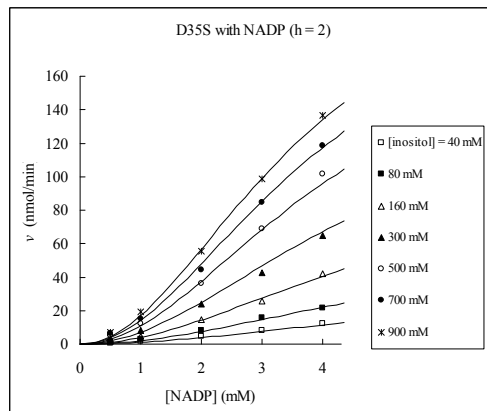
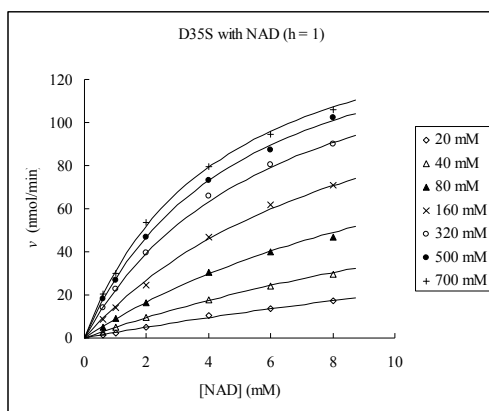
Appendix 2. NOE difference spectrometry of (\pm)-4-*O*-(1-allyl-4-methylene-1,2,3-triazole)-*myo*-inositol.



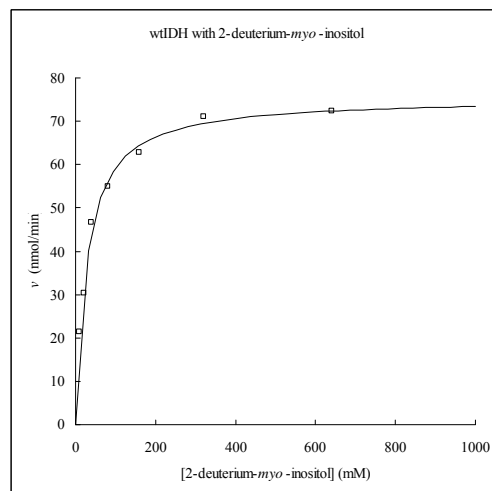
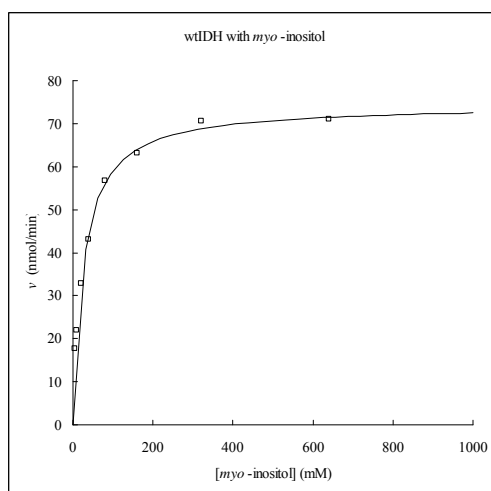
Appendix 3. Inhibitory activity (v_0/v_i) against concentrations of inhibitors.



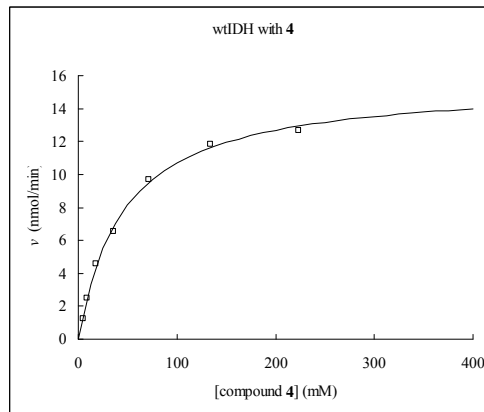
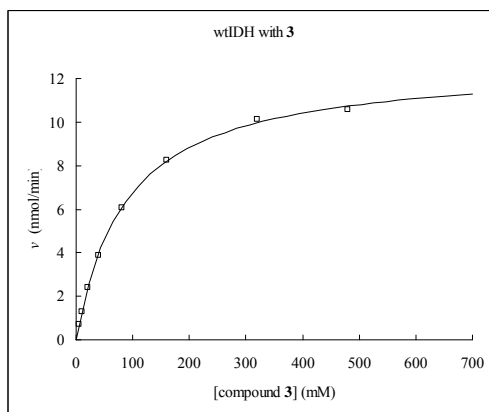
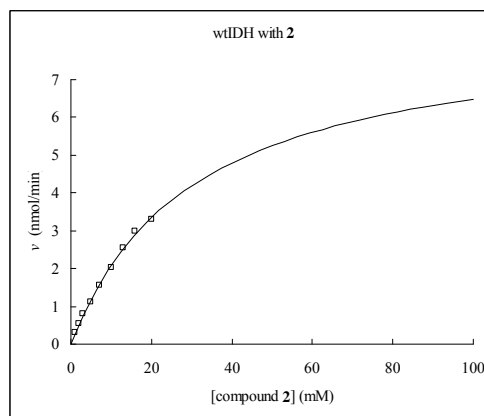
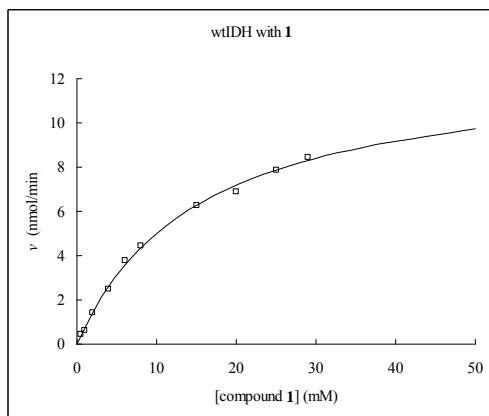
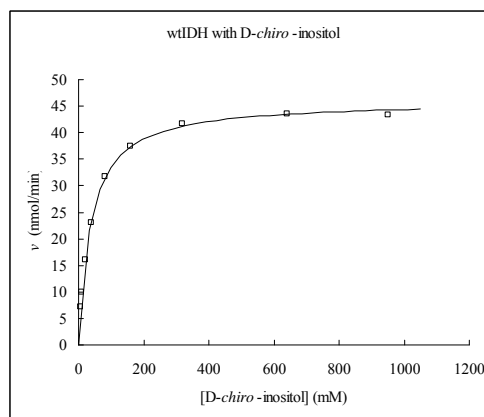
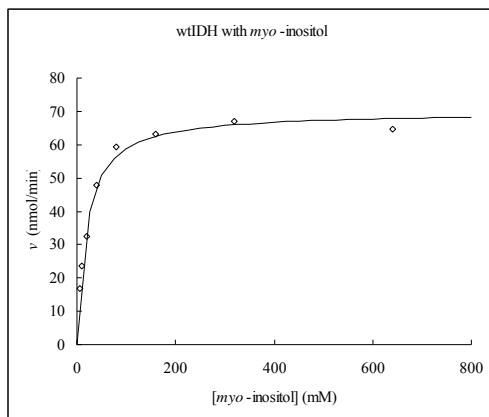
Appendix 4. Positive cooperativity demonstrated by mutants D35S and G14A/D35S with NADP⁺ or NAD⁺. No positive cooperativity observed with mutant D35S/V36R.



Appendix 5. Graphical representation of kinetic isotope effect measurement.



Appendix 6. Graphical representation of wild-type IDH using compounds 1, 2, 3, 4 , or D-*chiro*-inositol as the substrate.



Appendix 7. Graphical representation of IDH mutants using *myo*-inositol as the substrate.

